DEPARTMENT OF THE AIR FORCE

AIR UNIVERSITY

AIR FORCE INSTITUTE OF TECHNOLOGY

Wright-Patterson Air Force Base, Ohio

AFIT/GSO/AA/88D-2

AN ANALYSIS OF THE ATTITUDE STABILITY OF A SPACE STATION SUBJECT TO PARAMETRIC EXCITATION OF PERIODIC MASS MOTION

THESIS

Thomas E. Williams
Captain, USAF

AFIT/GSO/AA/88D-2

AFIT/GSO/AA/88D-2

AN ANALYSIS OF THE ATTITUDE STABILITY OF A SPACE STATION SUBJECT TO PARAMETRIC EXCITATION OF PERIODIC MASS MOTION

THESIS

Presented to the Faculty of the School of Engineering

of the Air Force Institute of Technology

Air University

In Partial Fulfillment of the

Requirements for the Degree of

Master of Science in Space Operations

Thomas E. Williams, B.S.

Captain, USAF

December 1988

Approved for public release; distribution unlimited

Preface

The purpose of this study was to determine how mass motion on a gravity gradient stabilized space station would alter the classical Lagrange stability region described by (Debra and Delp, 1961). The addition of mass motion to an orbiting space station introduces time varying moments of inertia into the equations of attitude motion. When the time variance is periodic, it is a source of parametric excitation.

The phenomenon of a parametrically excited system is also seen when eccentricity is introduced into the orbit of a gravity-gradient stabilized rigid body as shown by (Breakwell and Pringle, 1965). This study obtained similar results and shows that if masses move across the surface of a future space station, the gravity gradient torque will cause unstable attitude motion for certain configurations in the classical Lagrange region.

I would like to thank my thesis advisor, Dr. Curtis H. Spenny of the Department of Aeronautics and Astronautics, for his valued assistance in guiding me through this study. I would also like to thank Captain James Planeaux, also of the Department of Aeronautics and Astronautics, for his critical review of the final product. Finally, I would like to thank my wife Beverly for her patience and support; without it, this study would not have been possible.

Thomas E. Williams

Table of Contents

List of Figures

List of Symbols

a	Semi-Major Axis
a_T	Variable from Hill's Equation
A_{ij}	Elements of Direction Cosine Matrix
A_1, A_2	Coefficients of Assumed Solution to Order ϵ^0 Roll/Yaw Coupled Differential Equations
$\bar{A}_1, \bar{A}_2$	Complex Conjugates of A_1, A_2
A_1', A_2'	Derivative With Respect to T_1 of A_1, A_2
B	Body Principal Basis
$\hat{b}_1, \hat{b}_2, \hat{b}_3$	Orthogonal Directions of Body Principal Basis
D_0, D_1	Differential Operators
e	Eccentricity
$\underline{h}$	Angular Momentum of Space Station
I	Inertia Dyadic of the Space Station When Superscripted, Refers to Inertial Frame
I_1, I_2, I_3	Principal Moments of Inertia of the Space Station About Composite Center of Mass
I_{01}, I_{02} I_{03}	Principal Moments of Inertia of the Space Station Without Mass motion.
$\underline{M}$	External Gravity Torque
M_1, M_2, M_3	Body Components of $\underline{M}$
M	Reduced Mass of Moving Element
m_e	Mass of Moving Element
m_s	Mass of Sphere

$\underline{N}$	Vector Eccentric Orbital Rate
N	Scalar Eccentric Orbital Rate
n	Circular Orbital Rate
O	Orbit Basis
$\hat{o}_1, \hat{o}_2, \hat{o}_3$	Orthogonal Directions of Orbit Basis
p, r, y	Pitch, Roll, and Yaw Euler Angles
q_1, q_2, q_3	Variables of Hill's Equation
q_4	In Appendix A, these are Euler Parameters
$\underline{q}$	Quaternion
$\underline{R}$	Vector Radius From Earth Center to Space Station Center of Mass
R_1, R_2, R_3	Body Components of $\underline{R}$
R	Scalar Magnitude of $\underline{R}$
r_0, r_0'	Ratios of Moving Element Inertia to Pitch and Roll Inertias
r_1, r_2	Ratios of Principal Moments of Inertia
t	Time
t_p	Time Since Periapsis Passage
T	Dimensionless Time Variable
T_0, T_1	Time Scales
$\underline{u}$	Roll/Yaw Euler Angles in Method of Multiple Scales
${}^I\underline{w}^B$	Angular Velocity of Space Station With Respect to an Inertial Frame
${}^I\underline{w}^O$	Angular Velocity of Orbit Basis With Respect to an Inertial Frame
${}^O\underline{w}^B$	Angular Velocity of Space Station With Respect to Orbit Frame

z	Transformed Pitch Variable
Z	Skew-Symmetric Matrix
$\alpha_1, \alpha_2,$ λ_1, λ_2	Time Varying Coefficients of Coupled Roll/Yaw Equations
ϵ	Perturbation Parameter
μ	Characteristic Exponent
ω	Mass Motion Frequency
ω_1, ω_2	Resonant Frequencies

Abstract

The future space station will contain a mechanism that transports mass across large distances of its surface. Accordingly, this study will derive the equations of attitude motion for a gravity-gradient stabilized space station whose moments of inertia are varying with time. The equations are linearized, after which Hill's Equation is used to determine pitch stability, while the Method of Multiple Scales is used to determine the roll/yaw stability of the system. Results show that for certain frequencies of mass motion, attitude motion can grow unboundedly with time. Consequently, the shape of the classical Lagrange stability region is altered.

AN ANALYSIS OF THE ATTITUDE STABILITY OF A SPACE STATION SUBJECT TO PARAMETRIC EXCITATION OF PERIODIC MASS MOTION

I. Introduction

The proposed U.S. space station will be larger than any spacecraft previously built by man. As the station grows, it will become necessary to move maintenance and modification equipment over large distances of the space station surface. Hence, there is a need for a trolley apparatus that can transport large masses from section to section. This mass movement will affect the attitude stability of the space station. Research, therefore, is needed to determine the magnitude of this destabilizing motion and how it can be minimized, in order to design an adequate control system.

Objective

The objective of this study is to examine what happens to the pitch, roll, and yaw stability of a gravity-gradient stabilized space station when a trolley apparatus operates along a defined path. This study expands on the work John Chan (Chan, 1986) did with the pitch equation. The analysis continues by investigating the behavior of the coupled roll/yaw equations of attitude motion in order to define comprehensive conditions where mass movement will not lead

to large oscillations or to totally unstable attitude motion.

Methodology

The equations of motion are derived for a gravity-gradient stabilized space station whose moments of inertia are varying with time. The equations are then linearized, after which Hill's Equation and the Method of Multiple Scales are used to determine the pitch, roll, and yaw stability of the system. Stability boundaries are determined so that the effect of mass motion on the classical Lagrange gravity-gradient stability region is observed. The results are compared to the solutions obtained from numerical integration of the nonlinear equations for verification.

Scope

This study is restricted by the following conditions: (1) The only external torques acting on the spacecraft are gravitational environmental torques; (2) The spacecraft is small enough so that attitude motions have no significant effect on the orbital motion of the center of mass; (3) The orbit is circular.

II. Background Theory

The purpose of this Chapter is to provide some background theory on gravity-gradient stabilization and torques on spacecraft due to mass motion. An overview is provided on the analytical methods used to determine the stability of the linearized equations of motion. Specifics on each of the methods, however, are provided in Chapters V and VI.

Spacecraft Torques

The purpose of this section is to survey specific spacecraft torques and describe their origins and characteristics. (Hughes, 1986: 232) points out that the most striking characteristic of spacecraft torques is their minuteness. In terms of familiar terrestrial experience, they are intuitively negligible. On closer examination however, there are no "large" torques in space, and hence minor influences play major roles in governing the attitude dynamics of spacecraft. To help distinguish between the many different torques acting on spacecraft, they are divided into two categories: internal and external.

Internal Torques

Internal torques are usually defined as torques exerted on the main body of a spacecraft by internal moving

parts. Internal moving parts include reaction wheels, flexible booms or solar arrays, scanning or rastering instruments, liquids inside partially filled tanks, and moving crew members. For the purposes of this study, internal torques will also include torques caused by the motion of mass along the surface of a spacecraft. This is an obvious extension because all internal torques on spacecraft are in a sense self-generated.

The effect of mass motion on the stability of spacecraft has been studied before. Research and experience have shown that disturbances due to mass motion are a function of the amplitude of the motion and the ratio of the moving mass to the spacecraft's moment of inertia. (Thomson, 1985: 1087) showed analytically that if crew members on a space station moved periodically, they could rock a station and cause it to tumble. In addition, (Chubb, 1975: 277) used flight data from Skylab to show that while crew members were jogging, the station experienced substantial angular deviation from its nominal attitude.

It should be pointed out, however, that the crew motion discussed in the previous articles was over small distances and that the ratios of the crew members' inertias to the space stations' moment of inertias were small. Research, therefore, is required to examine the movement of relatively large masses over large distances.

External Torques

External torques arise through the interaction of a vehicle with its environment. They include gravitational, aerodynamic, radiation, and magnetic torques. This study will concentrate specifically on the gravitational environmental torque.

The Earth's gravitational field is one of the dominant sources of attitude disturbance torques on a spacecraft in low-earth orbit. Any nonsymmetrical object of finite dimensions in orbit is subject to a gravitational torque because of the variation in the Earth's gravitational force over the object. This variation is caused by the inverse square gravitational force field that surrounds the earth. The result is a gravity-gradient torque which will try to align a spacecraft's minimum moment of inertia axis with the local vertical (radius vector drawn from center of the earth)(Wertz, 1985: 566).

The principle of gravity-gradient stabilization can be explained simply by considering the attitude motion of the dumbbell satellite in Fig. 1, where the orbital frame of reference is $\hat{o}_1$, $\hat{o}_2$, and $\hat{o}_3$ with the origin at the center of mass of the body, the axis $\hat{o}_1$ directed away from the center of the earth, axis $\hat{o}_2$ tangent to the orbit in the direction of motion, and axis $\hat{o}_3$ normal to the orbit plane. The body principal axes are represented by $\hat{b}_1$, $\hat{b}_2$, and $\hat{b}_3$. A deflection away from the local vertical causes a restoring

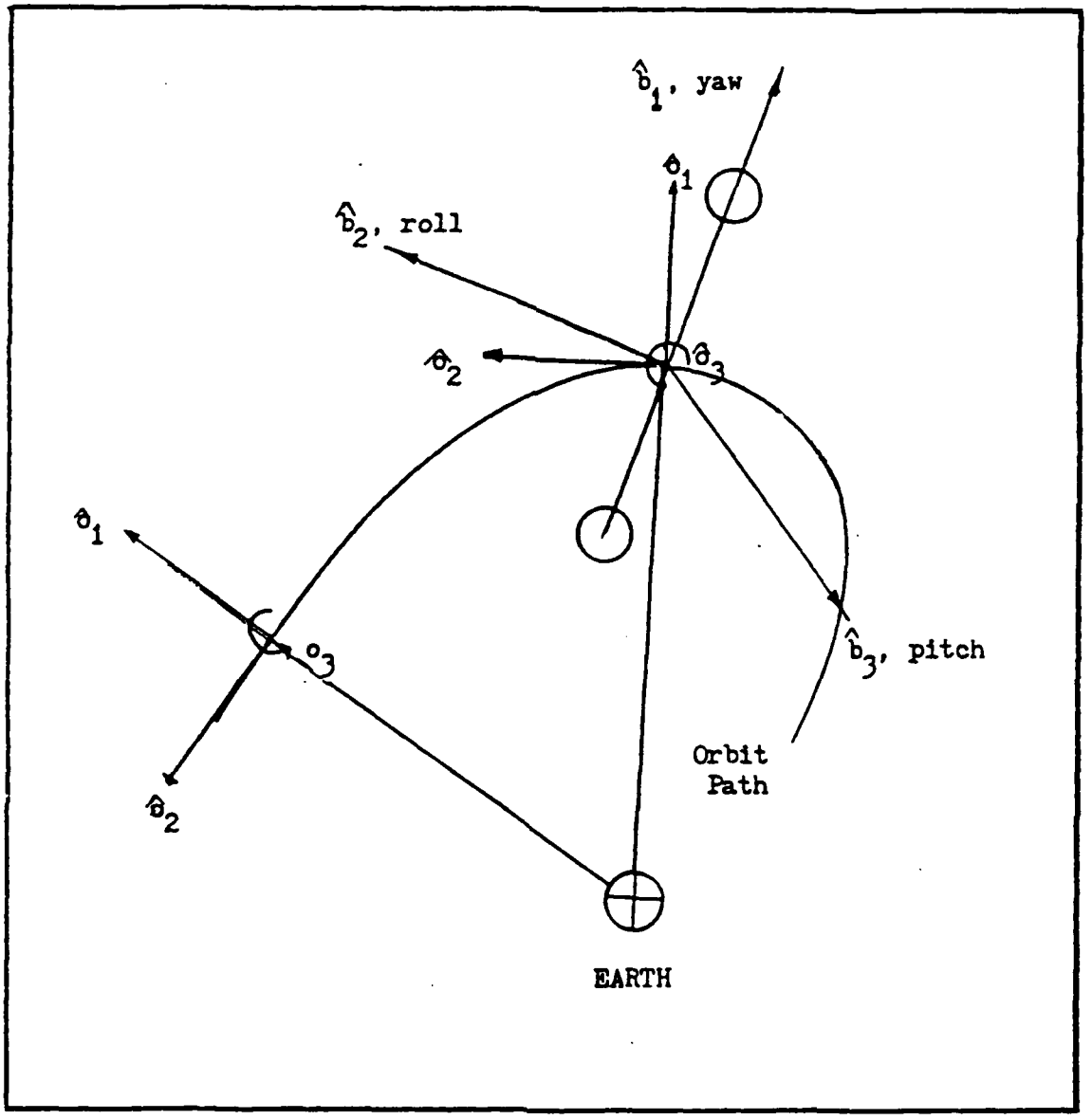

Fig. 1. Orbit and Body Axes

torque to be generated by the imbalance of forces acting on the spherical masses. The centrifugal force acting on the sphere furthest from the earth is greater than the gravitational force on it because these two forces are equal only at the center of mass. Since the oposite is true of the mass closet to the earth, a net torque is created which forces the masses toward a local vertical orientation (Kaplan, 1976: 199).

Gravity-gradient stabilization works not only for dumbbell satellites but for any spacecraft whose configuration lies within the regions shown in Fig. 2. For a rigid body in a circular orbit, the Lagrange region is statically stable whereas the Delp region is gyrically stable. Any inertia shape that lies outside of these regions would result in unstable motion. Moreover, when flexibility effects are considered with a quasi-rigid body, the Delp region loses its gyrically stable character while the Lagrange region becomes asymptotically three-axis stable (Hughes, 1986: 318). At the same time, Chan (20) points out that having mass motion along the body axis $\hat{b}_1$ (see Fig. 1) of a space station whose inertia shape is in the Delp region would correspond to mass motion along the shortest axis of the station inertia ellipsoid. Therefore, the Delp region will not be considered here.

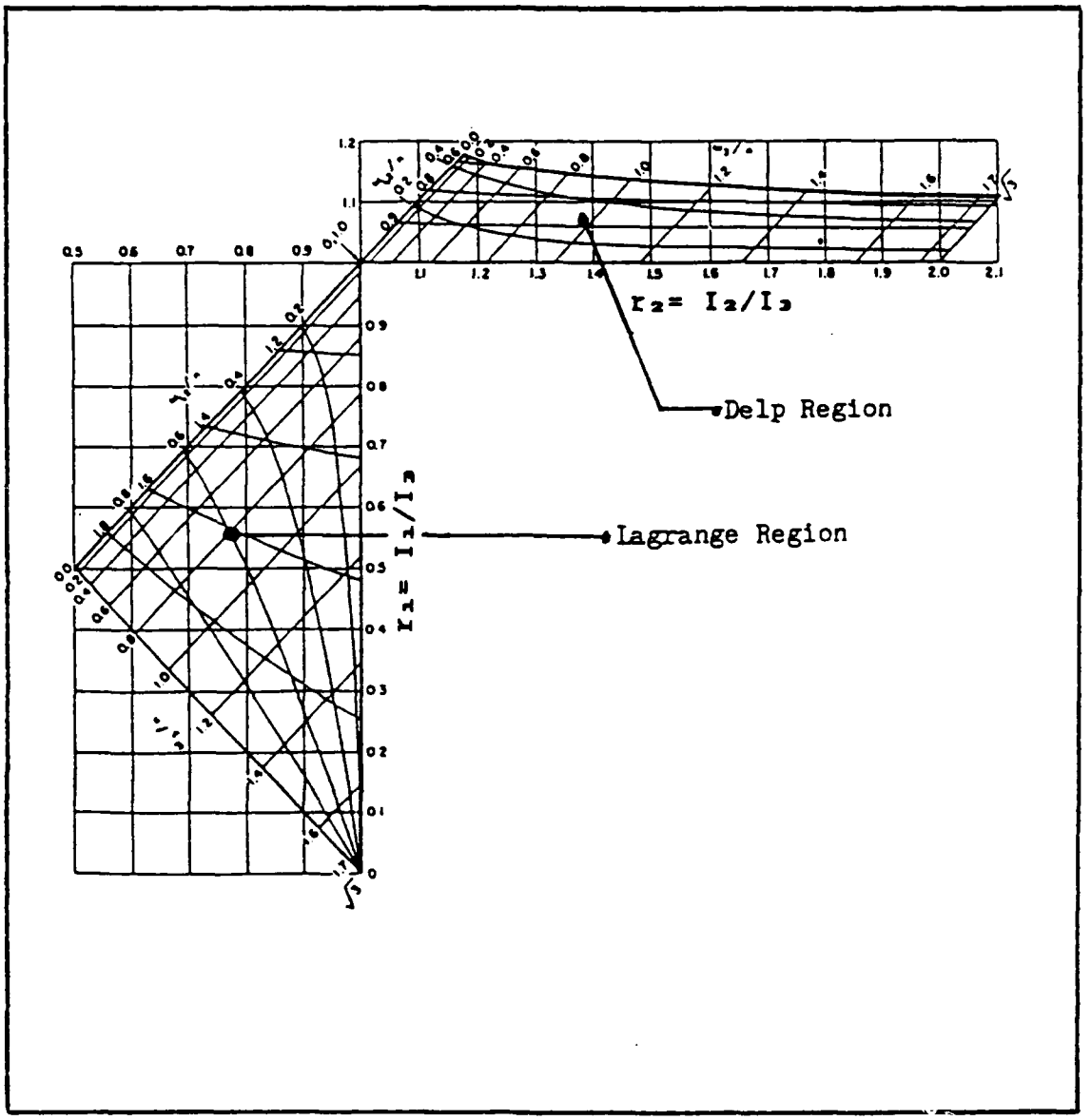

(Debra and Delp, 1961: 14)

Fig. 2.

Attitude Stability and Natural Frequencies of a Rigid Body in a Circular Orbit Plotted Versus r_1 and r_2

Analytical Methods

When an elevator that moves along the $\hat{b}_1$ axis is added to a dumbbell satellite (Fig. 3), the satellite will "bob" up and down along this axis in order to maintain the center of mass orbital path. If the satellite is deflected from the local vertical, however, periodic mass movement will exaggerate the torque caused by the gravity-gradient and result in large oscillations in the satellite's attitude. This phenomenon is known as parametric excitation and results when the coefficients of the equations of attitude motion vary periodically with time.

In an attempt to find an analytical solution for these equations, they must first be linearized. The results, detailed in Chapter IV, show linearized pitch, roll, and yaw equations where the roll and yaw equations are coupled. Many theories exist that determine the behavior of systems governed by linear ordinary differential equations with periodic coefficients. This study, however, will focus on Hill's equation and a generalized form of Hill's equation called Mathieu's equation that (Chan, 1986) used to conduct the pitch analysis. In addition, the Method of Multiple Scales is used to analyze the coupled roll/yaw equations.

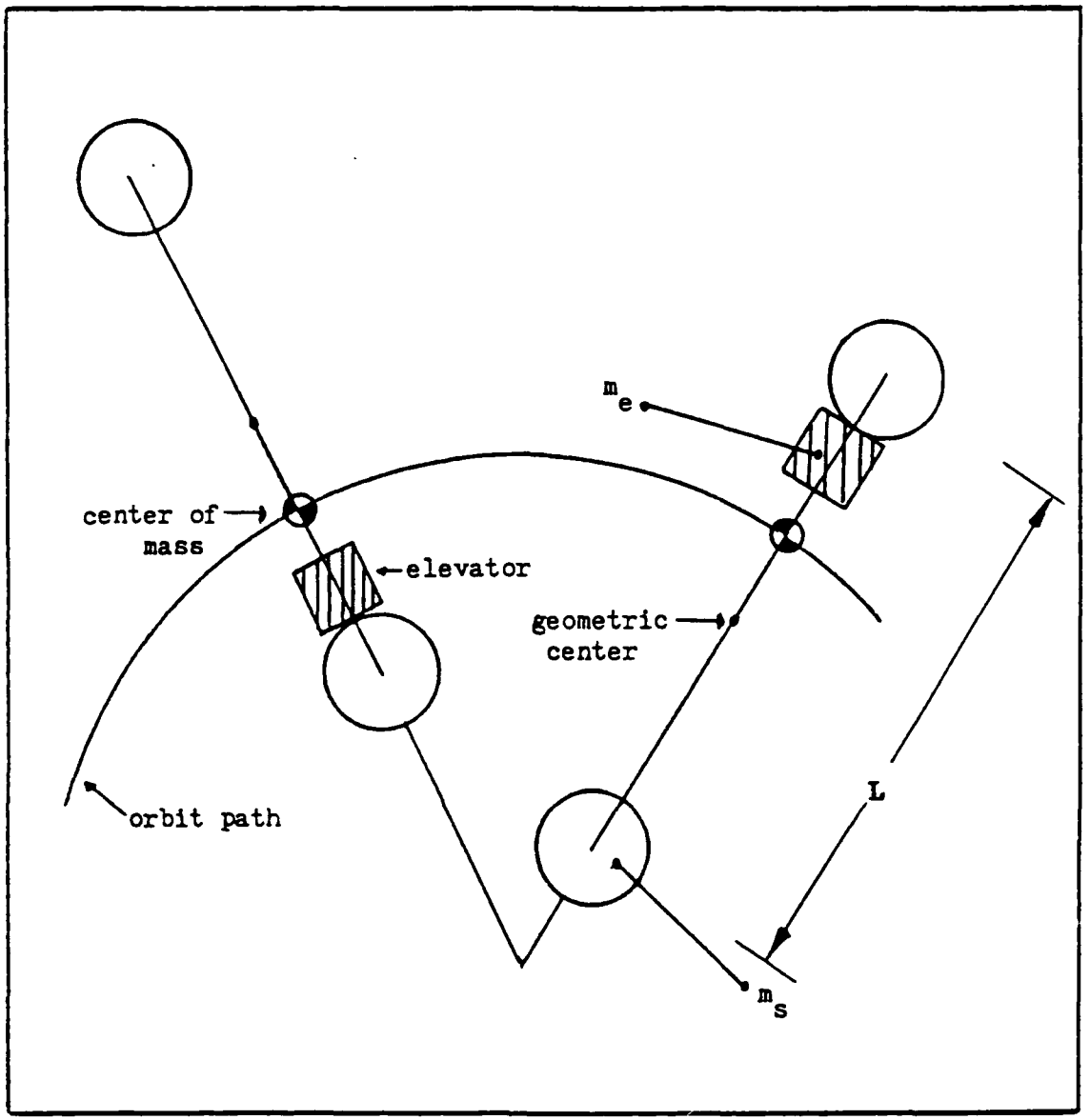

Fig. 3. Center of Mass - Dumbbell Configuration

III. Derivation of the Equations of Motion

The equations of attitude motion of a gravity-gradient stabilized spacecraft of arbitrary shape, for the conditions specified in Chapter I, are well known and can be seen in (Kaplan, 1976: 201). A difference occurs in this study, however, when a moving mass is added. This difference results in the principal moments of inertia of the spacecraft becoming a function of time.

The time varying moments of inertia were taken into account by (Chan, 1986) and resulted in three Euler moment equations

$$I_1\dot{w}_1 + \dot{I}_1 w_1 + (I_3 - I_2)w_2 w_3 = (3\mu/R^5)(I_3 - I_2)R_2 R_3 \qquad (1)$$

$$I_2\dot{w}_2 + \dot{I}_2 w_2 + (I_1 - I_3)w_3 w_1 = (3\mu/R^5)(I_1 - I_3)R_1 R_3 \qquad (2)$$

$$I_3\dot{w}_3 + \dot{I}_3 w_3 + (I_2 - I_1)w_1 w_2 = (3\mu/R^5)(I_2 - I_1)R_1 R_2 \qquad (3)$$

Eqs. (1), (2), and (3) differ from standard Euler equations for a gravity-gradient stabilized body (Kaplan, 1976: 201) because of the $\dot{I}w$ terms which permit the introduction of mass movement along an arbitrary axis. Their derivation is summarized below for completeness.

The formulation begins with an inverse square formulation of gravitational torques given in vector form by Wertz (567)

$$\underline{M} = (3\mu/R^5)\,[\underline{R} \times (I \cdot \underline{R})] \qquad (4)$$

where $\underline{R}$ is the radius vector from earth center to the mass center of the spacecraft, and μ=GM is the earth's gravitational constant. Since it is stated in Chapter I that there is no attitude/orbit coupling, Eq. (4) in body component form becomes

$$M_1 = (3\mu/R^5)[(I_3 - I_2)R_2R_3] \tag{5c}$$

$$M_2 = (3\mu/R^5)[(I_1 - I_3)R_1R_3] \tag{5b}$$

$$M_3 = (3\mu/R^5)[(I_2 - I_1)R_1R_2] \tag{5c}$$

Recall that the reaction of this gravity-gradient torque ($\underline{M}$) about a rigid body's center of mass is equal to the time rate of change of the body's angular momentum ($\underline{h}$) with respect to an inertial frame

$$\underline{M} = {}^{I}\frac{d}{dt}(\underline{h}) \quad . \tag{6}$$

Eq. (6) becomes

$$\underline{M} = {}^{B}\frac{d}{dt}[I\cdot{}^{I}\underline{w}^{B}] + {}^{I}\underline{w}^{B} \times [I\cdot{}^{I}\underline{w}^{B}] \tag{7}$$

since

$$\underline{h} = I\cdot{}^{I}\underline{w}^{B} \tag{8}$$

where I is the inertia dyadic of the space station and ${}^{I}\underline{w}^{B}$ is the angular velocity of the body frame with respect to the inertial frame.

Because the origin of the body reference frame b_i is located at the geometric center of the space station, mass motion will cause it to translate in space relative to the center of mass. Therefore, the first term in Eq. (7) becomes

$$\frac{{}^{B}d}{dt}[I\cdot{}^{I}\underline{w}^{B}] = I\cdot\frac{{}^{B}d}{dt}[{}^{I}\underline{w}^{B}] + {}^{I}\underline{w}^{B}\cdot\frac{{}^{B}d}{dt}[I] \tag{9a}$$

or in matrix form,

$$\frac{{}^{B}d}{dt}[I\cdot{}^{I}\underline{w}^{B}] = \begin{bmatrix} I_1 & 0 & 0 \\ 0 & I_2 & 0 \\ 0 & 0 & I_3 \end{bmatrix} \begin{Bmatrix} \dot{w}_1 \\ \dot{w}_2 \\ \dot{w}_3 \end{Bmatrix} + \begin{bmatrix} \dot{I}_1 & 0 & 0 \\ 0 & \dot{I}_2 & 0 \\ 0 & 0 & \dot{I}_3 \end{bmatrix} \begin{Bmatrix} w_1 \\ w_2 \\ w_3 \end{Bmatrix} \tag{9b}$$

$$= \begin{Bmatrix} I_1\dot{w}_1 + \dot{I}_1 w_1 \\ I_2\dot{w}_2 + \dot{I}_2 w_2 \\ I_3\dot{w}_3 + \dot{I}_3 w_3 \end{Bmatrix} \tag{9c}$$

In addition, the second term of Eq. (7) becomes

$${}^{I}\underline{w}^{B} \times [I\cdot{}^{I}\underline{w}^{B}] = \begin{vmatrix} \hat{b}_1 & \hat{b}_2 & \hat{b}_3 \\ w_1 & w_2 & w_3 \\ I_1w_1 & I_2w_2 & I_3w_3 \end{vmatrix} \tag{10a}$$

or

$${}^{I}\underline{w}^{B} \times [I\cdot{}^{I}\underline{w}^{B}] = \begin{Bmatrix} (I_3 - I_2)w_2w_3 \\ (I_1 - I_3)w_1w_3 \\ (I_2 - I_1)w_1w_2 \end{Bmatrix} \tag{10b}$$

Substituting Eqs. (5), (9c), and (10b) into Eq. (7) will yield Eqs. (1), (2), and (3).

As pointed out by (Chan, 1986: 6) the orientation of the body cannot be determined from Eqs. (1), (2), and (3). Therefore, relationships are needed between these Euler moment equations and angles specifying the orientation of the body. One way of doing this is with Euler angles.

The direction cosine matrix using a 3-1-2 sequence of rotations between the $\hat{o}$ frame and the $\hat{b}$ frame is

$$A_{312}(p,y,r) = A_2(r)\, A_1(y)\, A_3(p)$$

$$= \begin{bmatrix} crcp-sysrsp & crsp+sysrcp & -cysr \\ -cysp & cycp & sy \\ srcp+sycrsp & srsp-sycrcp & cycr \end{bmatrix} \qquad (11)$$

where the Euler angles p, y, and r represent

p ≡ pitch angle ≡ body rotation about $\hat{o}_3$

y ≡ yaw angle ≡ body rotation about $\hat{o}_1$

r ≡ roll angle ≡ body rotation about $\hat{o}_2$

and c = cosine and s = sine.

The expressions for the rotation angles in terms of the elements of the direction cosine matrix are

$$p = -\arctan\,(A_{21}/A_{22}) \qquad (12a)$$

$$y = \arcsin\,(A_{23}) \qquad (12b)$$

$$r = -\arctan\,(A_{13}/A_{33}) \qquad (12c)$$

The angular velocity of the body frame with respect to the orbit frame is

$$\begin{Bmatrix} {}^{O}w_1^B \\ {}^{O}w_2^B \\ {}^{O}w_3^B \end{Bmatrix} = \begin{Bmatrix} -\dot{p}\cos(y)\sin(r) + \dot{y}\cos(r) \\ \dot{p}\sin(y) + \dot{r} \\ \dot{p}\cos(y)\cos(r) + \dot{y}\sin(r) \end{Bmatrix} \quad (13)$$

Since we need the angular velocity of the body frame with respect to the inertial frame ${}^{I}\underline{w}^{B}$

$${}^{I}\underline{w}^{B} = {}^{I}\underline{w}^{O} + {}^{O}\underline{w}^{B} \quad (14)$$

where ${}^{I}\underline{w}^{O} = N\hat{o}_3$ (N = scalar eccentric orbital rate).

Therefore, Eq. (14) becomes

$$\begin{Bmatrix} w_1 \\ w_2 \\ w_3 \end{Bmatrix} = \begin{bmatrix} A_{11} & A_{12} & A_{13} \\ A_{21} & A_{22} & A_{23} \\ A_{31} & A_{32} & A_{33} \end{bmatrix} \begin{Bmatrix} 0 \\ 0 \\ N \end{Bmatrix} + \begin{Bmatrix} -\dot{p}\cos(y)\sin(r) + \dot{y}\cos(r) \\ \dot{p}\sin(y) + \dot{r} \\ \dot{p}\cos(y)\cos(r) + \dot{y}\sin(r) \end{Bmatrix} \quad (15)$$

or,

$$w_1 = A_{13}N - \dot{p}\cos(y)\sin(r) + \dot{y}\cos(r) \quad (16a)$$

$$w_2 = A_{23}N + \dot{p}\sin(y) + \dot{r} \quad (16b)$$

$$w_3 = A_{33}N + \dot{p}\cos(y)\cos(r) + \dot{y}\sin(r) \quad (16c)$$

The Euler angle rates can now be solved in terms of the angular velocity and Euler angles:

$$\dot{p} = [(w_3 - A_{33}N)\cos(r) - (w_1 - A_{13}N)\sin(r)]\sec(y) \quad (17a)$$

$$\dot{y} = (w_1 - A_{13}N)\cos(r) + (w_3 - A_{33}N)\sin(r) \quad (17b)$$

$$\dot{r} = -[(w_3 - A_{33}N)\cos(r) - (w_1 - A_{13}N)\sin(r)]\tan(y) + (w_2 - A_{23}N) \quad (17c)$$

A computer simulation of a gravity-gradient stabilized

space station with mass movement can now be generated by solving Eqs. (1), (2), and (3) simultaneously with Eqs. (17a), (17b), (17c) for given values of $\dot{I}$.

Although the geometric significance of Euler angles is more apparent, computationally they are not as efficient as Euler's symmetric parameters q_1, q_2, q_3, and q_4. Appendix A details how Euler symmetric parameters (known as quaternions) are used instead of Eqs. (17) in the nonlinear program of this study.

IV. Linearization

The $\dot{I}w$ terms in the Euler moment Eqs. (1), (2), and (3) of Chapter III permit the introduction of mass movement along an arbitrary axis. If a trolley apparatus is constrained to move along the body axis ($\hat{b}_1$), then the term $\dot{I}_1$ vanishes. This leaves us with

$$I_1\dot{w}_1 + (I_3 - I_2)w_2w_3 = (3\mu/R^5)\,(I_3 - I_2)R_2R_3 \qquad (18a)$$

$$I_2\dot{w}_2 + \dot{I}_2w_2 + (I_1 - I_3)w_3w_1 = (3\mu/R^5)\,(I_1 - I_3)R_3R_1 \qquad (18b)$$

$$I_3\dot{w}_3 + \dot{I}_3w_3 + (I_2 - I_1)w_1w_2 = (3\mu/R^5)\,(I_2 - I_1)R_1R_2 \qquad (18c)$$

For small p, y, and r, the direction cosine matrix becomes

$$A\,(p,y,r) = \begin{bmatrix} 1 & p & -r \\ -p & 1 & y \\ r & -y & 1 \end{bmatrix} \qquad (19)$$

In order to get the components of the radius vector $\underline{R}$, we can write

$$\begin{Bmatrix} R_1 \\ R_2 \\ R_3 \end{Bmatrix} = \begin{bmatrix} 1 & p & -r \\ -p & 1 & y \\ r & -y & 1 \end{bmatrix} \begin{Bmatrix} R \\ 0 \\ 0 \end{Bmatrix} \qquad (20)$$

or,

$$\begin{Bmatrix} R_1 \\ R_2 \\ R_3 \end{Bmatrix} = \begin{Bmatrix} R \\ -Rp \\ Rr \end{Bmatrix} \qquad (21)$$

In addition, the angular velocity of the orbit frame with

respect to the inertial frame ${}^{I}\underline{w}^{O}$ can be written as

$$ {}^{I}\underline{w}^{O} = \begin{bmatrix} 1 & p & -r \\ -p & 1 & y \\ r & -y & 1 \end{bmatrix} \begin{Bmatrix} 0 \\ 0 \\ N \end{Bmatrix} = \begin{Bmatrix} -rN \\ yN \\ N \end{Bmatrix} \tag{22} $$

where $\underline{N} = N\hat{o}_3$ is the orbital rate.

Since the angular velocity of the body frame with respect to the orbital frame ${}^{O}\underline{w}^{B}$ can be expressed as

$$ {}^{O}\underline{w}^{B} = \dot{y}\hat{b}_1 + \dot{r}\hat{b}_2 + \dot{p}\hat{b}_3 \tag{23} $$

${}^{I}\underline{w}^{B}$ becomes

$$ w_1 = -rN + \dot{y} \tag{24a} $$

$$ w_2 = yN + \dot{r} \tag{24b} $$

$$ w_3 = N + \dot{p} \tag{24c} $$

Differentiating Eqs. (24) with respect to time in the body frame to obtain

$$ \dot{w}_1 = \ddot{y} - (\dot{r}N + r\dot{N}) \tag{25a} $$

$$ \dot{w}_2 = \ddot{r} + (\dot{y}N + y\dot{N}) \tag{25b} $$

$$ \dot{w}_3 = \ddot{p} + \dot{N} \tag{25c} $$

For small orbit eccentricity e, let N and R be approximated by

$$ N = n\,[1 + 2e\cos(nt_p)] \tag{26} $$

$$ R = a\,[1 - e\cos(nt_p)] \tag{27} $$

where $n = (\mu/a^3)^{.5}$ is the mean motion, and t_p is the time since periapsis passage. Differentiating Eq. (26) with respect to time leads to

$$\dot{N} = -2n^2 e\sin(nt_p) \tag{28}$$

After substituting Eqs. (21), (24), and (25) into Eqs. (18), the Euler Moment equations become

$$I_1(\ddot{y}-\dot{r}N-\dot{N}r)+(I_3-I_2)(\dot{r}+yN)(\dot{p}+N)=(3\mu/R^5)(I_3-I_2)(-pR)(rR) \tag{29}$$

$$I_2(\ddot{r}+\dot{y}N+\dot{N}y)+\dot{I}_2(\dot{r}+yN)+(I_1-I_3)(\dot{p}+N)(\dot{y}-rN) = (3\mu/R^5)(I_1-I_3)(rR)(R) \tag{30}$$

$$I_3(\ddot{p}+\dot{N})+\dot{I}_3(\dot{p}+N)+(I_2-I_1)(\dot{y}-rN)(\dot{r}+yN) = (3\mu/R^5)(I_2-I_1)(R)(-pR) \tag{31}$$

Substitute N and $\dot{N}$ from Eqs (26) and (28) into the above equations and delete the products of quantities assumed to be small, such as $\dot{p}y$ and pe. Finally, substitute μ/R^3 for N^2 and Eqs. (29), (30), and (31) become

$$I_1\ddot{y} + (I_3-I_2-I_1)n\dot{r} + (I_3-I_2)n^2 y = 0 \tag{32}$$

$$I_2\ddot{r} + (I_2+I_1-I_3)n\dot{y} - 4(I_1-I_3)n^2 r + \dot{I}_2(\dot{r}+yn) = 0 \tag{33}$$

$$I_3[\ddot{p}-2n^2 e\sin(nt_p)] + 3n^2(I_2-I_1)p + \dot{I}_3(\dot{p}+n) = 0 \tag{34}$$

It should be noted that the pitch equation, Eq. (34), is uncoupled from the coupled yaw and roll equations, Eqs. (32) and (33). In addition, as stated in (Chan, 1986: 13), these equations are nearly identical to those derived by Kaplan (204) for a gravity-gradient stabilized rigid body. The only difference is the existence of the $\dot{I}$ terms due to mass motion.

V. Pitch Analysis

The objective of this chapter is to obtain an analytical solution to the linearized pitch equation using Hill's Method. The results are compared to those obtained using Mathieu's equation (Chan, 1986) and to the numerical solutions of the nonlinear system.

The previous work done by Chan on this subject used Mathieu's equation to determine the inertia shapes in the Lagrange stability region that would not remain stable when the system was parametrically excited by mass movement. This chapter begins by reviewing the theory and derivations that lead to the use of Mathieu's and Hill's equations and then recaps the results Chan realized. The remaining work concentrates on using Hill's equation to find unstable configurations and comparing the results to those of (Chan, 1986).

Theory/Derivations

The pitch equation was shown to be decoupled from the roll and yaw equations in the previous chapter. After rearranging Eq. (34)

$$\ddot{p} + \left(\frac{\dot{I}_3}{I_3}\right)\dot{p} + 3n^2\left(\frac{I_2 - I_1}{I_3}\right)p + \left(\frac{\dot{I}_3}{I_3}\right)n = 2n^2 e\sin(nt_p) \qquad (35)$$

we should note that what is left is a linear ordinary differential equation of the form

$$\ddot{p} + 2P(t)\dot{p} + R^2(t)p = Q(t) \tag{36}$$

where the coefficients are time varying and defined as follows:

$$P(t) = .5\ (\dot{I}_3 / I_3) \tag{37}$$

$$R^2(t) = 3n^2[(I_2 - I_1)/ I_3] \tag{38}$$

$$Q(t) = -(\dot{I}_3 / I_3)n + 2n^2 e\sin(t_p) \tag{39}$$

By introducing the variable transformation

$$p = z\ e^{-\int P(t)dt} \tag{40}$$

Chan (15) showed that Eq. (36) becomes

$$\ddot{z} + [R^2 - P^2 - \dot{P}]z = Qe^{\int Pdt} \tag{41}$$

In addition, if the mass motion is chosen to be sinusoidal, then the coefficient of z is a periodic function of time and can be expanded to

$$[R^2 - P^2 - \dot{P}] = [a_T + 16q_1\cos 2T + 16q_2\cos 4T + 16q_3\cos 6T + 16q_4\cos 8T] \tag{42}$$

where Appendix B details this expansion as well as demonstrates that the final form of the transformed, homogeneous pitch equation is that of Hill's equation

$$\ddot{z} + [\theta_0 + 2\sum_{i=1}^{4} \theta_i \cos(2iT)]z = 0 \tag{43}$$

where $\theta_0 = a_T$ and $\theta_i = 8q_i$.

The general solution to Hill's equation is

$$z = c_1 e^{\mu T}\phi\ (T,\sigma) + c_2 e^{-\mu T}\phi\ (T,-\sigma) \tag{44}$$

where the stability of the system will be determined by the

characteristic exponent μ (Hayashi, 1964: 341). Meirovitch (282) shows that the determination of μ is not an easy matter. However, since μ depends on the parameters θ_0 and θ_1, it is possible to represent solutions to Eq. (44) by a parameter space defined by these quantities. Meirovitch (282) states that "the parameter space can be divided into regions of bounded and unbounded motions with periodic motions providing the surfaces separating these regions." If the parameter space, however, is truncated to the two parameters θ_0 and θ_1, the boundary surfaces become boundary curves. This lead Chan (18) to use a specialized form of Hill's equation called Mathieu's equation

$$\ddot{z} + (a_T + 16q_1\cos 2T)z = 0 \qquad (45)$$

to determine the stability of the pitch equation. The result is Fig. 4, which shows regions of bounded and unbounded motion as a function of the parameters a_T and q_1. This type of representation is referred to as a Strutt diagram.

Summary of Previous Results

In order to simplify the analysis, Chan needed to determine which regions of instability are of concern. Appendix B shows that the parameters a_T and q_1 are a function of the variables r_0, r_1, r_2 and (n/ω) where they are defined as $r_0 = \frac{ML^2}{4I_{03}}$, $r_1 = \frac{I_{01}}{I_{03}}$, $r_2 = \frac{I_{02}}{I_{03}}$, n = circular

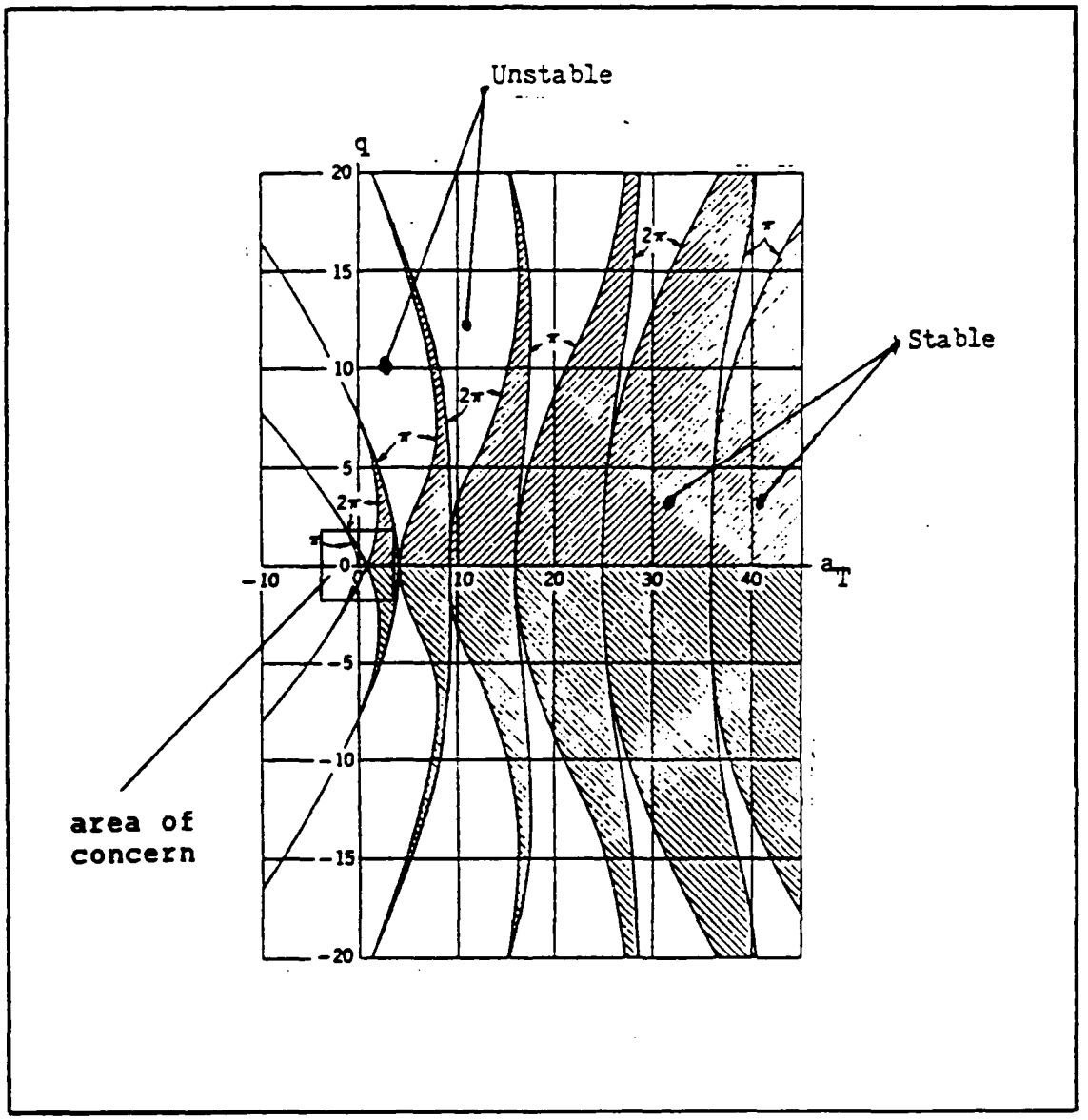

(Meirovitch, 1970: 286)

Fig. 4. Strutt Diagram

orbital frequency, and ω = mass (trolley) motion frequency. The stability of the solution to Eq. (45) will therefore depend on the station's inertia shape (r_1, r_2), orbit rate to mass motion frequency ratio (n/ω), and the ratio of effective trolley inertia to pitch inertia r_0. Since this study is only concerned with inertia parameters(r_1, r_2) that lie in the classical Lagrange region and because a_T and q_1 are a function of r_1 and r_2, Chan (19) mapped the Lagrange inertia region (Fig. 2) into the Strutt diagram (Fig. 4). The result is a polygon shape where, for a single r_0 value, the Lagrange region that is triangular in r_1-r_2 space maps into a line segment in the a_T-q_1 space (see Fig. 5). Because a point in the two-dimensional a_T-q_1 plane will transform into a line segment in the r_1-r_2 plane, Figs. 6 and 7 show how it is easy to determine unstable space station configurations. In Fig. 6, at r_0=.25, points 2 and 8 represent what Chan (22) calls "fence posts" enclosing points of instability. The lines in Fig. 7 that correspond to those points are the boundaries that define the approximate zone of instability. Any space station with a r_1-r_2 combination that falls within this zone will be theoretically unstable in pitch. In addition, as r_0 decreases, the number of points enclosed by the "fence posts" decreases. Therefore, the width of the instability zone in the r_1-r_2 plane would also decrease.

Each of the diagrams shown, have r_0 values ranging from

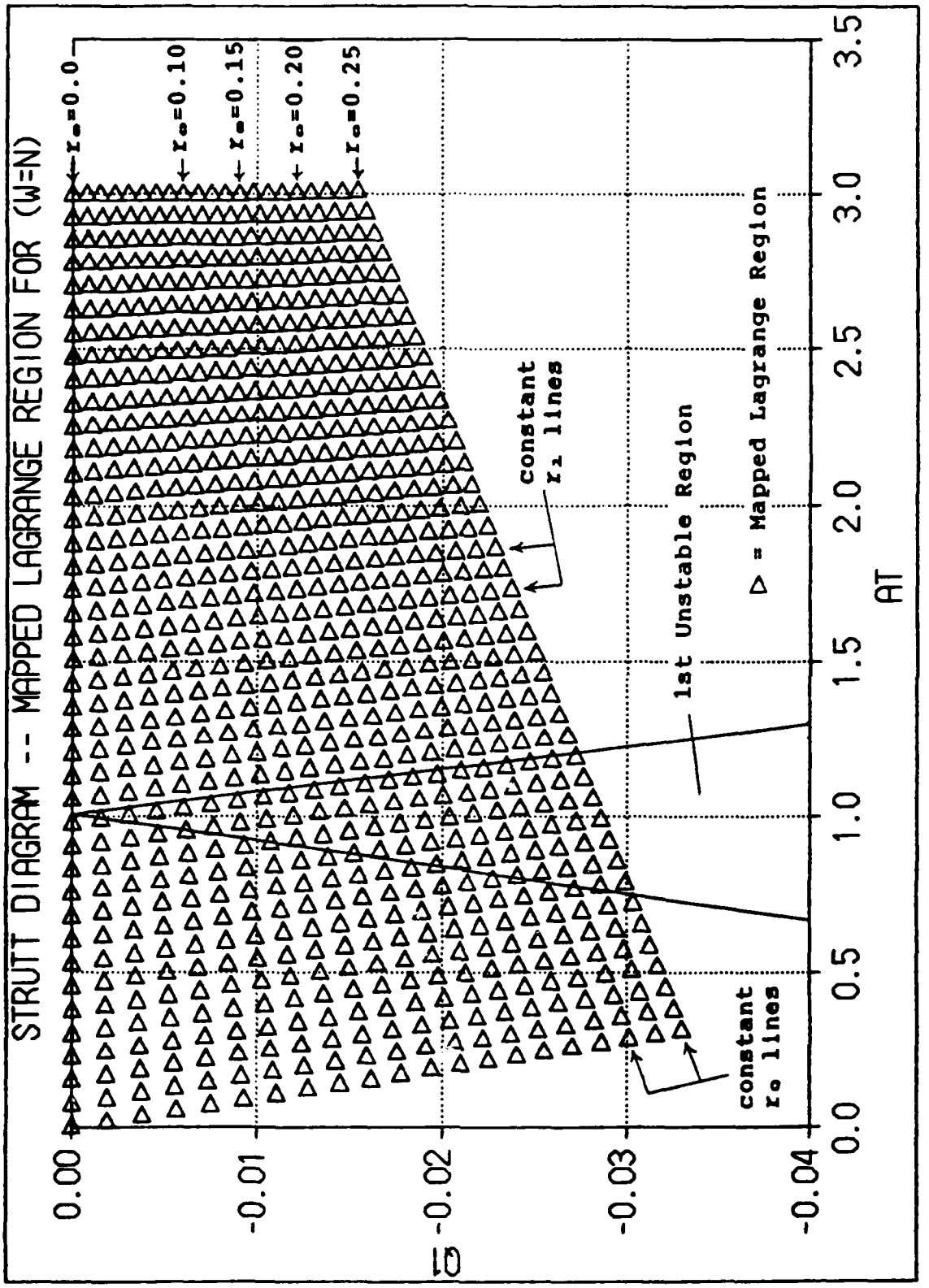

Fig. 5. Strutt Diagram With Mapped Lagrange Region For (w=n)

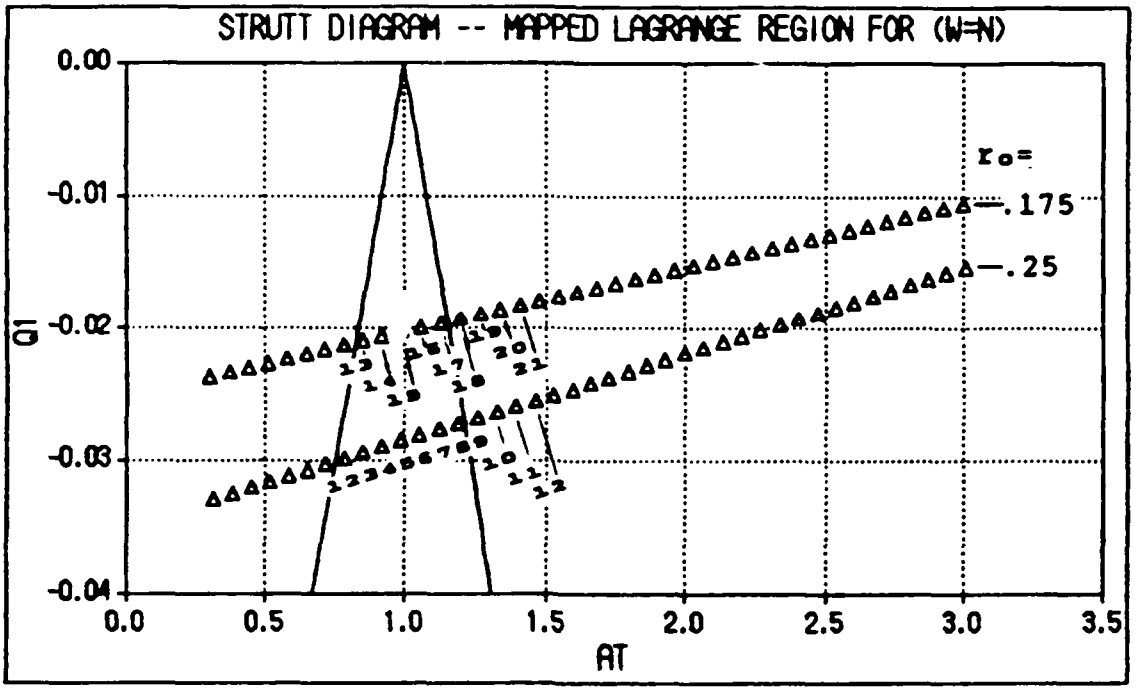

Fig. 6. Enclosed Points of Instability

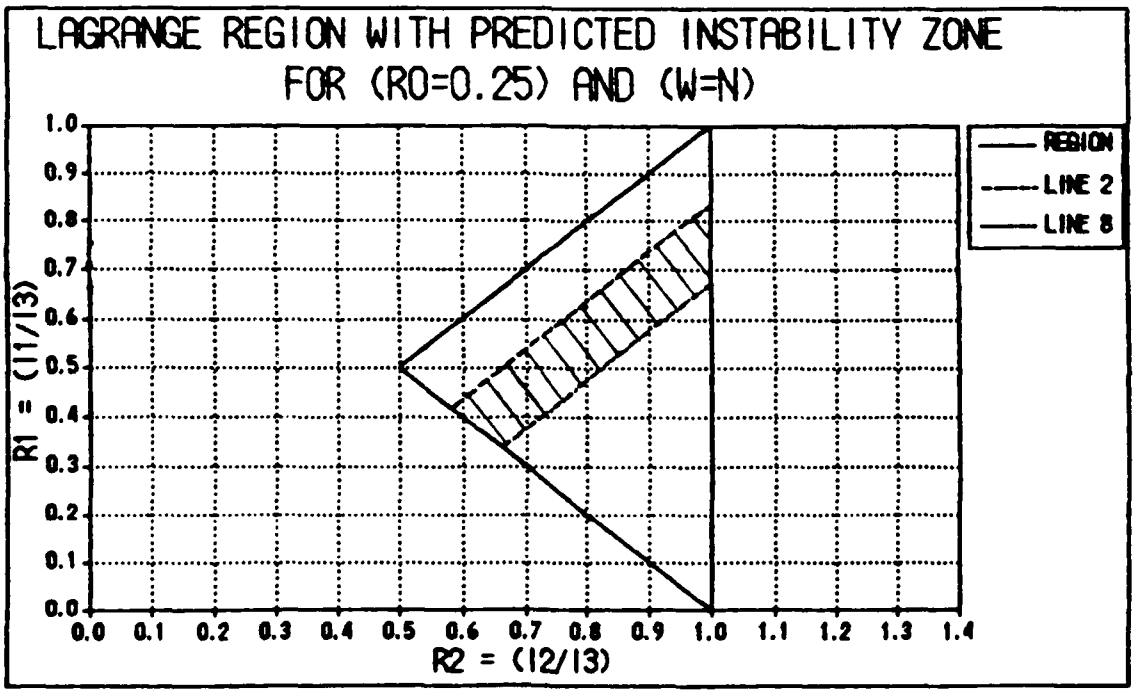

Fig. 7. Points of Instability Mapped Into r_1-r_2 Space

0 to .25. The lower limit $r_0 = 0$ denotes a null trolley mass. The chosen upper limit $r_0 = .25$ corresponds to the elevator mass being equal to a single sphere mass of a dumbbell configuration space station. In addition, each diagram corresponds to a fixed trolley frequency (ω) where $n \leq \omega \leq$ [illegible]. The lower limit, $\omega = n$ (trolley frequency = orbital rate), sets a reasonable lower bound on trolley speed.

By mapping the Lagrange region onto a Strutt diagram, (Chan, 1986) showed that when ω was at the lower limit only a small part of the first unstable region was of concern (see Fig. 8). But when ω is increased, even that region becomes of no concern. Fig. 9 shows that as ω increases, the mapped Lagrange region moves towards the origin of the Strutt diagram and away from the first unstable region. As this occurs, the "fence posts" no longer have any points to enclose. It is from this analysis that Chan (22) states that if ω is greater than 1.8 times the orbital rate, then all space station configurations are stable in pitch when mass motion is along the yaw axis $\hat{b}_1$.

The validity of this argument comes into question, however, when recalling the derivation in Appendix B where the pitch equation is written as

$$\ddot{z} + [a_T + 16q_1\cos 2T + 16q_2\cos 4T + 16q_3\cos 6T + 16q_4\cos 8T]z = 0 \qquad (46)$$

When (Chan, 1986) used Mathieu's equation to determine pitch

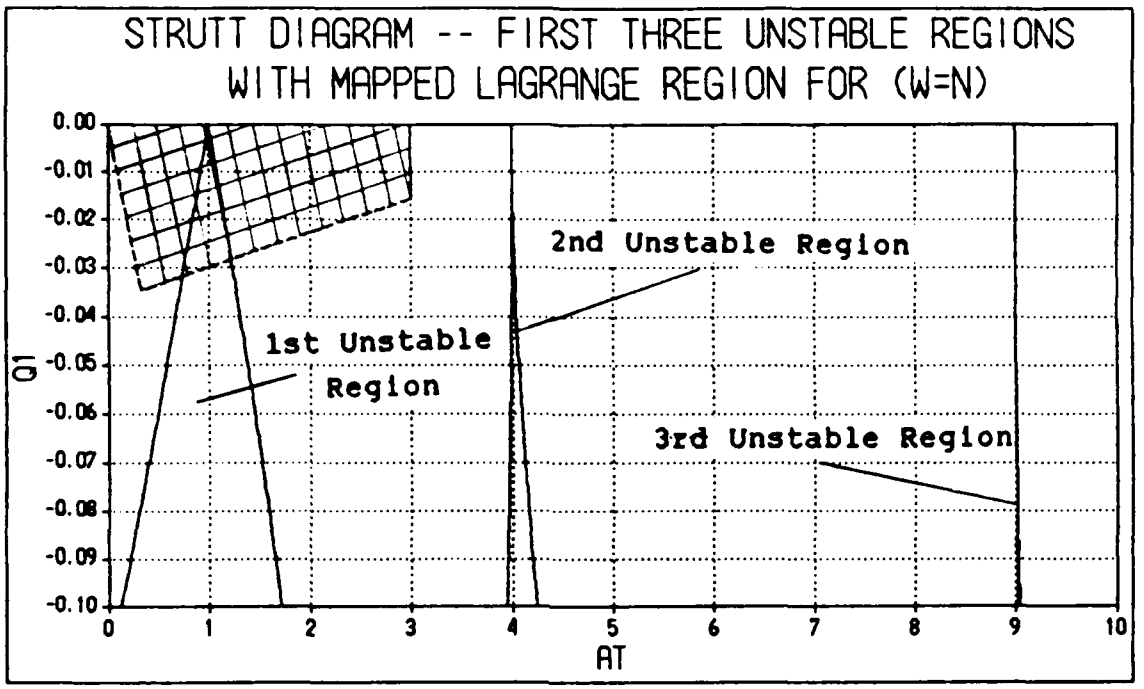

Fig. 8. Overlap of Mapped Lagrange Region With Unstable Regions From Strutt Diagram

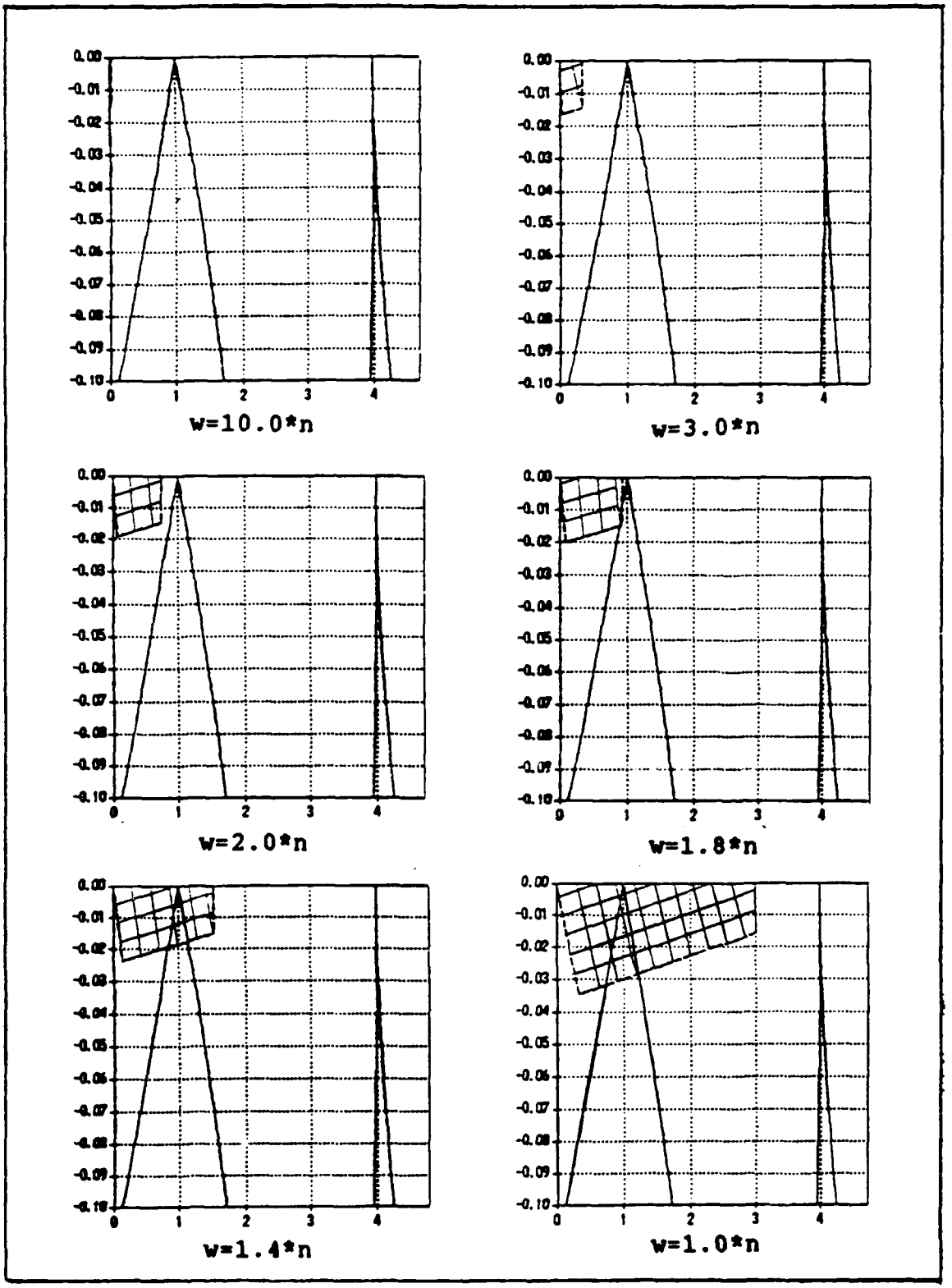

Fig. 9. Migration of Mapped Lagrange Region With Variation of w

stability of the system, he essentially ignored the q_2, q_3, and q_4 terms that are present in the Hill's equation. Chan (19) used the fact that both the Hill and Mathieu equations are linear to state that each q_i term can be examined independently. As a result, Chan (21) makes a reasonable statement that the q_3 and q_4 terms can be ignored since they are not functions of r_1 or r_2 and because they are small (on the order of $\times 10^{-4}$). At this point, however, Chan (21) states that since q_2 is also a function of the variables r_0, r_1, r_2, and (n/ω), a Strutt diagram can be developed in the a_T-q_2 plane (see Fig. 10). Chan (21) goes on to say that due to the location of the mapped Lagrange region to the horizontal axis, no additional unstable configurations are added to those obtained from the Strutt diagram in the a_T-q_1 plane. As a result, Chan (21) also drops the q_2 term.

Conducting the pitch analysis by using the full pitch equation (all q_i terms) demonstrates that the preceding arguments are not totally valid. The next section, detailing Hill's method, shows how the zones of instability for specific r_0 and ω values in the r_1-r_2 plane are different than those predicted by Mathieu Theory.

Hill's Equation

Determining the boundaries of the instability zones using Hill's equation is quite different from the methods used by (Chan, 1986). The main difference is that a Strutt

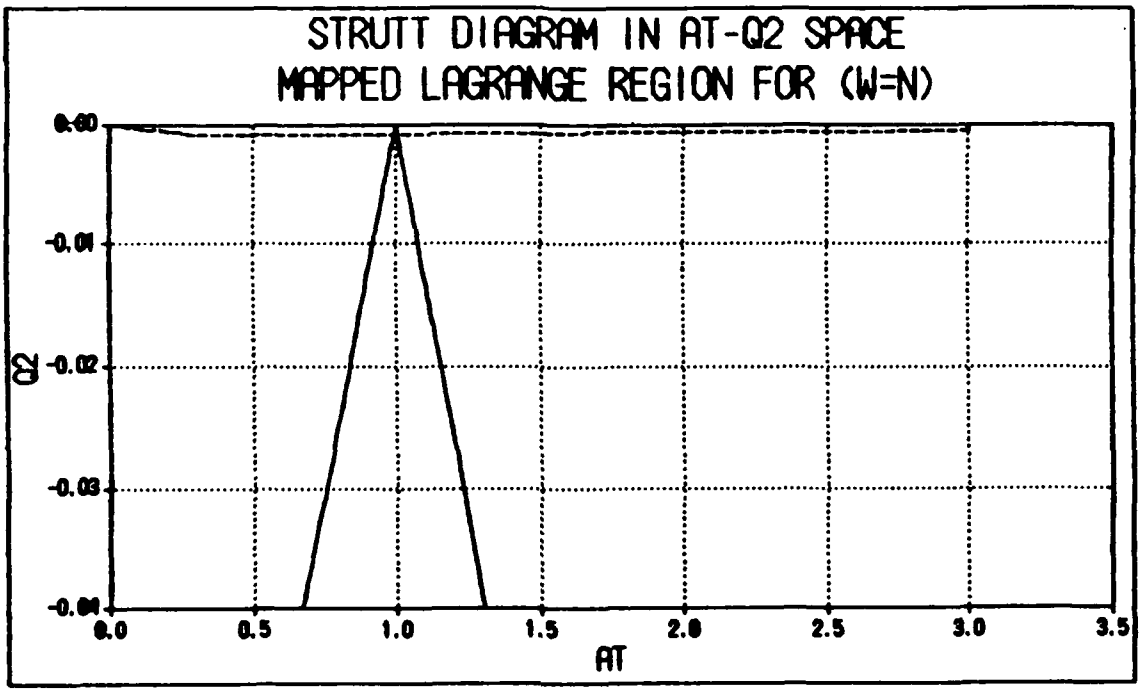

Fig. 10. Strutt Diagram in A_T-Q_2 Space With Mapped Lagrange Region For (w=n)

diagram can no longer be used to determine which space station configurations result in unbounded solutions to the pitch equation. The reason for this, discussed in the theory section, is that the parameter space representing bounded and unbounded solutions would be in several dimensions. Fortunately, Hill's equation is a well studied differential equation with solutions defined by (Hayashi, 1964:341).

For the unbounded solution corresponding to the first Mathieu unstable region, the characteristic exponent μ, shown in Eq. (44), is given by

$$\mu = \frac{1}{2}\theta_1\sin(2\sigma) + \frac{1}{8}\theta_1\theta_2\sin(2\sigma) + \frac{1}{24}\theta_2\theta_3\sin(2\sigma) - \frac{3}{128}\theta_1^3\sin(2\sigma) + \frac{1}{28}\theta_1^2\theta_2\sin(4\sigma) + \frac{5}{384}\theta_1^2\theta_3\sin(2\sigma) + \frac{7}{288}\theta_1\theta_2^2\sin(2\sigma) + \frac{17}{4608}\theta_1\theta_3^2\sin(2\sigma) + \frac{1}{96}\theta_2^3\theta_3\sin(2\sigma) + \frac{1}{1152}\theta_1\theta_2\theta_3\sin(4\sigma) + \cdots\cdots \quad (47)$$

in which the parameter σ is determined by

$$\theta_0 = K3 + K1\cos(2\sigma) + K2\cos(4\sigma) \quad (48a)$$

where

$$K1 = \theta_1 + \frac{1}{4}\theta_1\theta_2 + \frac{1}{12}\theta_2\theta_3 - \frac{1}{64}\theta_1^3 + \frac{5}{192}\theta_1^2\theta_3 - \frac{1}{144}\theta_1\theta_2^2 - \frac{1}{2304}\theta_1\theta_3^2 + \frac{1}{48}\theta_2^2\theta_3 \quad (48b)$$

$$K2 = \frac{1}{8}\theta_1^2 + \frac{5}{64}\theta_1^2\theta_2 + \frac{13}{576}\theta_1\theta_2\theta_3 \quad (48c)$$

$$K3 = 1 - \frac{1}{4}\theta_1^2 - \frac{1}{6}\theta_2^2 - \frac{1}{16}\theta_3^2 - \frac{11}{192}\theta_1^2\theta_2 - \frac{13}{192}\theta_1\theta_2\theta_3 \quad (48d)$$

and where $\theta_0 = a_T$ and $\theta_i = 8q_i$.

The task of finding the instability zones

initially appears to be quite complicated. However, the boundaries between stable and unstable solutions are defined by only two cases: (1) $\mu = 0$, $\sigma = 0^0$, and (2) $\mu = 0$, $\sigma = -90^0$. Substitution of these σ values into Eq. (48a) yields

$$\theta_0 = K3 + K1 + K2 \qquad (\text{for } \sigma = 0^0) \qquad (49a)$$

$$\theta_0 = K3 - K1 + K2 \qquad (\text{for } \sigma = -90^0) \qquad (49b)$$

Since θ_0, K1, K2, and K3 are a function of a_T and q_i, and the values of a_T and q_i are a function of r_1 and r_2, the boundaries of the instability zone in the r_1-r_2 plane are defined by r_1, r_2 combinations that satisfy Eqs. (49a) and (49b) for a given r_0 and ω.

Hayashi (342) goes on to define the unbounded solutions for other unstable regions, but they lie outside our area of interest and are not included in this analysis. Therefore, a comparison now can be made with the results of Mathieu's equation and to the nonlinear program.

Results/Observations

This section compares the analytical results generated by Mathieu's and Hill's equations with the numerical results generated by the computer code shown in Appendix D. Each of the methods are compared at mass motion frequencies (ω) ranging from 1.0*n to 2.0*n. In addition, at each ω, the methods will be compared at two r_0 values.

For comparison purposes, the test case run by the nonlinear code is the same case used by (Chan, 1986). A low

earth orbit of 150 km was used which yielded a circular orbit rate n = .001197 sec^{-1} and a period of 5250 seconds. All data points were run for a period of 1000 orbits, although unstable motion usually appeared by 100 orbits. Only at points close to the boundary between stable and unstable motion when μ is small did the simulation take more than 500 orbits, as would be expected, to go unstable. Examples of the output generated by the computer code for some of the data points shown if Fig. 6 are shown in Figs. 11 and 12. Each figure shows the progression from stable motion to unstable and then back to stable as r_1 is varied along a constant r_0 line. The fact that is evident from these figures is that the points predicted by the computer code to mark the beginning and end of unstable motion do not match the prediction by Mathieu's equation. This observation is illustrated more fully in the comparisons discussed next.

The following eight cases detail the comparison of each method as ω and r_0 vary: (1) $\omega = 1.0*n$, (r_0=.25, r_0=.175); (2) $\omega = 1.2*n$, (r_0=.25, r_0=.175); (3) $\omega = 1.4*n$, (r_0=.25, r_0=.20); (4) $\omega = 1.8*n$, (r_0=.25, r_0=.20). These cases are illustrated in r_1-r_2 space in Figs. (13) through (20).

Fig. 13 shows three predicted instability zones mapped into the classical Lagrange stability region. What is noticeable is that the Hill's analytical prediction falls within the Mathieu predicted instability zone. In

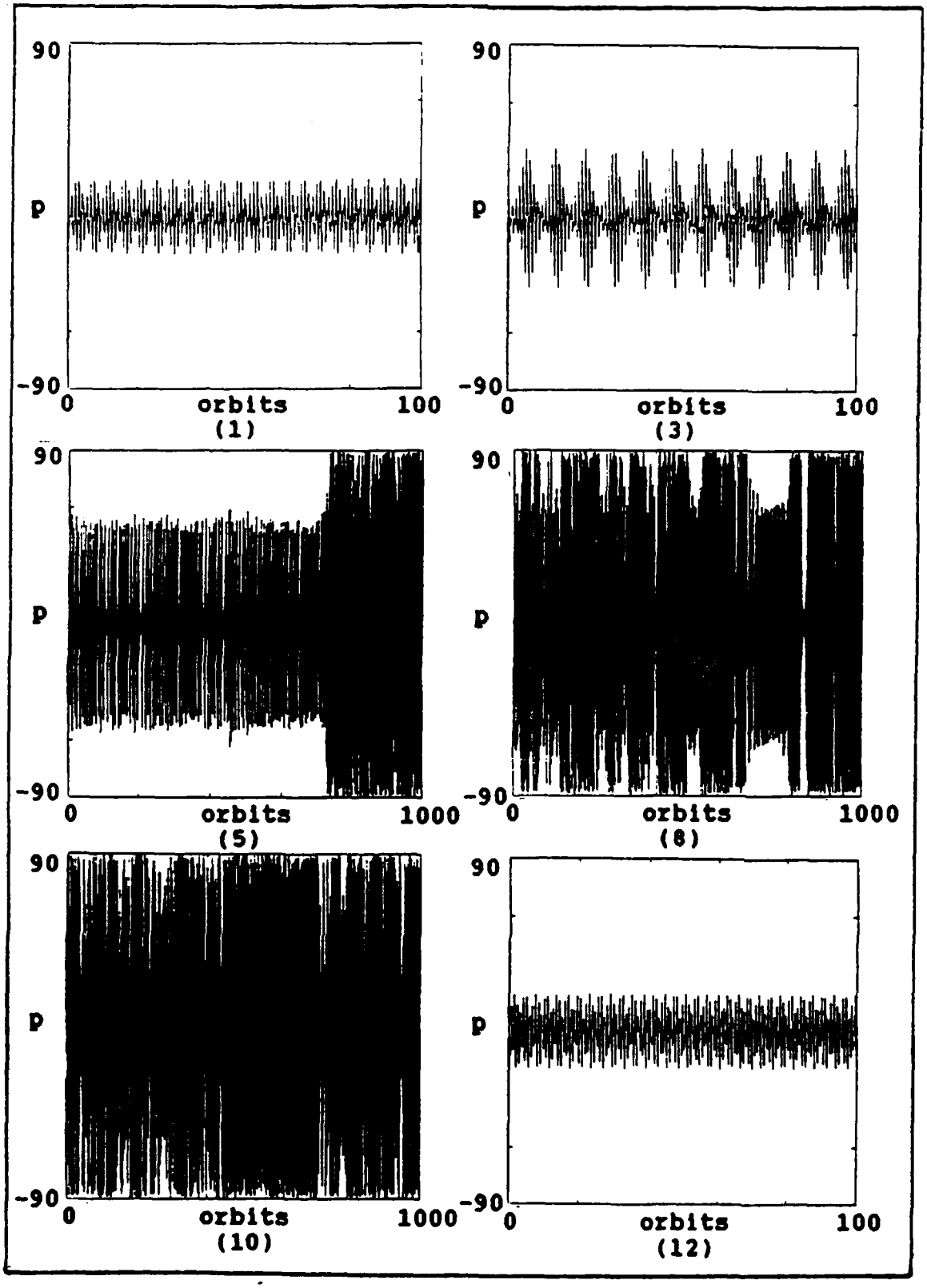

Fig. 11. Computer Runs (w=n, r_o=0.25)

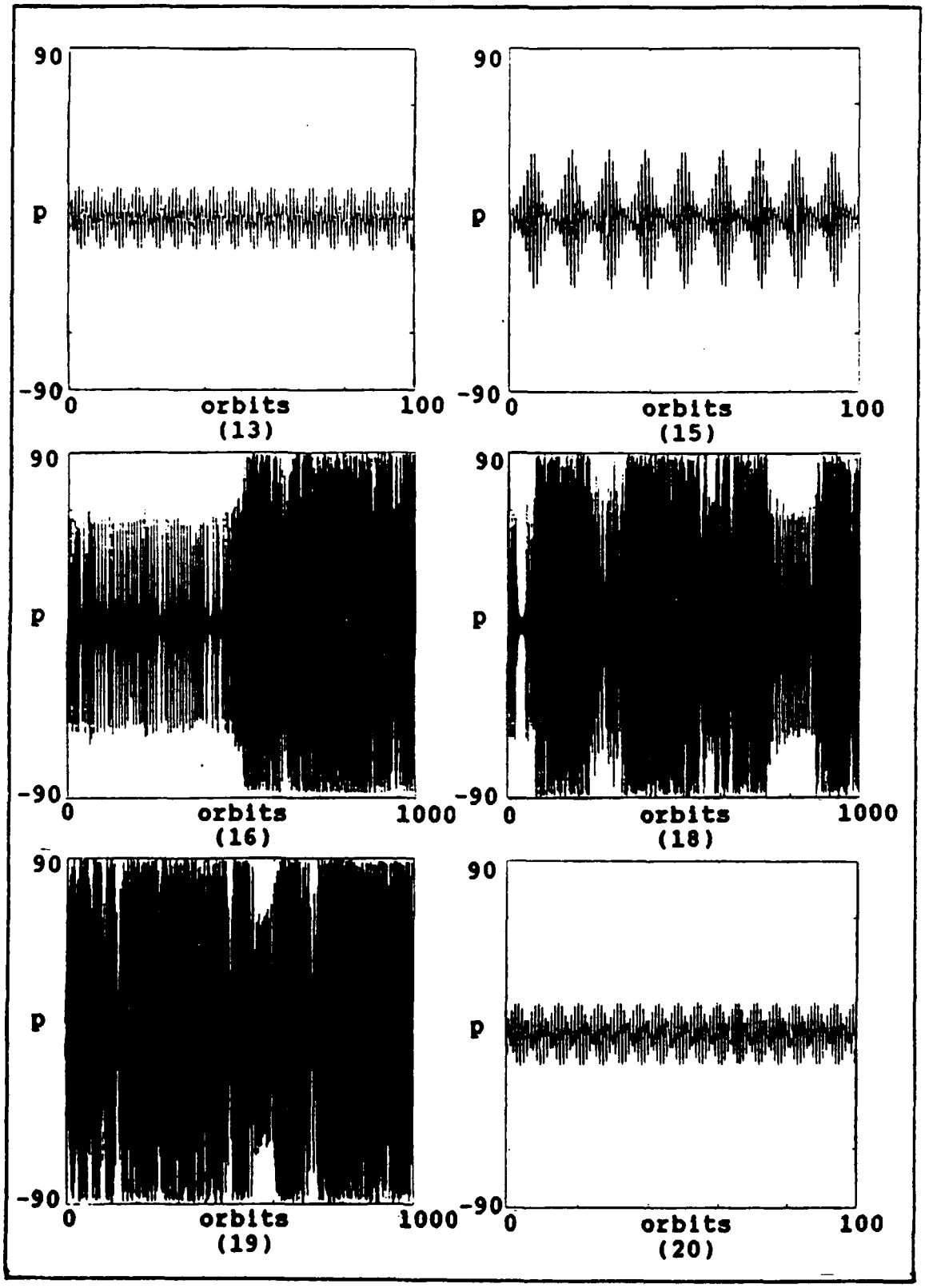

Fig. 12. Computer Runs (w=n, r_o=0.175)

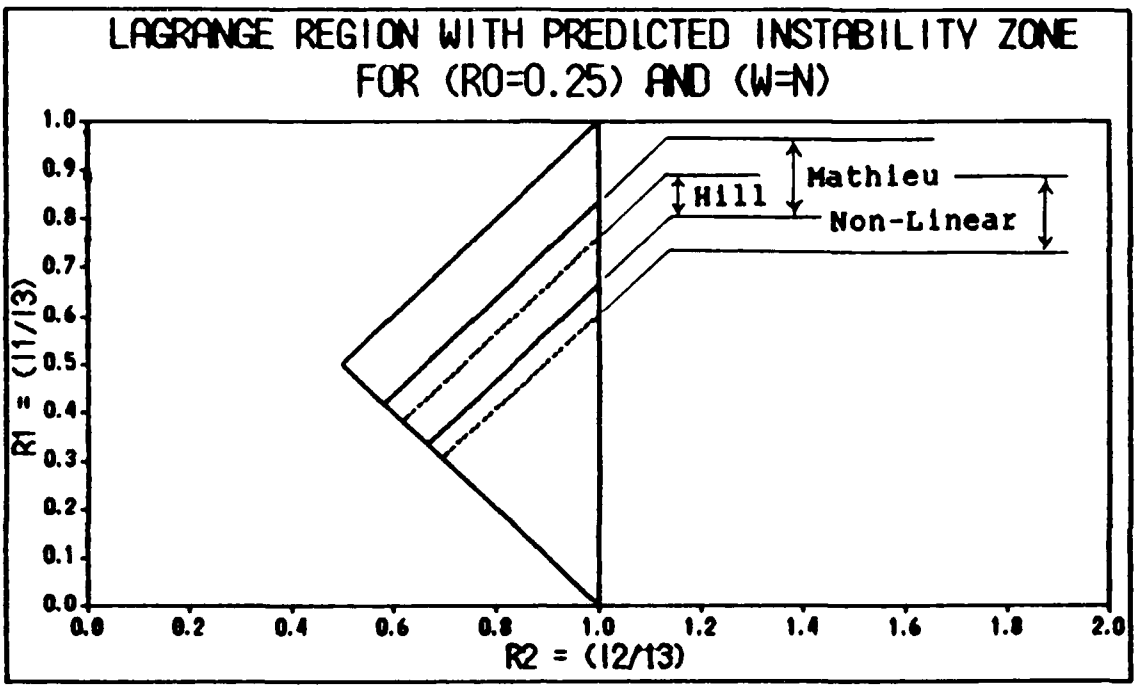

Fig. 13. Instability Zones For (r_o=.25) and (w=n)

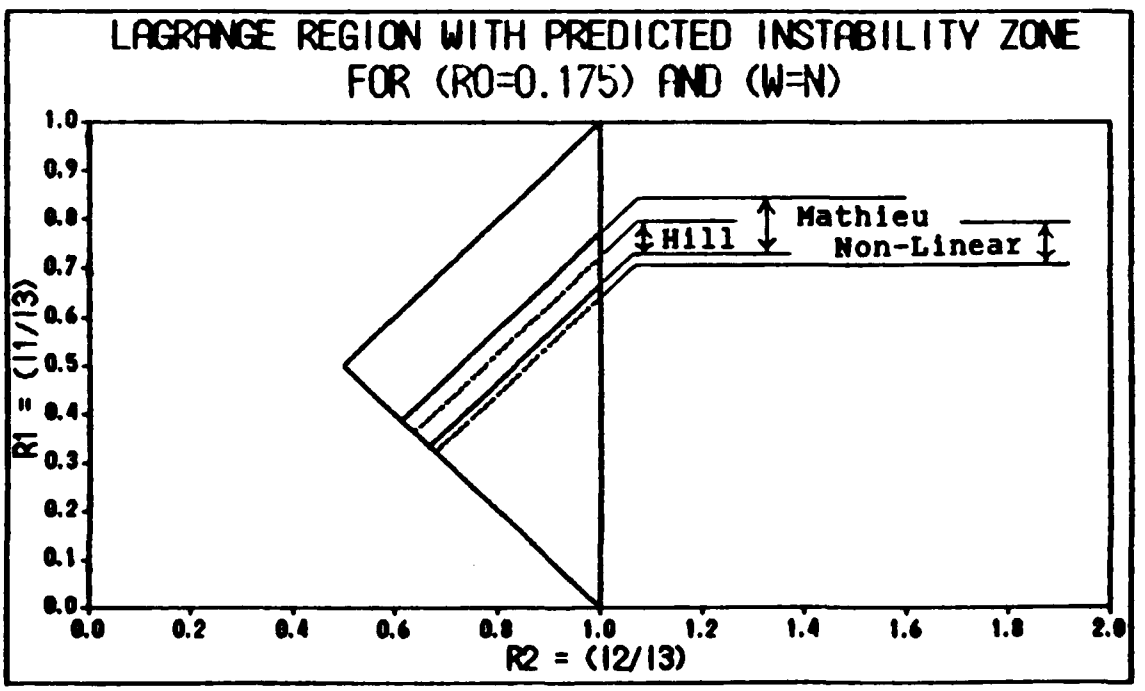

Fig. 14. Instability Zones For (r_o=.175) and (w=n)

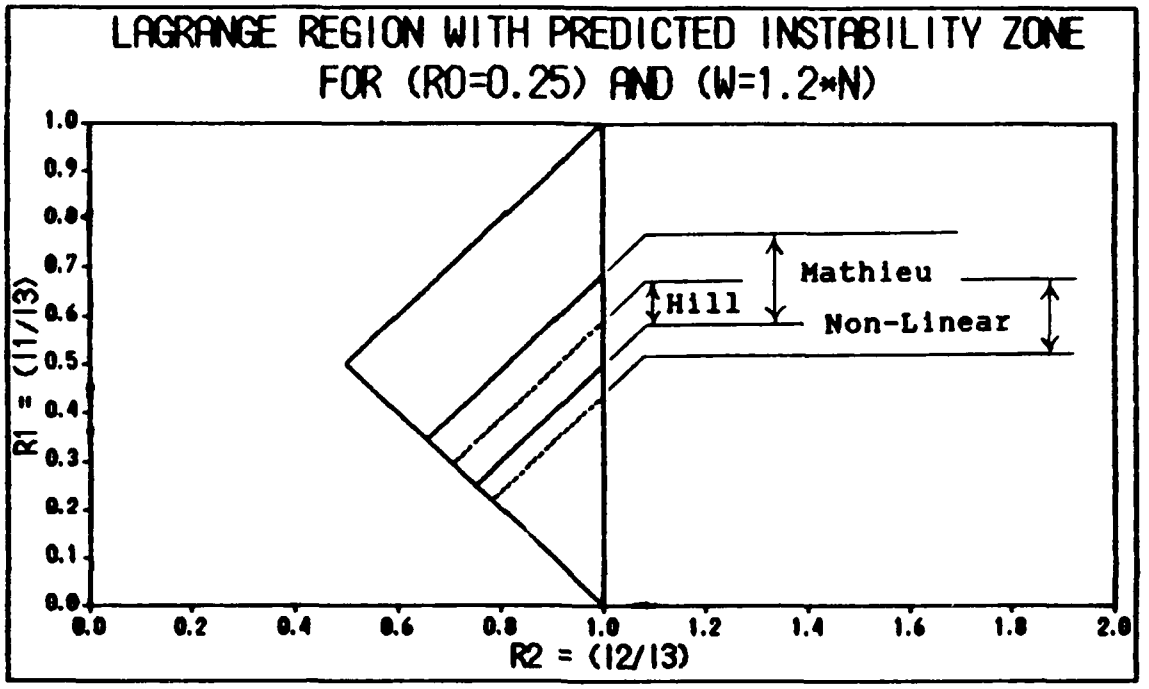

Fig. 15. Instability Zones For (r_o=.25) and (w=1.2*n)

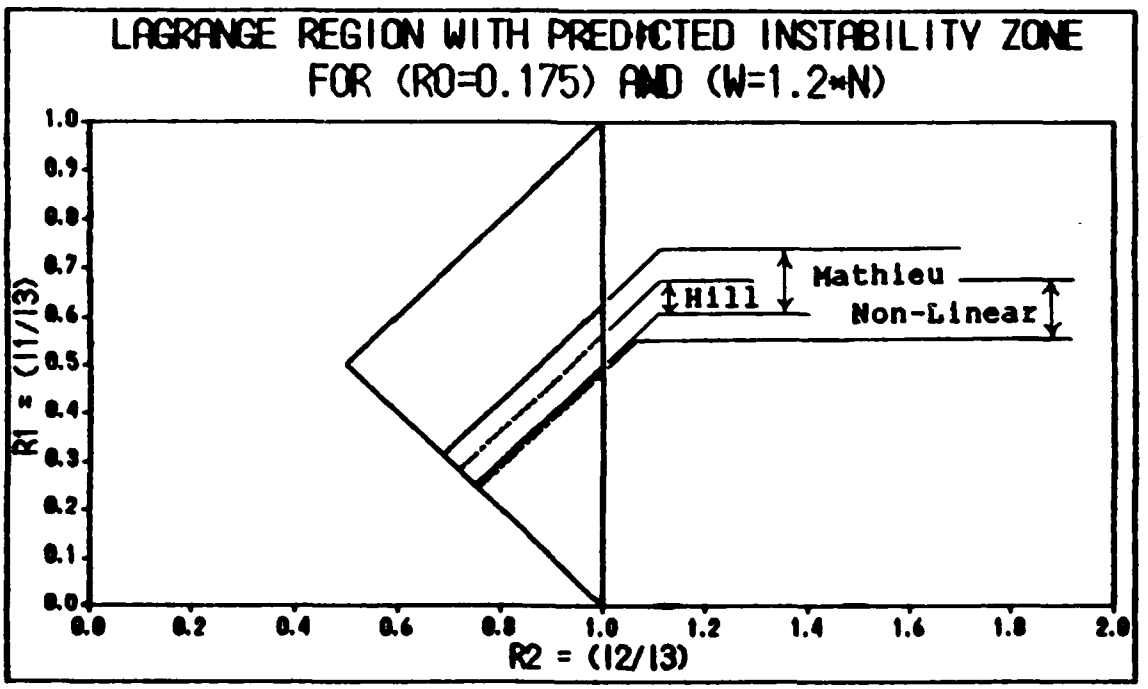

Fig. 16. Instability Zones For (r_o=.175) and (w=1.2*n)

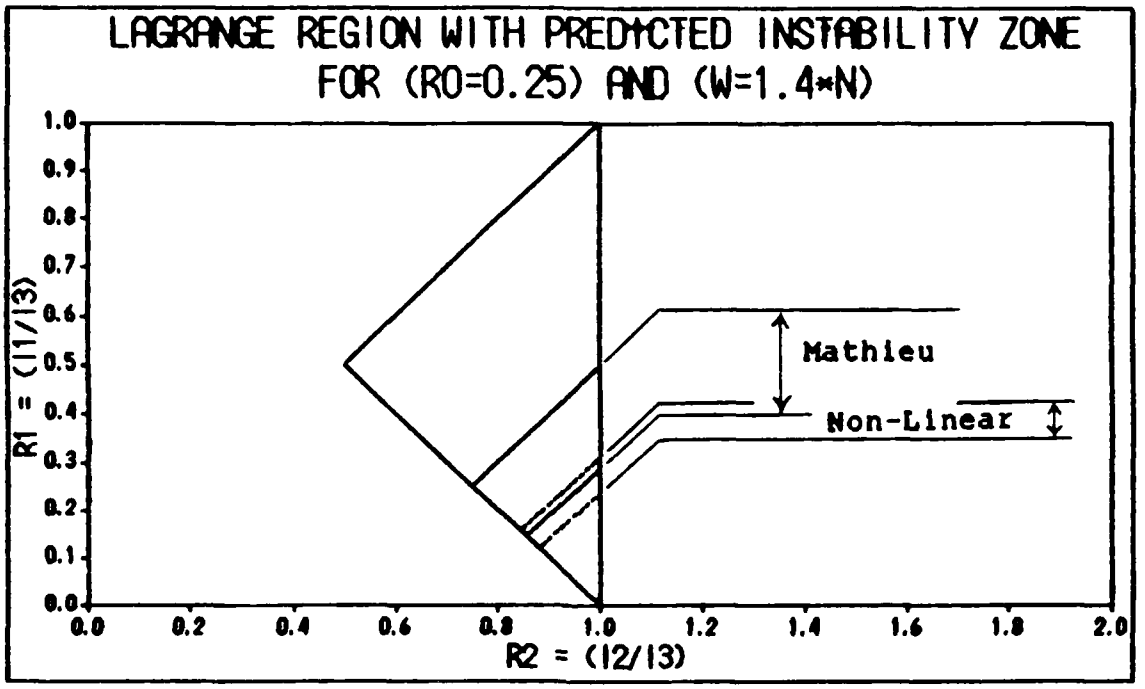

Fig. 17. Instability Zones For (r_o=.25) and (w=1.4*n)

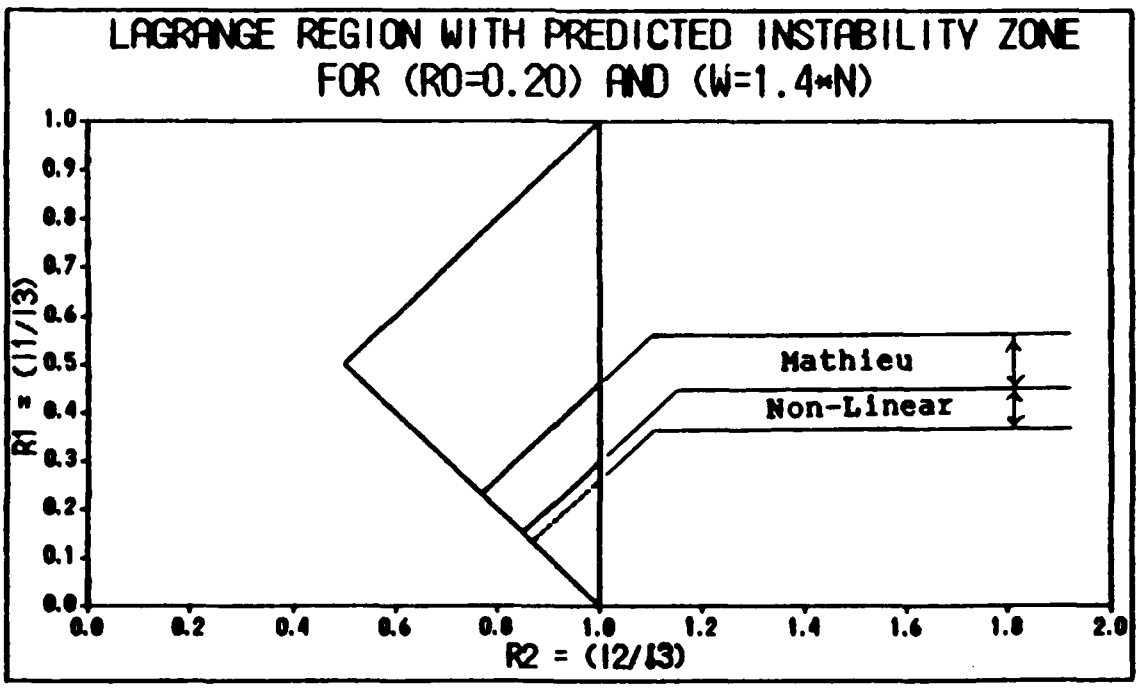

Fig. 18. Instability Zones For (r_o=.20) and (w=1.4*n)

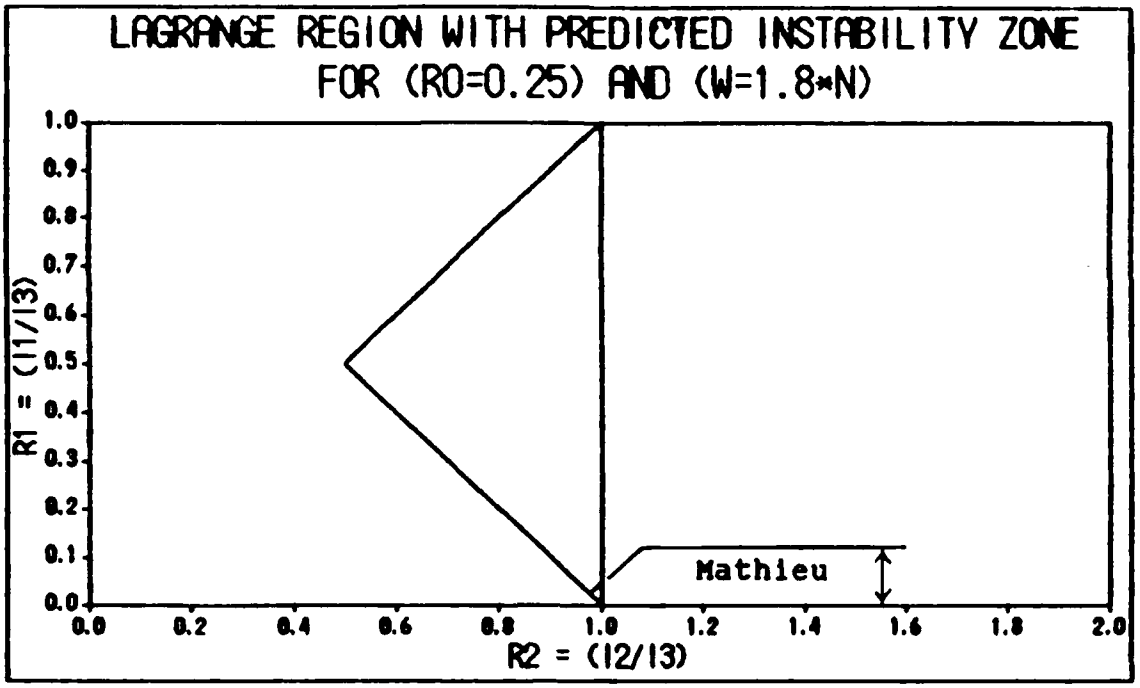

Fig. 19. Instability Zones For (r_o=.25) and (w=1.8*n)

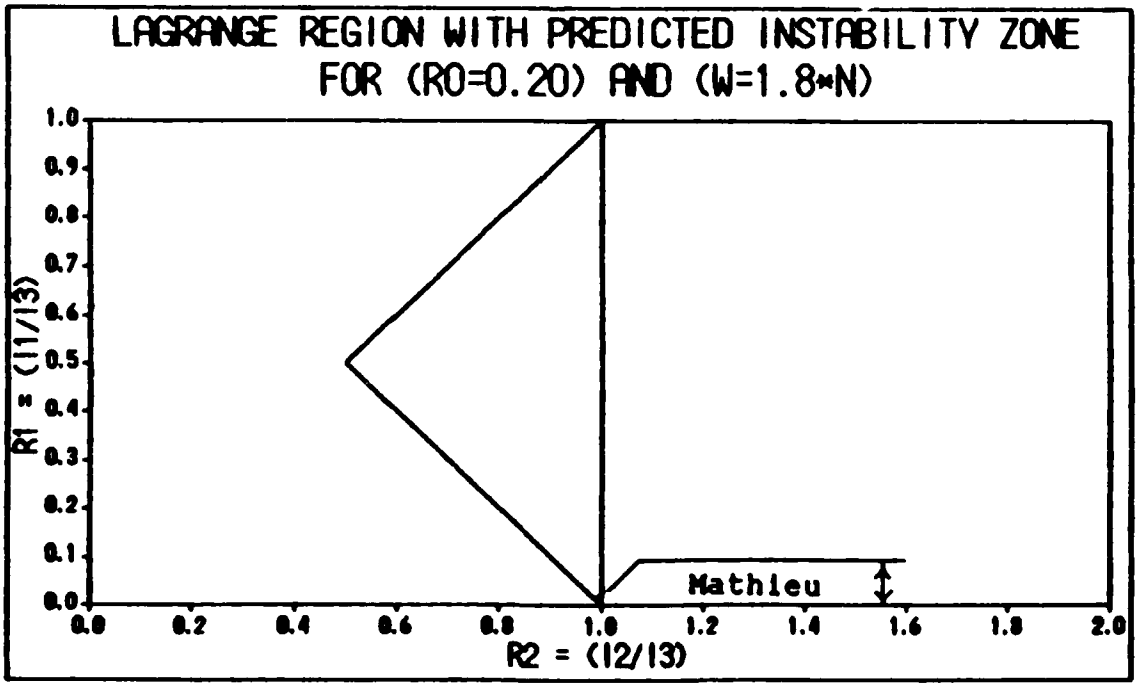

Fig. 20. Instability Zones For (r_o=.20) and (w=1.8*n)

fact, both methods share a common lower boundary due to the fact that Mathieu's equation is a specialized form of Hill's equation. Fig. 13 also reveals that both analytical methods miss the same portion of the instability zone predicted by the computer code. It should be noted, however, that although Fig. 13 gives the impression that the predictions by Hill's method and the nonlinear program share a common upper boundary, this is not the case. Due to the scale of the graph, the difference between boundaries is not obvious. As ω increases or r_0 decreases, however, the difference becomes more pronounced.

Fig. 14 shows that the common lower boundary of Hill's and Mathieu's predicted instability zones does not move much from its position in Fig. 13 as r_0 decreases. All of the other boundaries, however, will tend to collapse around this line. This tendency continues as r_0 decreases further until all that is left is a line at $r_0 \approx 0$. At $r_0 = 0$ (the null trolley mass) no instability remains. It should be noted that this collapsing phenomenon occurs in all the cases.

Another phenomenon observed is that as ω increases, the instability zones appear lower in the Lagrange region. This downward migration of the instability zones can be seen in the progression of graphs shown in Figs. (13) through (20). Figs. (19) and (20), for example, show that at $\omega = 1.8*n$ all that is left of the original instability zones is the tip of

the Lagrange region. When $\omega > 1.8*n$, no instability zones remain.

The predicted instability zones do not all disappear at the same time. The zone predicted by Hill's equation, for instance, disappears by the time $\omega = 1.3*n$. As a result, Figs. (17) and (18) show only two zones remaining. When $\omega = 1.7*n$, the zone predicted by the nonlinear equations vanishes leaving Figs. (19) and (20) with only one zone.

Based on this information, neither analytical method provides an excellent prediction of what the nonlinear equations are saying. Depending on the purpose of their use, however, the analytical methods maybe adequate for determining zones of pitch instability in the Lagrange region. Therefore, a summary of the results/observations is given below.

For $1.0*n \leq \omega < 1.3*n$, both analytical methods predict and miss the same portions of the nonlinear instability zone. In addition, Hill's method fails to predict any new instability zones that have not already been predicted by Mathieu's method. The conservative nature of Mathieu's method, however, eliminates an additional group of space station configurations that Hill's method does not.

For $1.3*n \leq \omega < 1.7*n$, Mathieu's method predicts a much larger instability zone than the one predicted by the nonlinear equations. However, the nonlinear zone hovered

around the lower boundary of Mathieu's zone. Given that Hill's method disappeared, Mathieu's analytical solution is better than nothing because it predicts the approximate neighborhood of the nonlinear zone.

For $1.7*n \leq \omega < 1.9*n$, Mathieu's method still predicts an instability zone when, according to the nonlinear program, an instability zone no longer exists.

And finally, for $\omega \geq 1.9*n$, no instability zones are predicted by any method.

VI. Roll/Yaw Analysis

The objective of this chapter is to obtain an analytical solution to the coupled roll/yaw equations using the Method of Multiple Scales. This method is used because the analytical technique in Chapter V is not applicable to two-dimensional problems. The results are compared to the numerical solutions of the nonlinear system for verification.

The chapter begins by reviewing the theory behind using perturbation techniques to solve parametrically excited systems. The Method of Multiple Scales is then introduced, followed by a discussion on the existing resonance conditions. The remainder of the chapter discusses the results obtained and the comparison to the numerical solutions.

Theory

The linearized roll and yaw equations of attitude motion were shown to be coupled in Chapter IV. Re-writing Eqs. (32) and (33) yields

$$\ddot{y} + \left(\frac{I_3 - I_2 - I_1}{I_1}\right) n\dot{r} + \left(\frac{I_3 - I_2}{I_1}\right) n^2 y = 0 \qquad (50)$$

$$\ddot{r} - \left(\frac{I_3 - I_2 - I_1}{I_2}\right) n\dot{y} + 4\left(\frac{I_3 - I_1}{I_2}\right) n^2 r + \left(\frac{\dot{I}_2}{I_2}\right)(\dot{r} + yn) = 0 \qquad (51)$$

where each coefficient containing I is a function of time

due to mass motion. Since the mass motion is periodic and occurs in an environment where the gravity-gradient torque is the dominant factor affecting the attitude stability of the space station, the equations governing attitude motion are parametrically excited. The presence of this small disturbance term has a non-negligible cumulative effect because it acts over a long time.

There are several techniques available to provide a systematic way of estimating this cumulative effect. These techniques are generally referred to as "perturbation methods" because the nonlinear equations representing the non autonomous dynamical system are "quasi-linear". This means that the equations can be separated into one part containing linear terms and a second part containing small nonlinear terms known as perturbations (Meirovitch, 1970: 294). The perturbation technique used in this study is known as the Method of Multiple Scales or Two-Timing.

Method of Multiple Scales

Appendix C details the expansion which shows Eqs.(50) and (51) are of the form

$$\ddot{u}_1 + \lambda_1 \dot{u}_2 + \alpha_1 u_1 = 0 \tag{52}$$

$$\ddot{u}_2 - \lambda_2 \dot{u}_1 + \alpha_2 u_2 + 2\varepsilon(f_{21} u_1 + f_{22} \dot{u}_2)\sin(2\omega t) + 2\varepsilon(f_{23} \dot{u}_1 + f_{24} u_2)\cos(2\omega t) = 0 \tag{53}$$

where

$$\underline{u} = \begin{bmatrix} u_1 \\ u_2 \end{bmatrix} = \begin{bmatrix} y \\ r \end{bmatrix} \tag{54}$$

and

ω = frequency of mass motion

$$\lambda_1 = \left(\frac{I_{03} - I_{02} - I_{01}}{I_{01}}\right) n \quad ; \quad \alpha_1 = \left(\frac{I_{03} - I_{02}}{I_{01}}\right) n^2$$

$$\lambda_2 = \left(\frac{I_{03} - I_{02} - I_{01}}{I_{02}}\right) (1-\epsilon) n \; ;$$

$$\alpha_2 = 4 \left[\left(\frac{I_{03} - I_{01}}{I_{02}}\right) - \epsilon \left(\frac{I_{03} - I_{02} - I_{01}}{I_{02}}\right)\right] n^2$$

$$f_{21} = n\omega \quad ; \quad f_{22} = \omega \quad ;$$

$$f_{23} = -(1/2)\left(\frac{I_{03} - I_{02} - I_{01}}{I_{02}}\right) n$$

$$f_{24} = 2\left(\frac{I_{03} - I_{02} - I_{01}}{I_{02}}\right) n^2 \quad ; \quad 2\epsilon = \frac{r_0}{r_2}$$

When $\epsilon = 0$, we have a system of linear homogeneous differential equations with known solutions. The role of the parameter ϵ, therefore, is to separate out the small terms in Eq.(53). Meirovitch (295) states that the presence of such a parameter associated with the small terms enables us to effect the transition between the known and desired solutions.

At this point, the fundamental perturbation technique assumes a solution to Eqs. (52) and (53) in the form of a

power series in ε given by

$$u_m = u_{m0} + \varepsilon u_{m1} + \varepsilon^2 u_{m2} + \cdots \quad . \tag{56}$$

However, the method of multiple scales introduces new independent variables according to

$$T_n = \varepsilon^n t \quad \text{for } n = 0, 1, 2, \cdots \tag{57}$$

where $T_0 = t$; and $T_1 = \varepsilon t$.

The underlying idea, according to (Nayfeh, 1979: 56), is to arrive at a more convenient method of dealing with certain dynamical systems by considering "the expansion representing the response to be a function of multiple independent variables, or scales, instead of a single variable." As a result, the assumed solution becomes

$$u_m = u_{m0}(T_0, T_1) + \varepsilon u_{m1}(T_0, T_1) + \cdots \tag{58}$$

where the independent time scales are limited to T_0 and T_1 because a first order expansion is adequate for this study.

Expanding the time derivatives of Eq. (58) yields

$$\dot{u}_m = D_0 u_{m0} + \varepsilon D_1 u_{m0} + \varepsilon D_0 u_{m1} + \varepsilon^2 D_1 u_{m1} \tag{59}$$

where the operators

$$D_0 u_{mi} = \frac{\partial u_{mi}}{\partial T_0} \qquad (i = 1, 2) \tag{60a}$$

$$D_1 u_{mi} = \frac{\partial u_{mi}}{\partial T_1} \qquad (i = 1, 2) \tag{60b}$$

and

$$\frac{dT_n}{dt} = \frac{d\varepsilon^n t}{dt} \qquad (n = 0, 1) \tag{60c}$$

Similarly,

$$\ddot{u}_m = D_0^2 u_{m0} + 2\varepsilon D_0 D_1 u_{m0} + \varepsilon D_0^2 u_{m1} + \varepsilon^2 D_1^2 u_{m0} + \varepsilon^2 D_0 D_1 u_{m1} + \cdots \quad (61)$$

Substituting Eqs. (53) and (61) into Eqs. (52) and (53) and equating coefficients of like powers of ε yields

Order ε^0

$$D_0^2 u_{10} + \lambda_1 D_0 u_{20} + \alpha_1 u_{10} = 0. \quad (62a)$$

$$D_0^2 u_{20} - \lambda_2 D_0 u_{10} + \alpha_2 u_{20} = 0. \quad (62b)$$

Order ε^1

$$D_0^2 u_{11} + \lambda_1 D_0 u_{21} + \alpha_1 u_{11} = -2D_0 D_1 u_{10} - \lambda_1 D_1 u_{20} \quad (63a)$$

$$D_0^2 u_{21} - \lambda_2 D_0 u_{11} + \alpha_2 u_{21} = -2D_0 D_1 u_{20} - \lambda_2 D_1 u_{10} - 2(f_{21} u_{10} + f_{22} D_0 u_{20})\sin(2\omega t) - 2(f_{23} D_0 u_{10} + f_{24} u_{20})\cos(2\omega t) \quad (63b)$$

According to (Nayfeh, 1979: 332) the solutions to Eqs. (62a) and (62b) can be written in the form

$$u_{10} = A_1(T_1)\left[e^{i\omega_1 T_0}\right] + A_2(T_1)\left[e^{i\omega_2 T_0}\right] + cc \quad (64a)$$

$$u_{20} = \frac{i(\alpha_1 - \omega_1^2)}{\lambda_1 \omega_1} A_1\left[e^{i\omega_1 T_0}\right] + \frac{i(\alpha_1 - \omega_2^2)}{\lambda_1 \omega_2} A_2\left[e^{i\omega_2 T_0}\right] + cc \quad (64b)$$

where ω_1^2 and ω_2^2 are the solutions to the order ε^0 characteristic equation

$$\omega^4 - (\alpha_1 + \alpha_2 + \lambda_1\lambda_2)\omega^2 + \alpha_1\alpha_2 = 0. \quad (65)$$

It is assumed that ω_1 and ω_2 are real and positive, and that $\omega_2 > \omega_1$.

Now that the solutions to the linear homogeneous differential Eqs. (62a) and (62b) are known, we can

substitute them into Eqs. (63a) and (63b) to get

$$D_0^2 u_{11} + \lambda_1 D_0 u_{21} + \alpha_1 u_{11} =$$

$$- \frac{i(\alpha_1+\omega_1^2)}{\omega_1} A_1' \left(e^{i\omega_1 T_0} \right) - \frac{i(\alpha_1+\omega_2^2)}{\omega_2} A_2' \left(e^{i\omega_2 T_0} \right) \qquad (66)$$

$$D_0^2 u_{21} - \lambda_2 D_0 u_{11} + \alpha_2 u_{21} = \frac{2\alpha_1+\lambda_1\lambda_2-2\omega_1^2}{\lambda_1} A_1' \left(e^{i\omega_1 T_0} \right)$$

$$+ \frac{2\alpha_1+\lambda_1\lambda_2-2\omega_2^2}{\lambda_1} A_2' \left(e^{i\omega_2 T_0} \right)$$

$$-2\left(f_{21} - \frac{f_{22}(\alpha_1-\omega_1^2)}{\lambda_1} \right) A_1 \left(e^{i\omega_1 T_0} \right) \sin(2\omega t) \qquad (67)$$

$$-2\left(f_{21} - \frac{f_{22}(\alpha_1-\omega_2^2)}{\lambda_1} \right) A_2 \left(e^{i\omega_2 T_0} \right) \sin(2\omega t)$$

$$+2i\left(f_{23}\omega_1 + \frac{f_{24}(\alpha_1-\omega_1^2)}{\lambda_1\omega_1} \right) A_1 \left(e^{i\omega_1 T_0} \right) \cos(2\omega t)$$

$$+2i\left(f_{23}\omega_2 + \frac{f_{24}(\alpha_1-\omega_2^2)}{\lambda_1\omega_2} \right) A_2 \left(e^{i\omega_2 T_0} \right) \cos(2\omega t)$$

where A_1' and A_2' are derivatives of A_1 and A_2 with respect to T_1. Since, $\sin(2\omega t) = \frac{e^{i2\omega T_0} - e^{-i2\omega T_0}}{2i} = \frac{-i}{2}\left(e^{i2\omega T_0} - e^{-i2\omega T_0} \right)$

and $\cos(2\omega t) = \frac{1}{2}\left(e^{i2\omega T_0} + e^{-i2\omega T_0} \right)$, Eq. (67) becomes

$$D_0^2 u_{21} - \lambda_2 D_0 u_{11} + \alpha_2 u_{21} = \frac{2\alpha_1+\lambda_1\lambda_2-2\omega_1^2}{\lambda_1} A_1' \left(e^{i\omega_1 T_0} \right)$$

$$+ \frac{2\alpha_1+\lambda_1\lambda_2-2\omega_2^2}{\lambda_1} A_2' \left(e^{i\omega_2 T_0} \right)$$

$$+ i\left[f_{21} + f_{23}\omega_1 + \left(f_{24} - f_{22}\omega_1\right)\frac{(\alpha_1 - \omega_1^2)}{\lambda_1\omega_1}\right] A_1\left[e^{i(2\omega+\omega_1)T_0}\right]$$

$$- i\left[f_{21} - f_{23}\omega_1 - \left(f_{24} + f_{22}\omega_1\right)\frac{(\alpha_1 - \omega_1^2)}{\lambda_1\omega_1}\right] \bar{A}_1\left[e^{i(2\omega-\omega_1)T_0}\right] \qquad (68)$$

$$+ i\left[f_{21} + f_{23}\omega_2 + \left(f_{24} - f_{22}\omega_2\right)\frac{(\alpha_1 - \omega_2^2)}{\lambda_1\omega_2}\right] A_2\left[e^{i(2\omega+\omega_2)T_0}\right]$$

$$- i\left[f_{21} - f_{23}\omega_2 - \left(f_{24} + f_{22}\omega_2\right)\frac{(\alpha_1 - \omega_2^2)}{\lambda_1\omega_2}\right] \bar{A}_2\left[e^{i(2\omega-\omega_2)T_0}\right]$$

where $\bar{A}_1$ and $\bar{A}_2$ are the complex conjugates of A_1 and A_2.

Resonance

Fortunately, it is not necessary to find the solutions to Eqs. (66) and (68) in order to determine the system's stability. This study needs only to look at the terms

$$\left[e^{i(2\omega+\omega_1)T_0}\right] \quad ; \quad \left[e^{i(2\omega-\omega_1)T_0}\right]$$

$$\left[e^{i(2\omega+\omega_2)T_0}\right] \quad ; \quad \left[e^{i(2\omega-\omega_2)T_0}\right] \qquad (69)$$

from Eq. (68). The reason for this stems from Eq. (65) and the determination of ω_1 and ω_2. The frequencies ω_1 and ω_2 are the resonant frequencies of the unperturbed equations of motion. When the mass motion frequency ω takes on a value such that one of the exponents in Eq. (66) goes to a resonant frequency (i.e. $i\omega_1 T_0$ or $i\omega_2 T_0$), secular terms will appear in the solution. Since secular terms grow indefinitely with time, large oscillations in attitude or

totally unstable motion can occur. The resonance phenomenon in this study occurs when a mass on the space station moves along the $\hat{b}_1$ axis with a frequency (ω) that meets one of the following conditions: (a) $\omega \approx .5(\omega_2 + \omega_1)$; (b) $\omega \approx .5(\omega_2 - \omega_1)$; (c) $\omega \approx \omega_2$; or (d) $\omega \approx \omega_1$. For example, when ω is at condition (a), $\left(e^{i(2\omega-\omega_1)T_0}\right)$ becomes $\left(e^{i(2*(.5\omega_2+\omega_1)-\omega_1)T_0}\right)$ which equals $\left(e^{i\omega_2 T_0}\right)$ which is a resonant frequency.

This problem of resonance and gravity-gradient stability has been studied before by (Breakwell and Pringle, 1965). In their study, Breakwell and Pringle (307) identified orbit eccentricity instead of mass motion as the forcing function. Fig. (21) contains dotted lines which represent what they call "external resonance" loci in the r_1, r_2 inertia parameter space. The authors stated that if a spacecraft had a configuration that fell on an external resonance line, orbit eccentricity would eventually cause unbounded attitude motion.

The types of resonance lines described by (Breakwell and Pringle, 1965) also appear in this study. The reason for this is that ω_1 and ω_2 are a function of r_0, r_1 and r_2. As a result, each resonance condition translates into constant value lines (loci) in the Lagrange region. To illustrate this concept, Figs. (22) through (25) show the constant value lines created by the resonance conditions (a) through (d) at $r_0 = .25$. Figs. (26) and (27) show how constant value

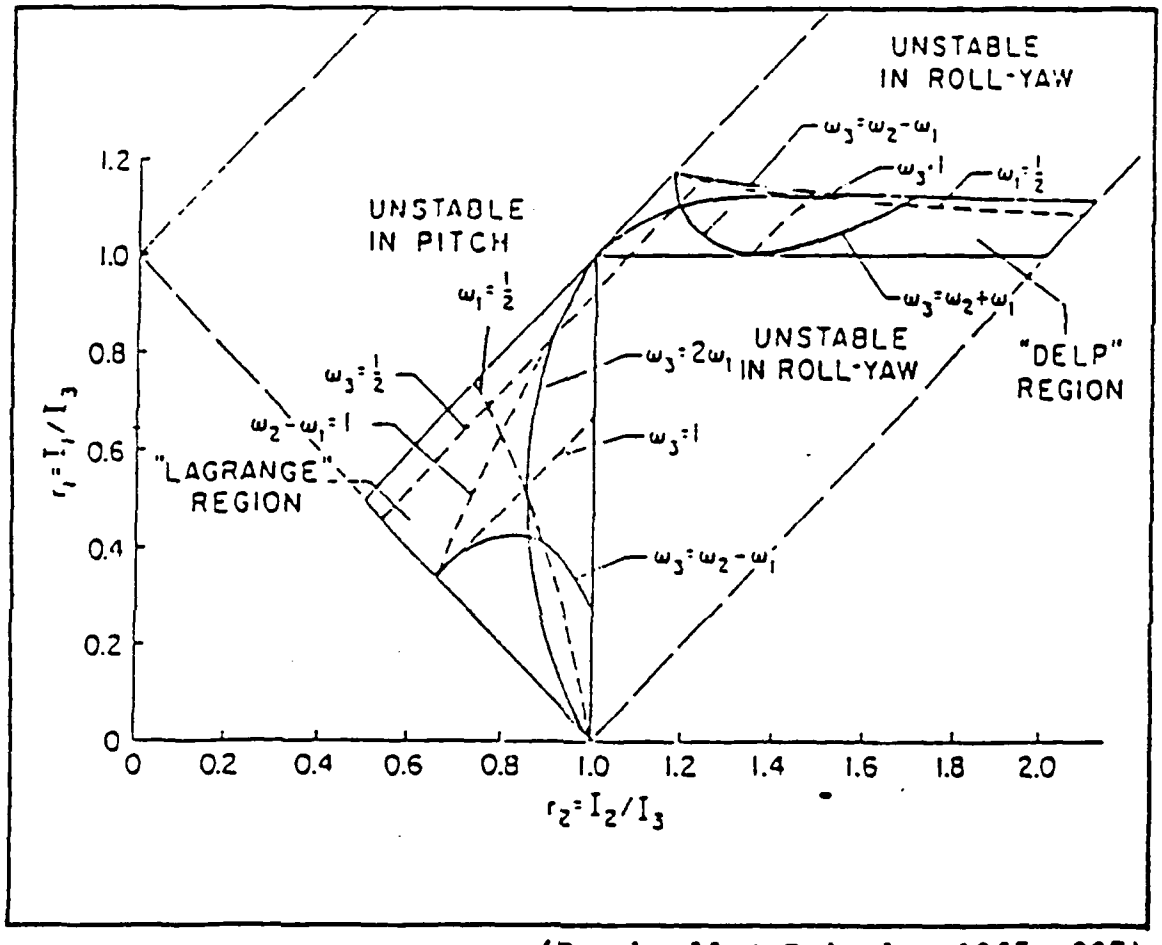

(Breakwell & Pringle, 1965: 307)

Fig. 21. Internal and External Resonance Lines in r_1, r_2 Inertia Parameter Space

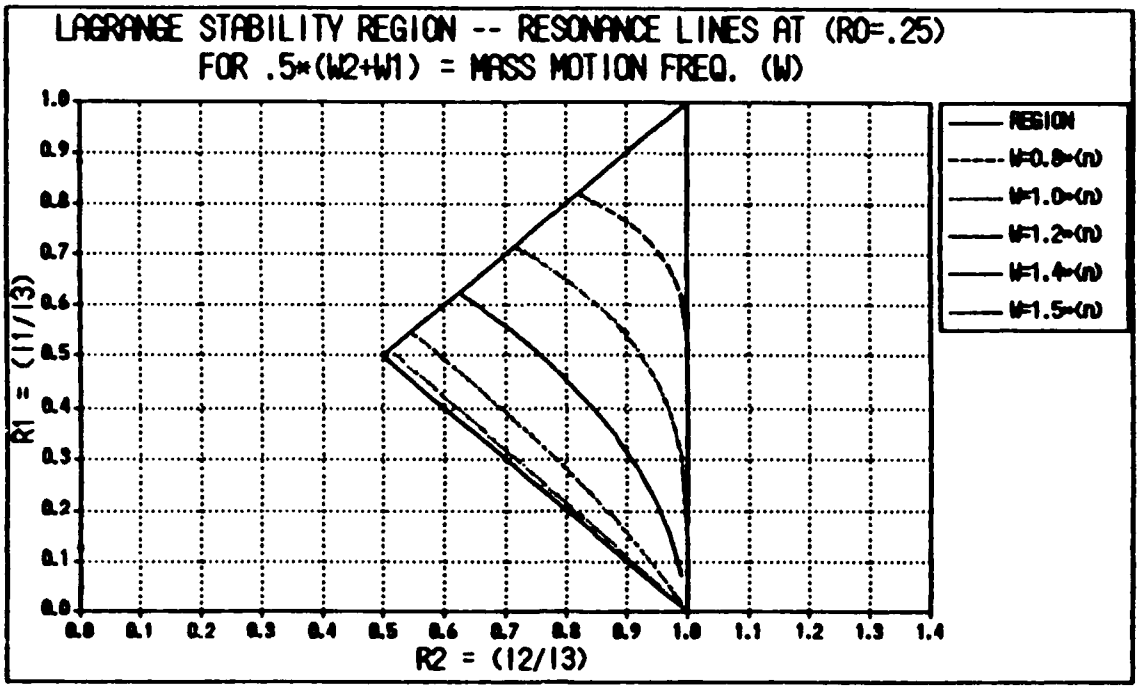

Fig. 22. Resonance Lines For .5(W2+W1)

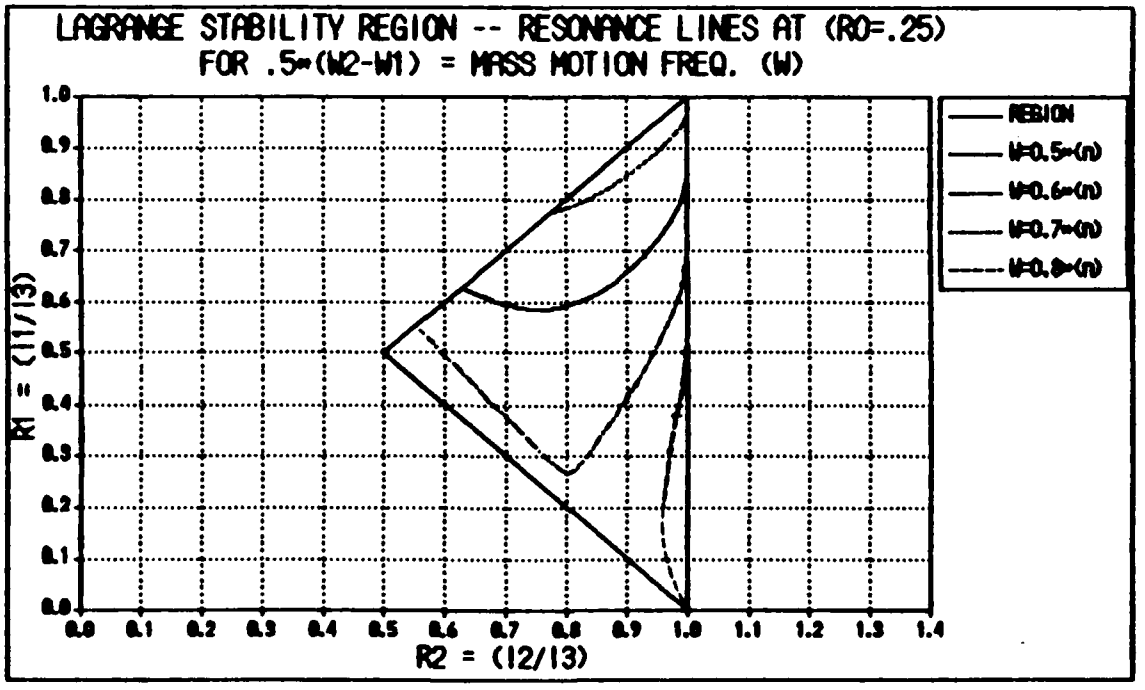

Fig. 23. Resonance Lines For .5(W2-W1)

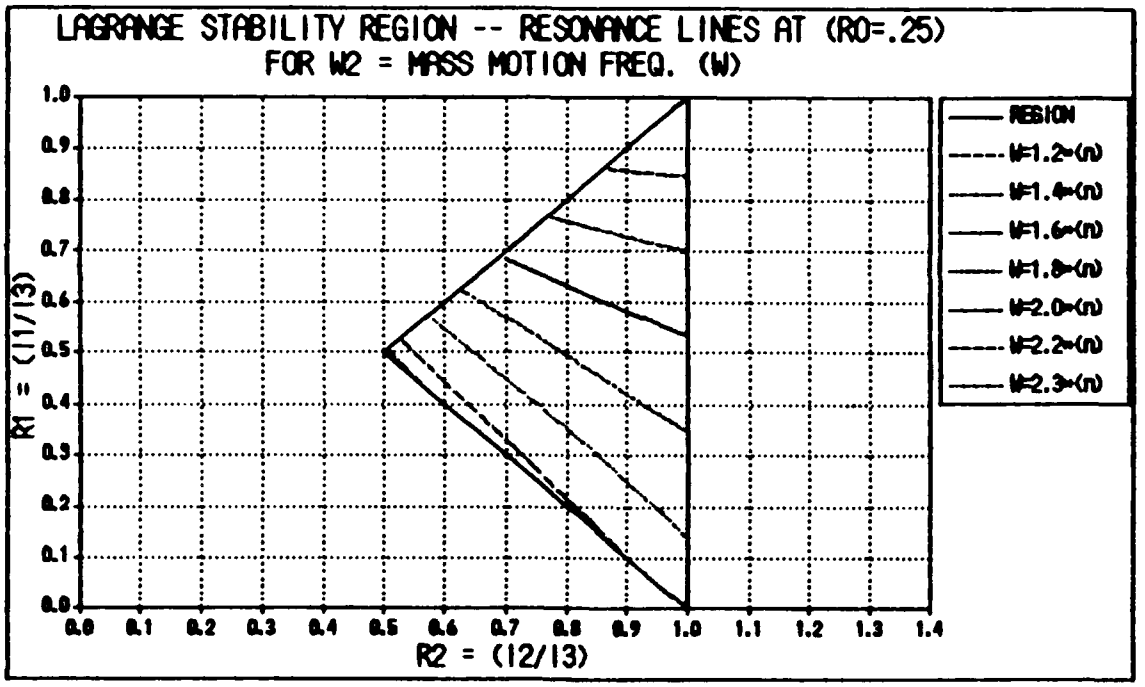

Fig. 24. Resonance Lines For W2

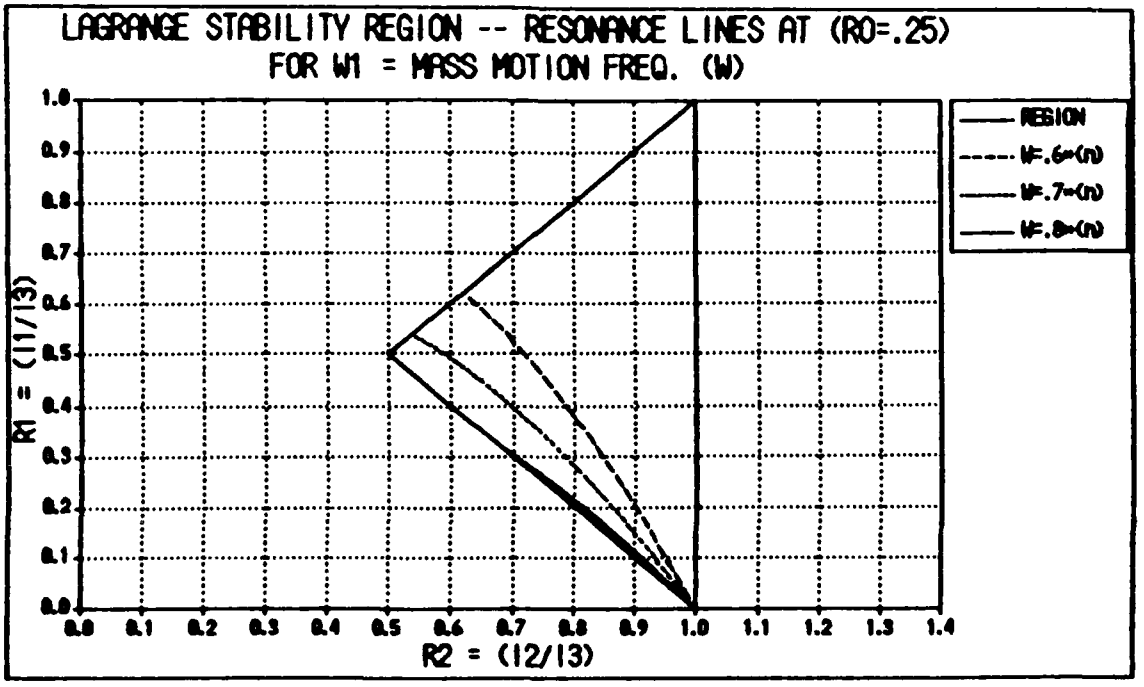

Fig. 25. Resonance Lines For W1

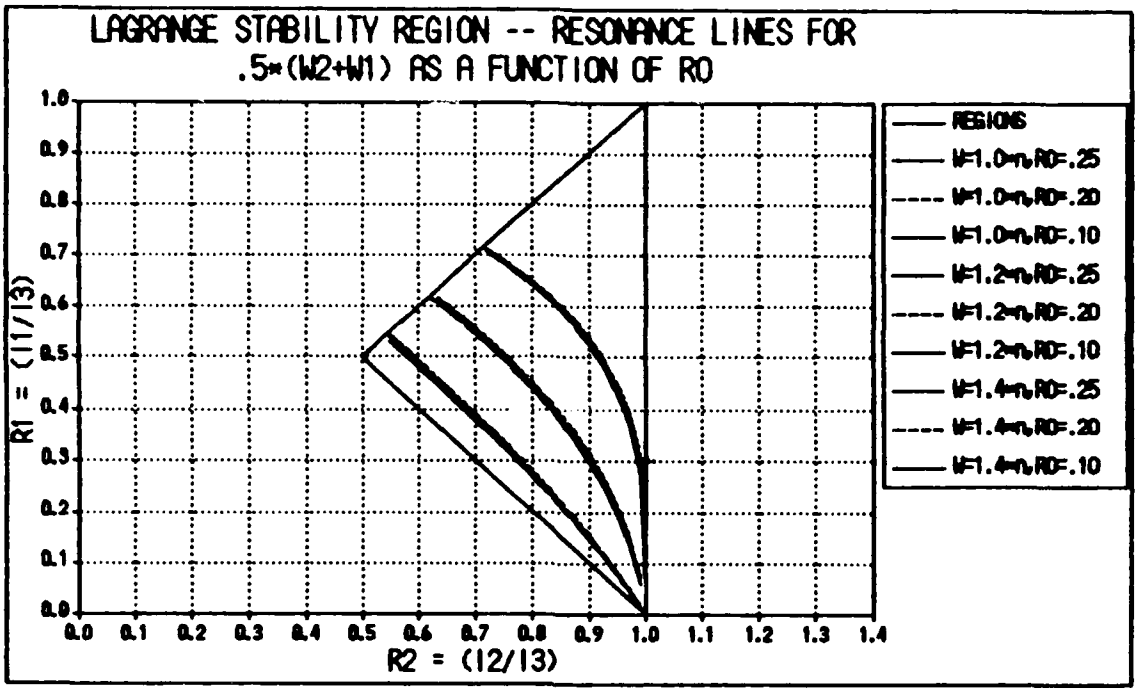

Fig. 26. Resonance Lines For .5(W2+W1) As A Function of r_o

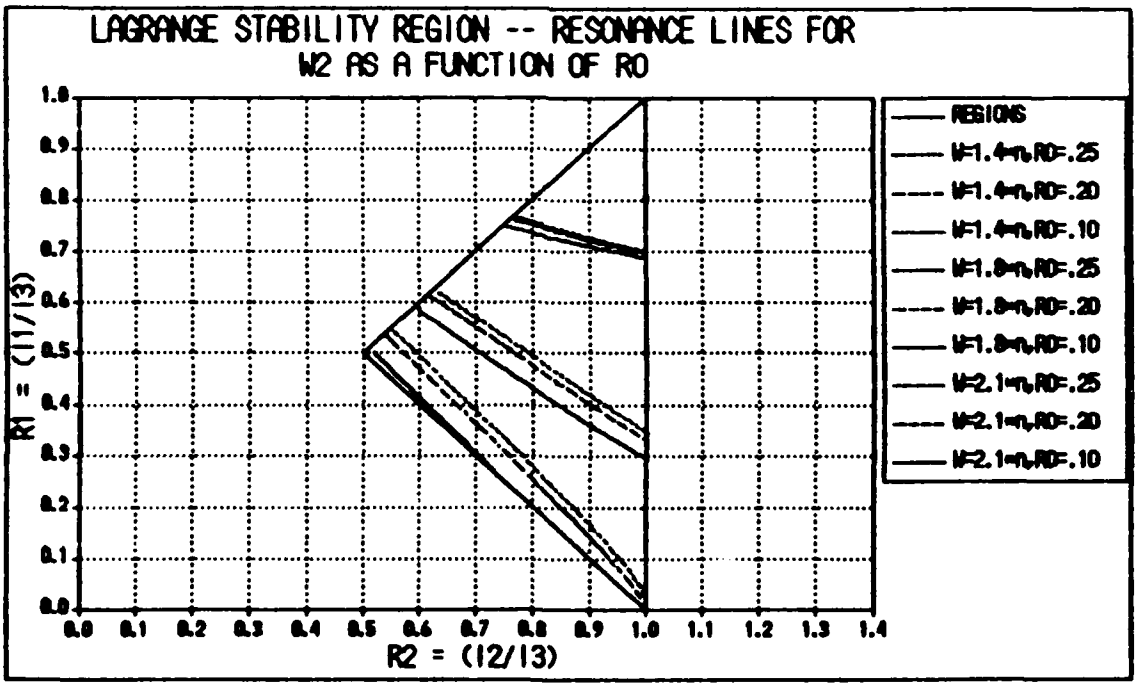

Fig. 27. Resonance Lines For W2 As A Function of r_o

lines for conditions (a) and (c) vary with r_0.

The lines in each figure represent where in the Lagrange region that the designated function equals a constant value. The values are varied in each figure to show the progression of the lines. For example, when a mass moves on a space station with a frequency (ω) equal to 1.0*n, the constant value line for $.5*(\omega_2+\omega_1)$ in Fig. (22) that corresponds to 1.0*n becomes a resonance line. In addition, as ω is varied so is the location of the corresponding line. It should be noted, however, that only two of the four resonance conditions listed previously result in resonance lines of concern. Figs. (23) and (25), for example, show the constant value lines for the resonance conditions $.5*(\omega_2-\omega_1)$ and ω_1. The figures reveal that in each case the functions do not exist in the Lagrange region for values of ω greater than 1.0*n. Figs. (22) and (24), however, reveal constant value lines for values of ω between 1.0*n and 2.3*n for the conditions (a) $\omega \approx .5*(\omega_2+\omega_1)$ and (c) $\omega \approx \omega_2$. Since the lower limit of ω was determined in Chapter V to be 1.0*n, this study will only look at the resonance lines generated by conditions (a) and (c).

In addition to the downward progression of the resonance lines due to increasing ω, Figs.(26) and (27) show a downward shift due to a decrease in r_0. The figures show that the shift is more noticeable in condition (c) and when ω is high.

In order to verify that resonance conditions (a) and (c) indeed lead to unstable motions, computer runs were conducted at a number of specific points on the different constant value lines for each condition. Two points, one from each condition, are shown in Figs. (28) and (29). The points illustrated were picked so that they would lie outside the pitch instability zones described in the previous chapter, in order to assure that the results were directly attributed to the resonance phenomenon. Fig. (28) shows that the pitch, roll, and yaw attitude motion for a point on the 1.0*n line of $.5*(\omega_2+\omega_1)$ is unstable. Fig. (29) reveals the same results for a point on the 1.4*n line of ω_2.

It should be realized, however, that the unstable motion associated with these resonance lines is not confined specifically to the lines themselves. As discussed earlier, the perturbation parameter ϵ associated with the small nonlinear terms enables us to effect the transition between the known and desired solutions. This transition acts as a band around the resonance lines to mark the change from stable to unstable motion. To illustrate this fact, Fig. (30) enlarges the area around the point used for Fig. (28). Two points are chosen at varied distances from the line. A computer run is conducted using the nonlinear program to see what happens to the stability of the equations at each point. Figs. (31) and (32) reveal that point (1) is still

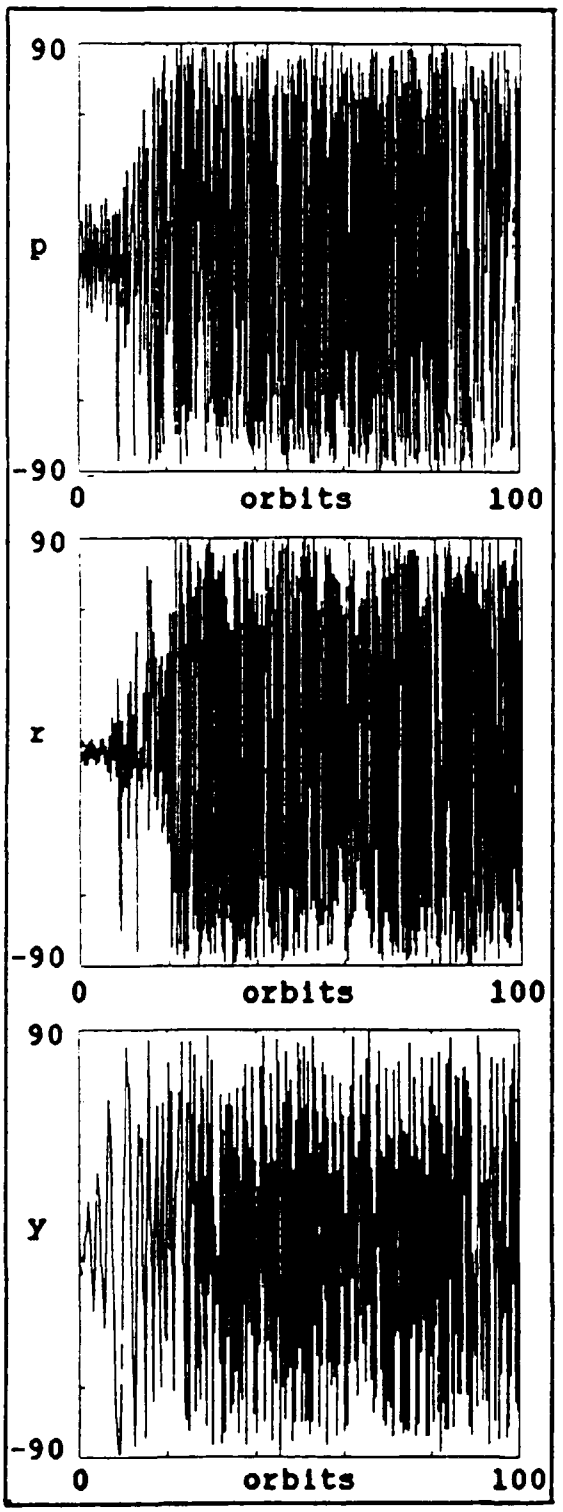

Fig. 28.
Computer Run For Resonance
Line .5(W2+W1) at (w=1.0*n)
(r_1=.6841,r_2=.76)

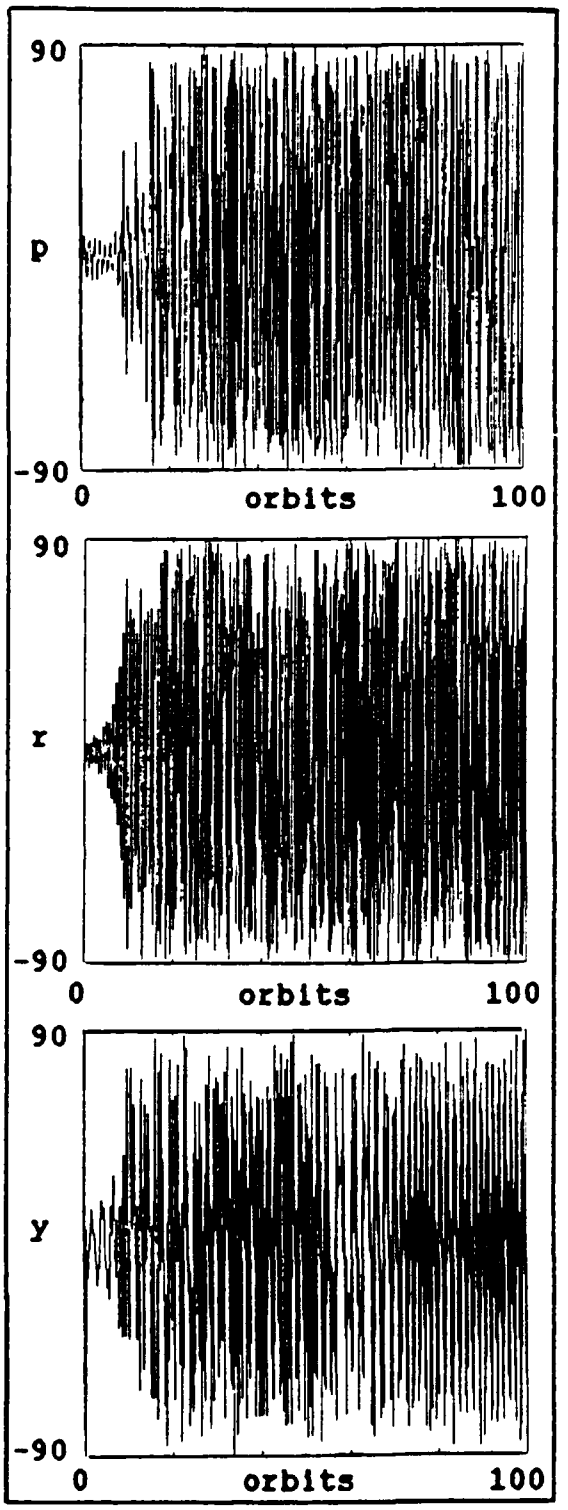

Fig. 29.
Computer Run For Resonance
Line W2 at (w=1.4*n)
(r_1=.73,r_2=.85)

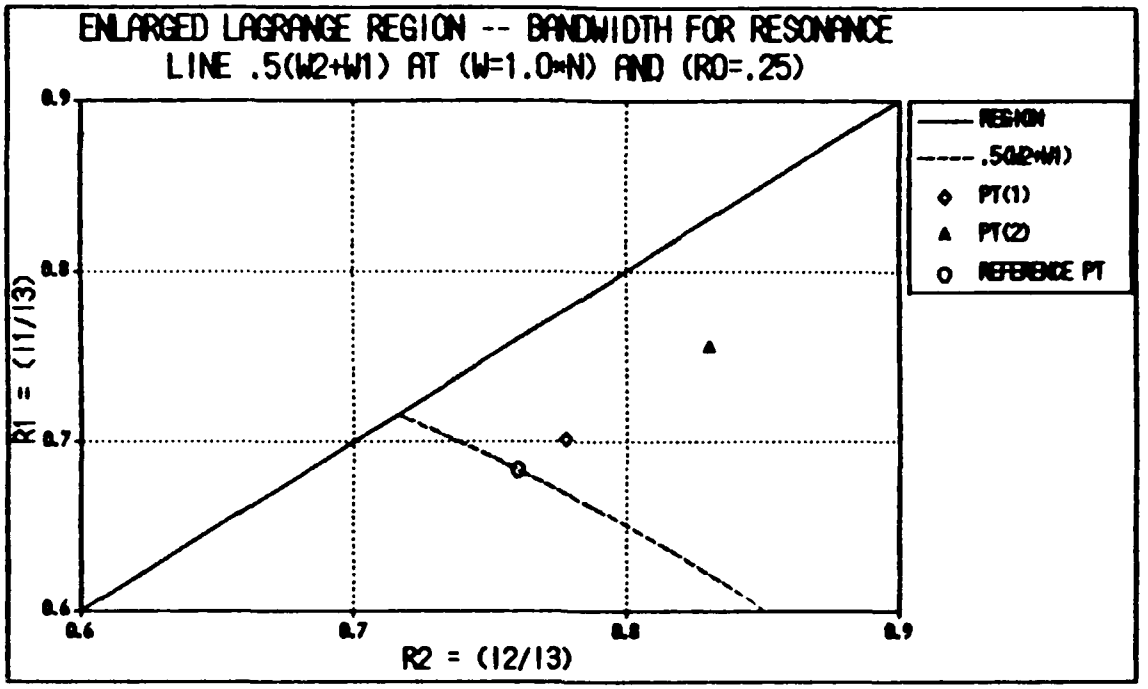

Fig. 30. Sample Bandwidth For Resonance Line .5(W2+W1) at (w=1.0*n)

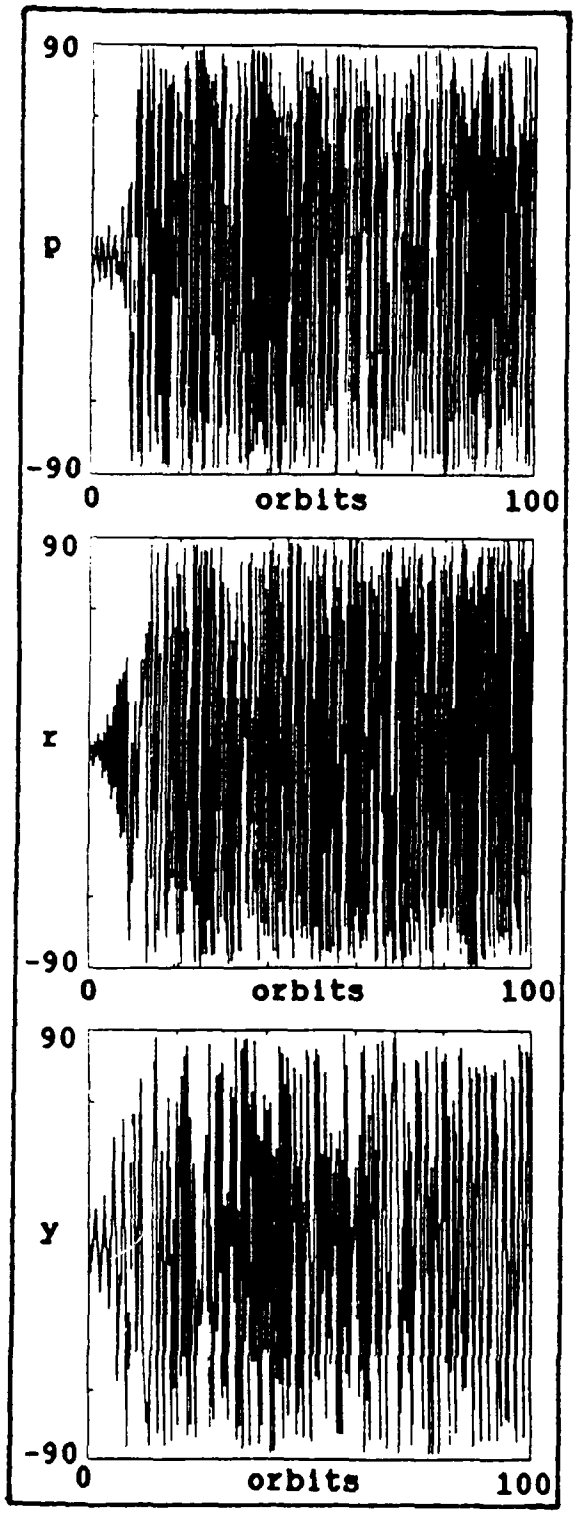

Fig. 31.
Computer Run For
Bandwidth Pt(1)

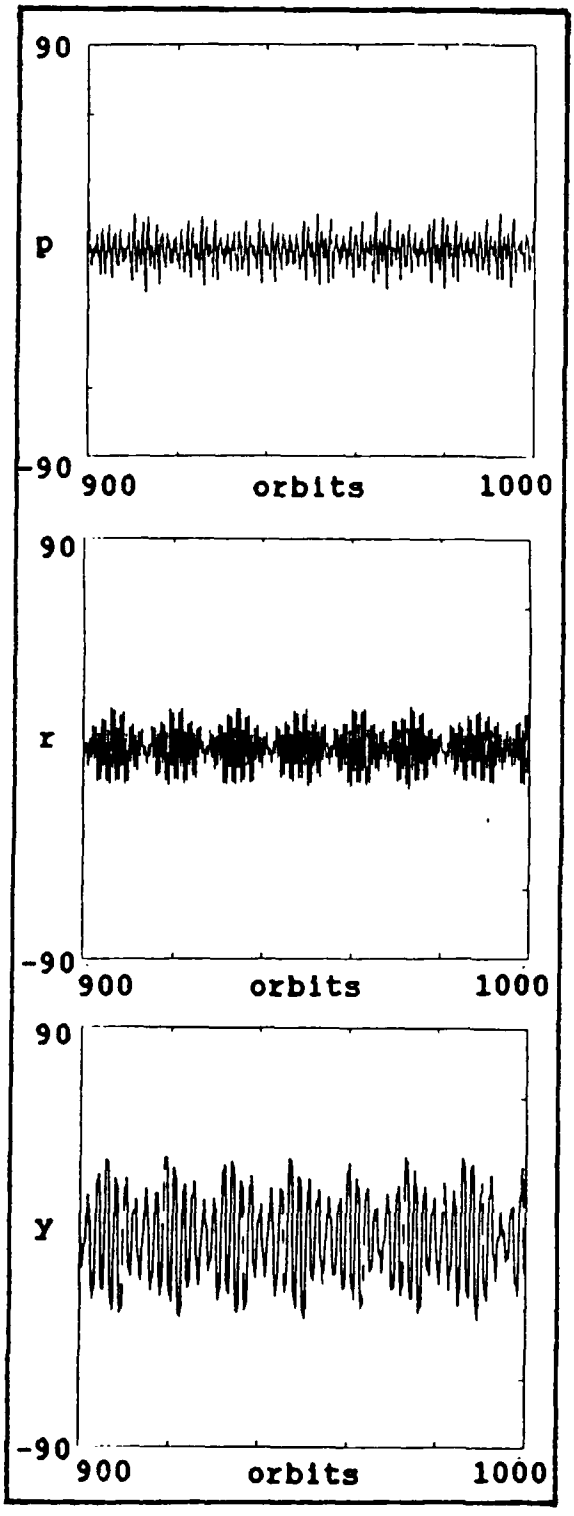

Fig. 32.
Computer Run For
Bandwidth Pt(2)

within the transition band where as point (2) is not. Although both points were run for 1000 orbits, only a portion of the data is presented so that the trends can be observed.

Mathematical approximation of the bandwidth around the resonance lines is possible and procedures are laid out in (Nayfeh, 1979). However, the bandwidths are a function of ϵ and therefore depend on r_0 and r_2. Although r_0 is a chosen constant, the value of r_2 varies along the resonance lines. Therefore, the bandwidth will have a tapered appearance with the width depending upon the location in the Lagrange region. For this study, it is considered sufficient to say that a band exists around the resonance lines and that it should be considered when making conclusions. Determination of the actual bandwidth is left for future studies.

Results

The main idea that this chapter attempted to present was that in the Lagrange region, resonance lines exist which represent space station configurations that result in unstable attitude motion for specific mass motion frequencies (ω). The lines that would cause concern at specific ω's are presented in Figs. (33) through (36). It should be noted that as ω increases, the resonance lines migrate towards the bottom of the Lagrange region. By the time $\omega=2.3*n$, no resonance lines remain. If a space station

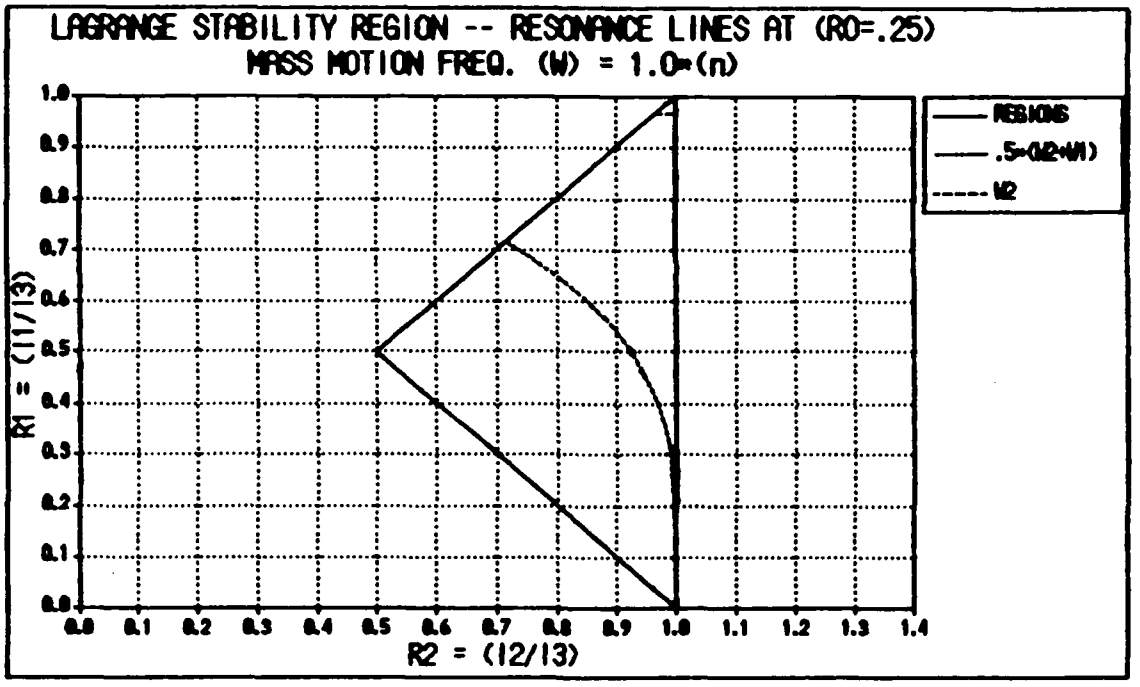

Fig. 33. Resonance Lines When (w=1.0*n)

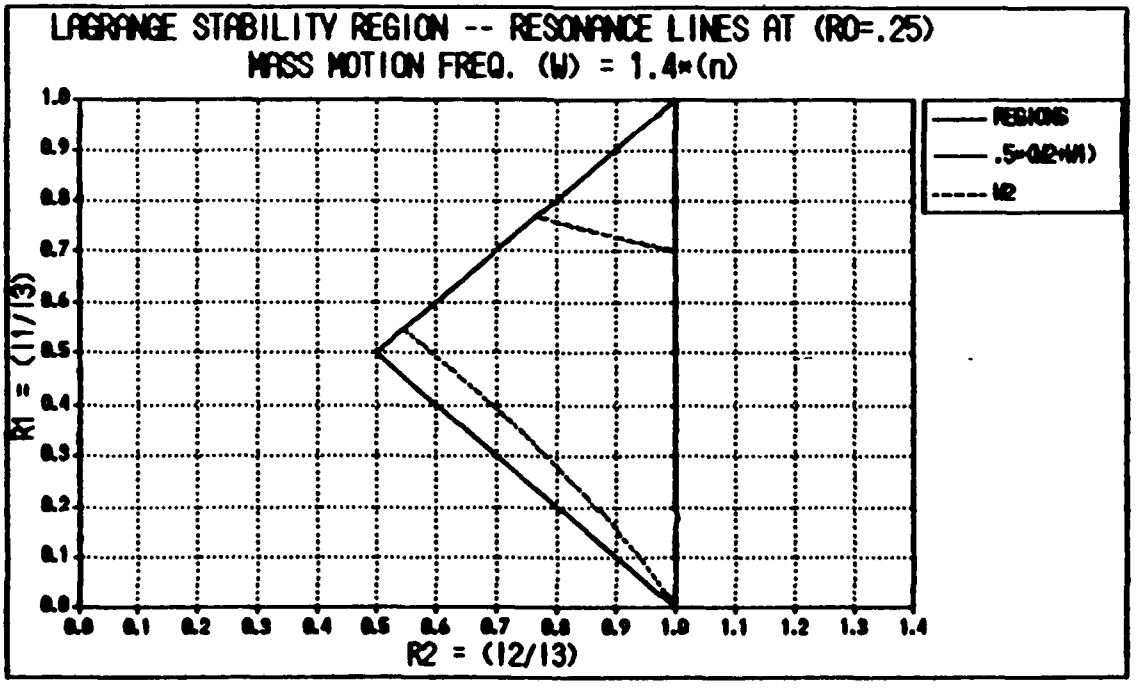

Fig. 34. Resonance Lines When (w=1.4*n)

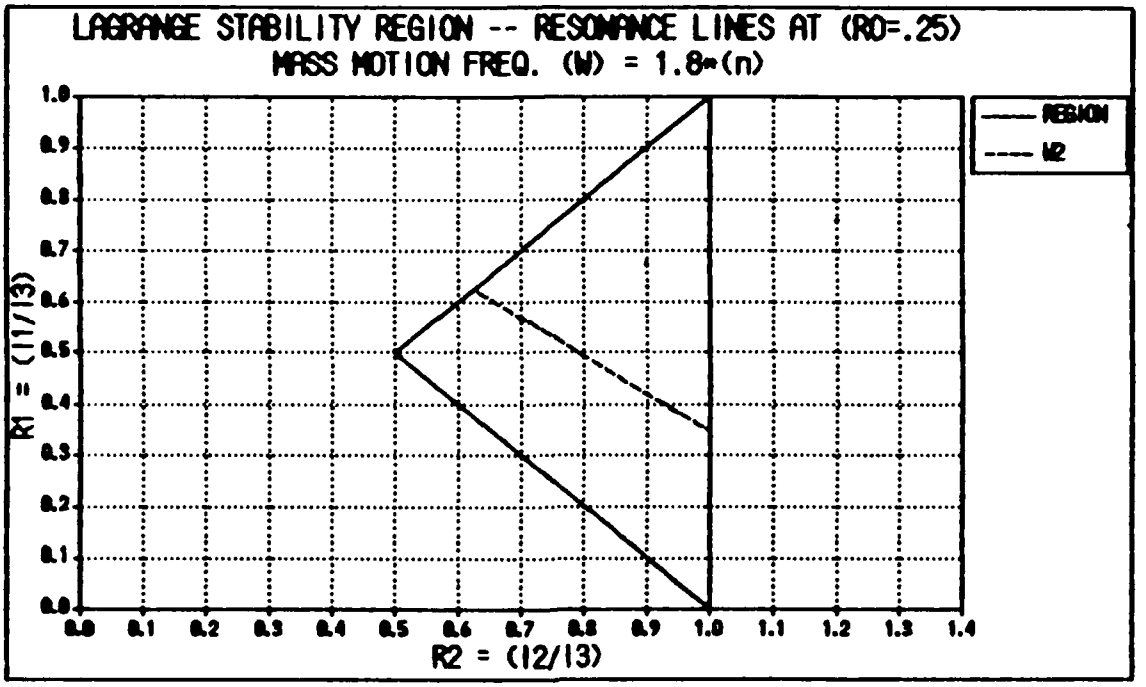

Fig. 35. Resonance Lines When (w=1.8*n)

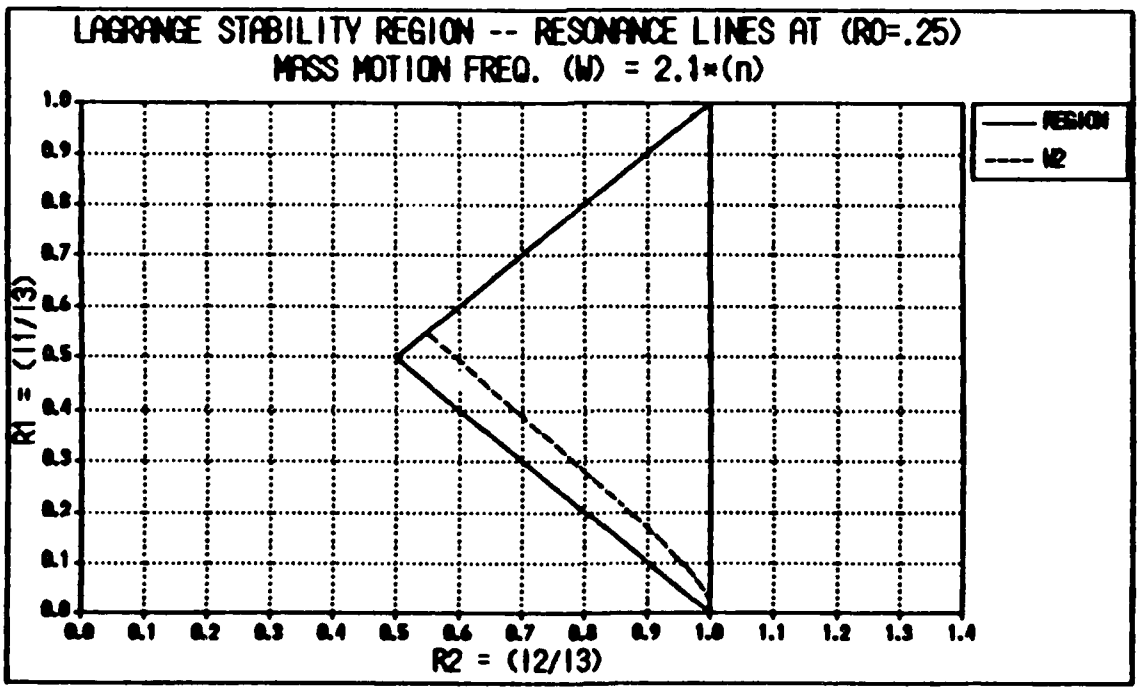

Fig. 36. Resonance Lines When (w=2.1*n)

is designed such that mass motion will occur along the $\hat{b}_1$ axis with a $1.0*n \leq \omega \leq 2.3*n$, then configurations which lie in the neighborhood of the resonance lines should be avoided or at least analyzed further with appropriate consideration given towards compensation.

VII. Conclusions and Recommendations

In order to make conclusions and recommendations on the analyses provided in Chapters V and VI, a composite of the results obtained in both chapters is formed. To accomplish this task, some ground rules are established.

In the pitch analysis conducted in Chapter V, two analytical methods and the numerical solutions were compared. Each method predicted a different instability zone and each method existed throughout a different range of mass motion frequencies (ω). Since neither analytical method exhibited superior qualities relative to the other, no preferred method was picked. Therefore, in order to simplify the overall analysis, the Mathieu analytical method is used to represent the pitch analysis because it was the most conservative and it existed over the largest range of applicable ω values.

In the roll/yaw analysis conducted in Chapter VI, resonance lines were determined for different values of ω. In addition, a band around each resonance line was found to exist. Because no analytical method is developed in Chapter V to determine a specific bandwidth, the composite analysis uses only the actual resonance lines.

When the findings from Chapters V and VI are combined under the ground rules stated above, the result is a composite of instability regions as a function of ω. Figs.

(37) and (38) show all the r_1, r_2 combinations that lead to unstable motion for the given mass motion frequency (ω).

Conclusions

A detailed discussion of the different analytical methods used in the pitch and roll/yaw analyses, along with the presentation of results, is located at the end of each of the respective chapters. Overall, the following conclusions can be drawn:

1. For the problem of a simple, gravity-gradient stabilized rigid body, the addition of mass motion results in time varying moments of inertia being introduced into the equations of motion.

2. The mass motion must be periodic and continuous over many orbital periods to induce parametric excitation.

3. A composite of the pitch and roll/yaw instability predictions when the mass motion is along the $\hat{b}_1$ axis yields the following: (1) for $1.0*n \leq \omega < 1.5*n$, there exists a zone of pitch instability along with two roll/yaw resonance lines; (2) for $1.5*n \leq \omega \leq 1.8*n$, there exists a zone of pitch instability along with one roll/yaw resonance line; (3) for $1.8*n < \omega < 2.3*n$, there exists one roll/yaw resonance line; (4) for $\omega \geq 2.3*n$, no predicted instabilities exist.

4. Mathieu and Hill analyses of the linearized pitch

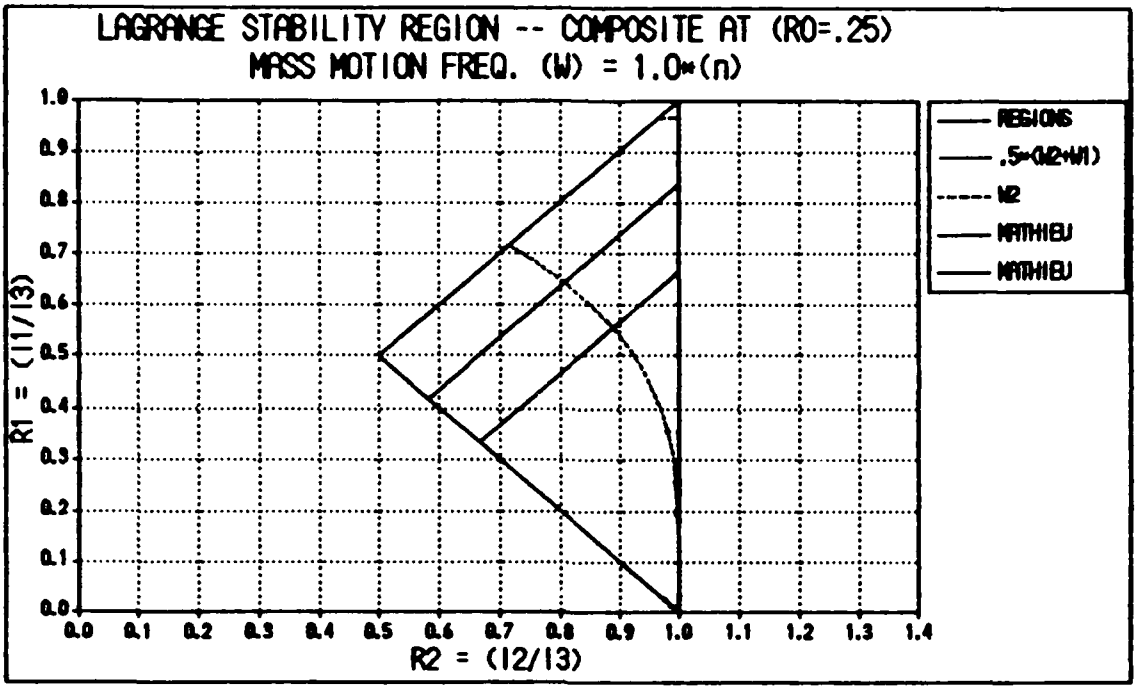

Fig. 37. Composite of All Unstable Space Station Configurations at (w=1.0*n) and (r_o=.25)

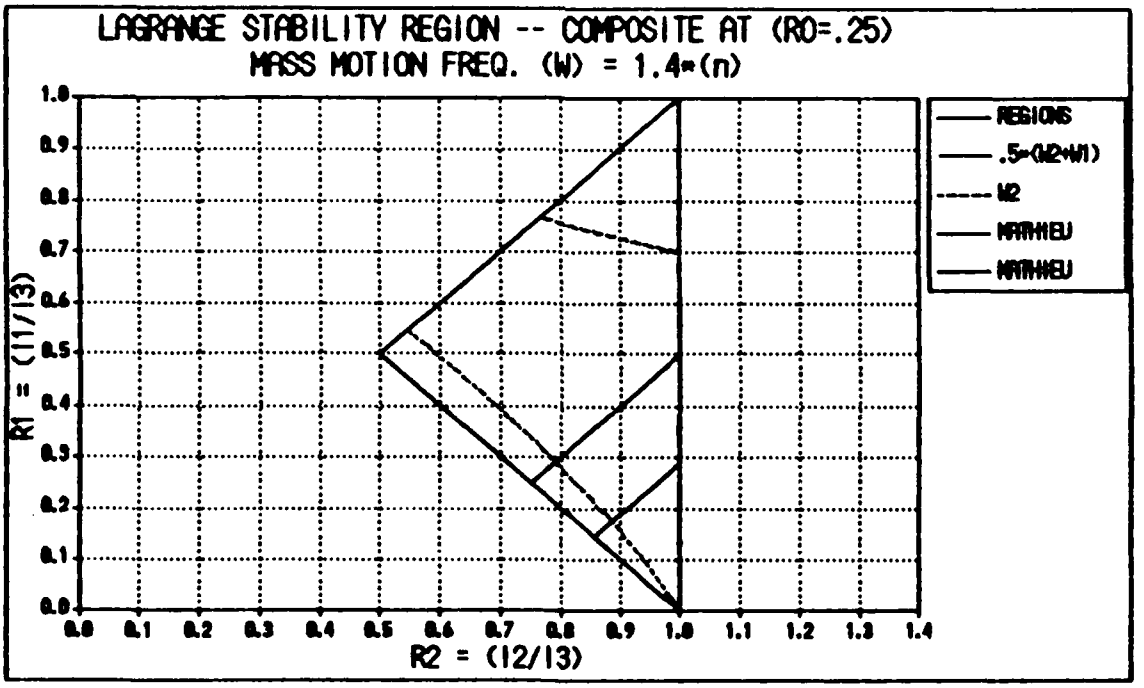

Fig. 38. Composite of All Unstable Space Station Configurations at (w=1.4*n) and (r_o=.25)

equation provide a 1st order prediction of unstable space station configurations resulting from mass motion. These methods should be used as a guide to establish a more precise location of unstable configurations using the nonlinear equations.

Recommendations

The following recommendations for further study are suggested:

1. Study of the problem of mass translation along other axes (i.e. $\hat{b}_2$ or $\hat{b}_3$) may provide the potential for additional information gain.
2. Introduction of other forcing functions, like eccentricity or the rotation of internal mass, to the rigid body problem is recommended.
3. Study of a more realistic mass motion problem that includes flexibility effects along with eccentricity for a specific configuration (i.e. proposed) is recommended.
4. Further study is recommended to better predict the roll/yaw instability regions by determining a mathematical approximation to the bandwidths around the resonance lines.

Appendix A

Equations of Motion Using Euler Parameters

As stated in Chapter III, quaternions are a more efficient parameterization of the attitude position of a spacecraft than Euler angles. The reason for this is that they are more compact than the direction cosine matrix. Quaternions require less computational time in simulations since there are only four parameters instead of nine and because they involve fewer trigonometric functions.

(Wertz, 1980: 512) describes the time differentiation of quaternions as

$$\frac{d}{dt}[\underline{q}] = (1/2)Z\underline{q} \tag{A-1}$$

where Z is the skew-symmetric matrix

$$Z = \begin{bmatrix} 0 & w_w & -w_v & w_u \\ -w_w & 0 & w_u & w_v \\ w_v & -w_u & 0 & w_w \\ -w_u & -w_v & -w_w & 0 \end{bmatrix} \tag{A-2}$$

and

$$\underline{q} = \begin{Bmatrix} q_1 \\ q_2 \\ q_3 \\ q_4 \end{Bmatrix} \tag{A-3}$$

and w_u, w_v, and w_w are the components of the angular velocity ${}^{O}\underline{w}^{B}$ expressed in the principal body basis. Since,

$$ {}^{I}\underline{w}^{B} = {}^{I}\underline{w}^{O} + {}^{O}\underline{w}^{B} \qquad \text{(A-4)} $$

or,

$$ \begin{Bmatrix} w_1 \\ w_2 \\ w_3 \end{Bmatrix} = \begin{Bmatrix} A_{13}n + w_u \\ A_{23}n + w_v \\ A_{33}n + w_w \end{Bmatrix} \qquad \text{(A-5)} $$

Solve for w_u, w_v, and w_w, and substitute them into Eq. (A-1) to get

$$ \dot{q}_1 = (1/2)(q_2 w_w - q_3 w_v + q_4 w_u) \qquad \text{(A-6a)} $$

$$ \dot{q}_2 = (1/2)(-q_1 w_w + q_3 w_u + q_4 w_v) \qquad \text{(A-6b)} $$

$$ \dot{q}_3 = (1/2)(q_1 w_v - q_2 w_u + q_4 w_w) \qquad \text{(A-6c)} $$

$$ \dot{q}_4 = (1/2)(-q_1 w_u - q_2 w_v - q_3 w_w) \qquad \text{(A-6d)} $$

Eqs. (A-6) can be rewritten as

$$ \dot{q}_1 = (1/2)[q_2(w_3 - A_{33}n) - q_2(w_2 - A_{23}n) + q_4(w_1 - A_{13}n)] \qquad \text{(A-7a)} $$

$$ \dot{q}_2 = (1/2)[-q_1(w_3 - A_{33}n) + q_3(w_1 - A_{13}n) + q_4(w_2 - A_{23}n)] \qquad \text{(A-7b)} $$

$$ \dot{q}_3 = (1/2)[q_1(w_2 - A_{23}n) - q_2(w_1 - A_{13}n) + q_4(w_3 - A_{33}n)] \qquad \text{(A-7c)} $$

$$ \dot{q}_4 = (1/2)[-q_1(w_1 - A_{13}n) - q_2(w_2 - A_{23}n) - q_3(w_3 - A_{33}n)] \qquad \text{(A-7d)} $$

Eqs. (A-7) are the equivalent set of kinematic equations to be solved simultaneously with Eqs. (1), (2), and (3) instead of Eqs. (17). In addition to Eqs. (A-7), the following relations are needed:

$$ q_1 = (1/4q_4)(A_{23} - A_{32}) \qquad \text{(A-8a)} $$

$$ q_2 = (1/4q_4)(A_{31} - A_{13}) \qquad \text{(A-8b)} $$

$$ q_3 = (1/4q_4)(A_{12} - A_{21}) \qquad \text{(A-8c)} $$

$$q_4 = (1/2)(1+A_{11}+A_{22}+A_{33}+A_{44})^{.5} \qquad \text{(A-8d)}$$

which give Euler parameters in terms of the elements of the direction cosine matrix A. Similarly, A in terms of $\underline{q}$ can be seen to be

$$A(\underline{q}) = \begin{bmatrix} q_1^2-q_2^2-q_3^2+q_4^2 & 2(q_1q_2+q_3q_4) & 2(q_1q_3-q_2q_4) \\ 2(q_1q_2-q_3q_4) & -q_1^2+q_2^2-q_3^2+q_4^2 & 2(q_2q_3+q_1q_4) \\ 2(q_1q_3+q_2q_4) & 2(q_2q_3-q_1q_4) & -q_1^2-q_2^2+q_3^2+q_4^2 \end{bmatrix} \qquad \text{(A-9)}$$

Appendix B

Expansion of Periodic Coefficient

The moments of inertia about the composite center of mass of a body that is symmetric about the yaw axis and has mass movement along the yaw axis, can be described by

$$I_1 = I_{01} \tag{B-1a}$$

$$I_2 = I_{02} + M\,[(L/2)\sin(\omega t)]^2 \tag{B-1b}$$

$$I_3 = I_{03} + M\,[(L/2)\sin(\omega t)]^2 \tag{B-1c}$$

where M is the reduced mass of the moving element. If the space station assumes the form of a dumbbell satellite, for example, $M = [m_e m_s/(m_e+m_s)]$ where m_e is the mass of the moving element and m_s is the mass of one of the spheres. I_{01}, I_{02}, and I_{03}, are the principal moments of inertia about the center of mass of a generic space station without the moving mass. Time derivatives of Eqs. (B-1) yields

$$\dot{I} = \dot{I}_2 = \dot{I}_3 = \frac{1}{2}\,[\omega M L^2 \sin(\omega t)\cos(\omega t)] \tag{B-2}$$

Inserting Eq. (B-2) into Eq. (37) gives us

$$P(t) = .5\left[\frac{.5\omega M L^2 \sin(\omega t)\cos(\omega t)}{I_{03} + .25 M L^2 \sin^2(\omega t)}\right] \tag{B-3}$$

Squaring P(t) gives

$$P^2(t) = .25\left[\frac{.25\omega^2 M^2 L^4 \sin^2(\omega t)\cos^2(\omega t)}{(I_{03} + M\,[(L/2)\sin(\omega t)]^2)^2}\right] \tag{B-4}$$

Taking a time derivative of P(t) yields

$$\dot{P}(t) = .25\ (\omega ML^2)[\omega C\cos^2(\omega t) - \omega C\sin^2(\omega t) - .5\omega ML^2C^2\sin^2(\omega t)\cos^2(\omega t)] \quad \text{(B-5)}$$

where $C = [I_{03} + .25ML^2\sin^2(\omega t)]^{-1}$.

Inserting Eqs. (B-1) into Eq. (38) will give

$$R^2(t) = 3n^2C\ [I_{02} + .25ML^2\sin^2(\omega t) - I_{01}] \quad \text{(B-6)}$$

Substituting Eqs. (B-4), (B-5), and (B-6) into the transformed pitch equation, Eq. (41), yields

$$\ddot{z} + \left\{3n^2C\left[I_{02} + .25ML^2\sin^2(\omega t) - I_{01}\right] - \frac{1}{16}\,C^2\omega^2M^2L^4\sin^2(\omega t)\cos^2(\omega t) - \frac{1}{4}\,\omega ML^2\left[C\omega\cos^2(\omega t) - C\omega\sin^2(\omega t) - \frac{1}{2}\,\omega ML^2C^2\sin^2(\omega t)\cos^2(\omega t)\right]\right\} z = 0. \quad \text{(B-7)}$$

The term $C = [I_{03} + .25ML^2\sin^2(\omega t)]^{-1}$ can be written in the form

$$C = \left(\frac{1}{I_{03}}\right)(1 + x)^{-1} \quad \text{(B-8)}$$

where $x = r_0\sin^2(\omega t)$ and $r_0 = \frac{ML^2}{4I_{03}}$.

By using the binomial series for $(1 + x)^{-1}$ and only keeping the first three terms we get

$$C = \left(\frac{1}{I_{03}}\right)(1 - x + x^2) \quad \text{(B-9)}$$

$$C^2 = \left(\frac{1}{I_{03}}\right)^2(1 - 2x + 3x^2) \quad \text{(B-10)}$$

The three term approximation for the binomial series comes from the fact that r_0 has a maximum value of .25, as discussed on page 27 of Chapter V. Substituting (B-9) and

(B-10) into (B-7) yields

$$\ddot{z} + \left\{\frac{3n^2}{I_{03}}\left[I_{02} + .25ML^2\sin^2(\omega t) - I_{01}\right](1 - x + x^2) - \right.$$

$$\frac{\omega^2 M^2 L^4}{16 I_{03}^2}\sin^2(\omega t)\cos^2(\omega t)(1 - 2x + 3x^2) - \qquad \text{(B-11)}$$

$$\frac{\omega^2 ML^2}{4I_{03}}\left[\cos^2(\omega t)(1 - x + x^2) - \sin^2(\omega t)(1 - x + x^2) - \right.$$

$$\left.\left.\frac{ML^2}{2I_{03}}\sin^2(\omega t)\cos^2(\omega t)(1 - 2x + 3x^2)\right]\right\} z = 0.$$

By defining the terms

$$A' = \frac{\omega^2 M^2 L^4}{16 I_{03}^2}\sin^2(\omega t)\cos^2(\omega t)$$

$$= \omega^2 r_0^2 \sin^2(\omega t)\cos^2(\omega t)$$

$$B' = \frac{\omega^2 ML^2}{4I_{03}} = \omega^2 r_0$$

$$C' = (\cos^2(\omega t) - \sin^2(\omega t)) = \cos(2\omega t)$$

$$D' = \frac{ML^2}{2I_{03}}\sin^2(\omega t)\cos^2(\omega t) = 2r_0\sin^2(\omega t)\cos^2(\omega t)$$

and

$$B'C' = \omega^2 r_0 \cos(2\omega t)$$

$$B'D' = 2\omega^2 r_0^2 \sin^2(\omega t)\cos^2(\omega t)$$

Eq. (B-11) becomes

$$\ddot{z} + \left\{\frac{3n^2}{I_{03}}\left[I_{02} + .25ML^2\sin^2(\omega t) - I_{01}\right](1 - x + x^2) - \right. \qquad \text{(B-12)}$$

$$\left. A'(1-2x+3x^2) - B'C'(1-x+x^2) + B'D'(1-2x+3x^2)\right\} z = 0.$$

But $3n^2\left(\frac{I_{02}}{I_{03}}\right) = 3n^2 r_2$; $3n^2\left(\frac{I_{01}}{I_{03}}\right) = 3n^2 r_1$

and $3n^2\frac{ML^2}{4I_{03}}\sin^2(\omega t) = 3n^2 r_0 \sin^2(\omega t)$

Therefore, Eq. (B-12) becomes

$$\ddot{z} + \Big\{3n^2 r_2 + 3n^2 r_0 \sin^2(\omega t) - 3n^2 r_1 - 3n^2 r_2 x - 3n^2 r_0 \sin^2(\omega t)x + 3n^2 r_1 x + 3n^2 r_2 x^2 + 3n^2 r_0 \sin^2(\omega t)x^2 - 3n^2 r_1 x^2 - A' + 2A'x - 3A'x^2 - B'C' + B'C'x - B'C'x^2 + B'D' - 2B'D'x + 3B'D'x^2\Big\}z = 0 \qquad \text{(B-13)}$$

By recalling that $x = r_0 \sin^2(\omega t)$ and grouping like terms, Eq. (B-13) becomes

$$\begin{aligned}\ddot{z} + \Big\{&3n^2 r_2 - 3n^2 r_1 + \left(3n^2 r_0 - 3n^2 r_2 r_0 + 3n^2 r_1 r_0\right)\sin^2(\omega t) \\ &+ \left(-3n^2 r_0 + 3n^2 r_2 r_0^2 - 3n^2 r_1 r_0^2\right)\sin^4(\omega t) + 3n^2 r_0^3 \sin^6(\omega t) \\ &+ \left(-\omega^2 r_0^2 + 2\omega^2 r_0^2\right)\sin^2(\omega t)\cos^2(\omega t) \\ &+ \left(-2\omega^2 r_0^3\right)\sin^4(\omega t)\cos^2(\omega t) + \left(3\omega^2 r_0^4\right)\sin^6(\omega t)\cos^2(\omega t) \\ &+ \left(\omega^2 r_0^2\right)\sin^2(\omega t)\cos(2\omega t) - \left(\omega^2 r_0^3\right)\sin^4(\omega t)\cos(2\omega t) \\ &- \omega^2 r_0 \cos(2\omega t)\Big\} z = 0. \end{aligned} \qquad \text{(B-14)}$$

By using the trigonometric identities

$$\sin^2(\omega t) = 1/2 - (1/2)\cos(2\omega t)$$

$$\sin^4(\omega t) = 3/8 - (1/2)\cos(2\omega t) + (1/8)\cos(4\omega t)$$

$$\sin^6(\omega t) = (5/16) - (15/32)\cos(2\omega t) + (3/16)\cos(4\omega t) - (1/32)\cos(6\omega t)$$

$$\cos^2(\omega t) - \sin^2(\omega t) = \cos(2\omega t)$$

$$\cos^2(\omega t)\sin^2(\omega t) = 1/8 - (1/8)\cos(4\omega t)$$

and grouping like terms of $\cos(2\omega t)$, $\cos(4\omega t)$, $\cos(6\omega t)$, and $\cos(8\omega t)$, Eq. (B-14) can be written as

$$\ddot{z} + \left[a_T + 16q_1\cos(2T) + 16q_2\cos(4T) + 16q_3\cos(6T) + 16q_4\cos(8T)\right] z = 0. \quad \text{(B-15)}$$

in which the independent variable has been changed from t to T through the definition $T = \omega t$, and the variables a_T, q_1, q_3, and q_4 are given by

$$a_T = (9/8)(n/\omega)^2 r_0^2 (r_2 - r_1 - 1) - (3/2)(n/\omega)^2 r_0 (r_2 - r_1 - 1) + 3(n/\omega)^2 (r_2 - r_1) + (15/16)(n/\omega)^2 r_0^3 + (15/128) r_0^4 + (1/8) r_0^3 - (1/8) r_0^2 \quad \text{(B-16)}$$

$$q_1 = (1/16)\left[(-3/2)(n/\omega)^2 r_0^2 (r_2 - r_1 - 1) + (3/2)(n/\omega)^2 r_0 (r_2 - r_1 - 1) - (45/32)(n/\omega)^2 r_0^3 - (3/32) r_0^4 - (3/8) r_0^3 + (1/2) r_0^2 - r_0\right] \quad \text{(B-17)}$$

$$q_2 = (1/16)\left[(3/8)(n/\omega)^2 r_0^2 (r_2 - r_1 - 1) + (9/16)(n/\omega)^2 r_0^3 - (3/32) r_0^4 + (3/8) r_0^3 - (3/8) r_0^2\right] \quad \text{(B-18)}$$

$$q_3 = (1/16)\left[-(3/32)(n/\omega)^2 r_0^3 - (3/32) r_0^4 - (1/8) r_0^3\right] \quad \text{(B-19)}$$

$$q_4 = (1/16)\left[-(3/128) r_0^4\right] \quad \text{(B-20)}$$

Appendix C

Expansion of the Roll/Yaw Periodic Coefficient

The roll and yaw equations of attitude motion were shown in Chapter IV to be

$$\ddot{y} + \left(\frac{I_3 - I_2 - I_1}{I_1}\right) n\dot{r} + \left(\frac{I_3 - I_2}{I_1}\right) n^2 y = 0 \qquad \text{(C-1)}$$

$$\ddot{r} - \left(\frac{I_3 - I_2 - I_1}{I_2}\right) n\dot{y} + 4\left(\frac{I_3 - I_1}{I_2}\right) n^2 r + \left(\frac{\dot{I}_2}{I_2}\right)(\dot{r} + yn) = 0 \qquad \text{(C-2)}$$

where each coefficient containing I is a function of time and contributes to exciting the attitude motion of the space station. These terms can be expanded in a manner similar to the pitch periodic coefficient in Appendix B.

$\left(\frac{\dot{I}_2}{I_2}\right)$ Coefficient

By recalling from Appendix B that

$$I_2 = I_{02} + M\,[(L/2)\sin(\omega t)]^2$$

and

$$\dot{I} = \dot{I}_2 = \frac{1}{2}\,[\omega ML^2 \sin(\omega t)\cos(\omega t)]$$

the perturbation term becomes

$$\left(\frac{\dot{I}_2}{I_2}\right) = \left[\frac{.5\omega ML^2 \sin(\omega t)\cos(\omega t)}{I_{03} + .25ML^2 \sin^2(\omega t)}\right] \qquad \text{(C-3)}$$

If we let $D = \left(I_2\right)^{-1}$, then

$$D = \left(\frac{1}{I_{02}}\right)\left(\frac{1}{1 + .25ML^2/I_{02}\sin^2(\omega t)}\right)$$

This can be written as

$$D = \left(\frac{1}{I_{02}}\right)(1 + x)^{-1} \qquad (C\text{-}4)$$

where $x = r_0'\sin^2(\omega t)$ and $r_0' = \frac{ML^2}{4I_{02}}$.

By substituting Eq. (C-4) into (C-3) we get

$$\left(\frac{\dot{I}_2}{I_2}\right) = \left[\frac{.5\omega ML^2}{I_{02}}\right]\sin(\omega t)\cos(\omega t)(1 - x + x^2) \qquad (C\text{-}5)$$

Expanding further,

$$\left(\frac{\dot{I}_2}{I_2}\right) = 2\omega r_0'\left[\sin(\omega t)\cos(\omega t) - \sin(\omega t)\cos(\omega t)\, x + \sin(\omega t)\cos(\omega t)\, x^2\right] \qquad (C\text{-}6)$$

and

$$\left(\frac{\dot{I}_2}{I_2}\right) = 2\omega r_0'\left[\sin(\omega t)\cos(\omega t) - \sin(\omega t)\cos(\omega t) r_0'\sin^2(\omega t) + \sin(\omega t)\cos(\omega t)\left(r_0'\sin^2(\omega t)\right)^2\right] \qquad (C\text{-}7)$$

Using similar trigonometric identities to those used in Appendix B, Eq. (C-7) becomes

$$\left(\frac{\dot{I}_2}{I_2}\right) = 2\omega r_0'\left[A\sin(2\omega t) + B\sin(3\omega t) + C\sin(4\omega t) + D\sin(5\omega t) + E\sin(6\omega t)\right] \qquad (C\text{-}8)$$

where

$$A = \left((1/2) - r_0'/4 + (r_0'/2)^2\right)$$

$$B = \left(-3r_0'^2/32\right)$$

$$C = \left(r_0'/8 - r_0'^2/32\right)$$

$$D = \left(-3r_0'^2/32\right)$$

$$E = \left(r_0'^2/32\right)$$

Since $r_2 = \left(\frac{I_{02}}{I_{03}}\right)$ and $r_0 = \frac{ML^2}{4I_{03}}$, then r_0' becomes $r_0' = \frac{r_0}{r_2}$.

Because r_0' has a maximum value of .25, then all terms that are of higher order than $\left(r_0'\right)^1$ can be ignored.

Eq. (C-8) then becomes

$$\left(\frac{\dot{I}_2}{I_2}\right) \approx 2\omega r_0'(1/2)\sin(2\omega t) = \omega r_0'\sin(2\omega t) = \omega \frac{r_0}{r_2} \sin(2\omega t) \qquad (C\text{-}9)$$

Substituting Eq. (C-9) into Eq. (C-2) yields at this point

$$\ddot{r} - \left(\frac{I_3 - I_2 - I_1}{I_2}\right) n\dot{y} + 4\left(\frac{I_3 - I_1}{I_2}\right) n^2 r + 2\varepsilon \left(n\omega y + \omega \dot{r}\right)\sin(2\omega t) = 0 \qquad (C\text{-}10)$$

where $2\varepsilon = \frac{r_0}{r_2}$.

$\left(\frac{I_3 - I_2 - I_1}{I_2}\right)$ Coefficient

Recalling again the relationships for I_2 and I_3 from Appendix B, the coefficient becomes

$$\left(\frac{I_3 - I_2 - I_1}{I_2}\right) = \left[\frac{I_{03} - I_{02} - I_{01}}{I_{02} + .25ML^2\sin^2(\omega t)}\right] \qquad (C\text{-}11)$$

$$= \left(I_{03} - I_{02} - I_{01}\right) D$$

where D is defined in Eq. (C-4).

By defining $\lambda 2 = \left(\frac{I_{03} - I_{02} - I_{01}}{I_{02}}\right) = \frac{1 - r_2 - r_1}{r_2}$

Eq. (C-11) becomes

$$\left(\frac{I_3 - I_2 - I_1}{I_2}\right) = \lambda 2\ (1 - x + x^2) \qquad (C\text{-}12)$$

$$= \lambda 2 - \lambda 2\ r_0' \sin^2(\omega t) + \lambda 2\ r_0'^2 \sin^4(\omega t)$$

Using trigonometric relationships, Eq. (C-12) becomes

$$\left(\frac{I_3 - I_2 - I_1}{I_2}\right) = \lambda 2 \left(1 - \frac{r_0'}{2} + \frac{3r_0'}{8}\right) \qquad (C\text{-}13)$$

$$+ \lambda 2 \left(\frac{r_0'}{2} + \frac{r_0'^2}{2}\right)\cos(2\omega t) + \lambda 2 \left(\frac{r_0'^2}{8}\right)\cos(4\omega t)$$

Recalling that $r_0' = \frac{r_0}{r_2} = 2\epsilon$, Eq. (C-13) can be written as

$$\left(\frac{I_3 - I_2 - I_1}{I_2}\right) = \lambda 2 \left(1 - \epsilon + \frac{3}{2}\epsilon^2\right) + \lambda 2 \left(\epsilon - \frac{1}{2}\epsilon^2\right)\cos(2\omega t)$$

$$+ \lambda 2 \left(\frac{1}{2}\epsilon^2\right)\cos(4\omega t) \qquad (C\text{-}14)$$

By ignoring terms that are of higher order than ϵ^1, Eq. (C-14) can be simplified to

$$\left(\frac{I_3 - I_2 - I_1}{I_2}\right) = \lambda 2 \left(1 - \epsilon\right) + \lambda 2\ \epsilon \cos(2\omega t) \qquad (C\text{-}15)$$

$\left(\frac{I_3 - I_1}{I_2}\right)$ Coefficient

This term can be written as

$$\left(\frac{I_3 - I_1}{I_2}\right) = \left[\frac{I_{03} + .25ML^2\sin^2(\omega t) - I_{01}}{I_{02} + .25ML^2\sin^2(\omega t)}\right]$$

$$= \left(\frac{1}{r_2} - \frac{r_1}{r_2} + x\right)\left(1 - x + x^2\right) \qquad \text{(C-16)}$$

By defining $\alpha 2 = \left(\frac{1-r_1}{r_2}\right)$, Eq. (C-16) becomes

$$\left(\frac{I_3 - I_1}{I_2}\right) = \left(\alpha 2 + x\right)\left(1 - x + x^2\right) \qquad \text{(C-17)}$$

$$= \alpha 2 + (1-\alpha 2)r_0'\sin^2(\omega t) + (\alpha 2 - 1)\, r_0'^2\sin^4(\omega t) + r_0'^3\sin^6(\omega t)$$

Using trigonometric relationships, Eq. (C-17) becomes

$$\left(\frac{I_3 - I_1}{I_2}\right) = \left(\alpha 2 + \epsilon - \alpha 2\epsilon + \frac{3}{2}\alpha 2\epsilon^2 - \frac{3}{2}\epsilon^2 + \frac{5}{2}\epsilon^3\right)$$

$$+ \left(\alpha 2\epsilon - \epsilon - 2\alpha 2e^2 + 2\epsilon^2 - \frac{15}{4}\epsilon^3\right)\cos(2\omega t)$$

$$+ \left(\frac{1}{2}\alpha 2e^2 - \frac{1}{2}\epsilon^2 + \frac{3}{2}\epsilon^3\right)\cos(4\omega t)$$

$$+ \left(-\frac{1}{4}\epsilon^3\right)\cos(6\omega t) \qquad \text{(C-18)}$$

Ignoring terms of higher order than ϵ^1 yields

$$\left(\frac{I_3 - I_1}{I_2}\right) = \left(\alpha 2 + \epsilon(1-\alpha 2)\right) + \left(\epsilon(\alpha 2 - 1)\cos(2\omega t)\right) \qquad \text{(C-19)}$$

$\left(\frac{I_3 - I_2 - I_1}{I_1}\right)$ and $\left(\frac{I_3 - I_2}{I_1}\right)$ Coefficients

The expansion of these coefficients yields

$$\left(\frac{I_3 - I_2 - I_1}{I_1}\right) = \left(\frac{I_{03} - I_{02} - I_{01}}{I_{01}}\right) = \left(\frac{1 - r_2 - r_1}{r_1}\right) \qquad (C\text{-}20)$$

$$\left(\frac{I_3 - I_2}{I_1}\right) = \left(\frac{I_{03} - I_{02}}{I_{01}}\right) = \left(\frac{1 - r_2}{r_1}\right) \qquad (C\text{-}21)$$

As a result, Eq. (c-1) remains essentially the same and does not contribute to the excitation of the system.

$$\ddot{y} + \left(\frac{I_{03} - I_{02} - I_{01}}{I_{01}}\right) n\dot{r} + \left(\frac{I_{03} - I_{02}}{I_{01}}\right) n^2 y = 0 \qquad (C\text{-}22)$$

Summary

Substituting Eqs. (C-15) and (C-19) into Eq. (C-10) yields

$$\ddot{r} - \lambda 2\left(1 - \epsilon\right) n\dot{y} + 4\left(\alpha 2 + \epsilon(1-\alpha 2)\right) n^2 r + \\ + 2\epsilon\left(n\omega y + \omega\dot{r}\right)\sin(2\omega t) = 0 \qquad (C\text{-}23) \\ + 2\epsilon\left(-\frac{1}{2}\lambda 2 n\dot{y} + 2(\alpha 2 - 1) n^2 r\right)\cos(2\omega t)$$

Appendix D

Appendix D contains the Fortran computer program used to numerically integrateEqs. (17a), (17b), (17c), (a-7a), (A-7b), (A-7c), and (A-7d).

```
      program nonlinear
c
c
      common /ham/ t,x(7,4),f(7,4),errest(7),n,h,i01,i02,i03,m,ll,
     +             w,e,sma,u,n4
      double precision t,x,f,errest,h,i01,i02,i03,m,ll,w,e,sma,u,n4,
     +                 z,phi,theta,psi,phidot,thetadot,psidot,
     +                 a,check,conversion
      dimension z(7),a(3,3)
      open(unit=8,file='pitch',status='new')
      open(unit=9,file='roll',status='new')
      open(unit=10,file='yaw',status='new')
      open(unit=11,file='input1',status='old')
      open(unit=12,file='input2',status='old')
c
      tlines=0.
c
c  read in number of equations, plotted points,
c  steps between printing, and timestep
c
      read (11,5) n,nprint,nstep,t,h
5     format(3I6,2f6.2)
      write(*,*) n,nprint,nstep,t,h
c
c  read in static inertias, and m,l,w,e,sma,u,n4
c
      read(12,*) i01,i02,i03
      write(*,*) i01,i02,i03
      read(12,*) m,ll,w
      write(*,*) m,ll,w
      read(12,*) e,sma,u
      write(*,*) e,sma,u
      n4=sqrt(u/sma**3)
c
c  read in initial conditions
      read(12,*) theta,phi,psi
      write(*,*) theta,phi,psi
      read(12,*) thetadot,phidot,psidot
      write(*,*) thetadot,phidot,psidot
c
c  convert euler angles to radian measure
      conversion = 0.01745329252
      theta = theta*conversion
      phi = phi*conversion
      psi = psi*conversion
c
c  compute initial direction cosine matrix
      a(1,1) = cos(phi)*cos(theta)-sin(phi)*sin(psi)*sin(theta)
      a(1,2) = cos(phi)*sin(theta)+sin(phi)*sin(psi)*cos(theta)
      a(1,3) = -sin(phi)*cos(psi)
      a(2,1) = -cos(psi)*sin(theta)
      a(2,2) = cos(psi)*cos(theta)
```

```
      a(2,3) = sin(psi)
      a(3,1) = sin(phi)*cos(theta)+cos(phi)*sin(psi)*sin(theta)
      a(3,2) = sin(phi)*sin(theta)-cos(phi)*sin(psi)*cos(theta)
      a(3,3) = cos(phi)*cos(psi)
c
c  compute initial angular velocity ( z(5),z(6),z(7) are w1,w2,w3)
      z(5) = a(1,3)*n4-thetadot*cos(psi)*sin(phi)+psidot*cos(phi)
      z(6) = a(2,3)*n4+thetadot*sin(psi)+phidot
      z(7) = a(3,3)*n4+thetadot*cos(psi)*cos(phi)+psidot*sin(phi)
c
c  compute initial quaternion
      z(4) = 0.5*sqrt(1.+a(1,1)+a(2,2)+a(3,3))
      z(1) = (0.25/z(4))*(a(2,3)-a(3,2))
      z(2) = (0.25/z(4))*(a(3,1)-a(1,3))
      z(3) = (0.25/z(4))*(a(1,2)-a(2,1))
c
c  check sum of quaternion components squared being equal to one
      check = z(1)**2+z(2)**2+z(3)**2+z(4)**2
c
c  rename variables for haming-suitable iteration
      x(1,1) = z(1)
      x(2,1) = z(2)
      x(3,1) = z(3)
      x(4,1) = z(4)
      x(5,1) = z(5)
      x(6,1) = z(6)
      x(7,1) = z(7)
c
c     initialize haming
      nxt = 0
      call haming(nxt)
      if(nxt .ne. 0) go to 50
      write (*,1)
1     format(2x,' haming did not initialize')
      stop
c
50    continue
c
c     integrate ode....two nested loops
c
      do 200 ipr = 1,nprint
c
      do 100 istp = 1,nstep
c
c     each call to haming advances one step...
      call haming(nxt)
c
100   continue
c
c     after nstp integration steps, print current values
      z(1) = x(1,nxt)
      z(2) = x(2,nxt)
```

```
      z(3) = x(3,nxt)
      z(4) = x(4,nxt)
      z(5) = x(5,nxt)
      z(6) = x(6,nxt)
      z(7) = x(7,nxt)
c
c  compute direction cosine matrix a, euler angles, check quaternion
c  also store data for plotter
      a(1,3) = 2*(z(1)*z(3)-z(2)*z(4))
      a(2,1) = 2*(z(1)*z(2)-z(3)*z(4))
      a(2,2) = -z(1)**2+z(2)**2-z(3)**2+z(4)**2
      a(2,3) = 2*(z(2)*z(3)+z(1)*z(4))
      a(3,3) = -z(1)**2-z(2)**2+z(3)**2+z(4)**2
c
      theta = atan(-a(2,1)/a(2,2))
      psi = asin(a(2,3))
      phi = atan(-a(1,3)/a(3,3))
c
c
      thetadot = ((z(7)-a(3,3)*n4)*cos(phi)-(z(5)-a(1,3)*n4)*
     +           sin(phi))/cos(psi)
      psidot = ((z(5)-a(1,3)*n4)*cos(phi)+(z(7)-a(3,3)*n4)*sin(phi))
      phidot = (z(6)-a(2,3)*n4)-
     +         ((z(7)-a(3,3)*n4)*cos(phi)-(z(5)-a(1,3)*n4)*
     +         sin(phi))*tan(theta)
c
      check = z(1)**2+z(2)**2+z(3)**2+z(4)**2
c
      tlines=tlines+1.
      torbits=t/5250.
      write(8,13) torbits,theta
13    format(1x,f12.6,1x,f12.6)
      write(9,13) torbits,phi
      write(10,13) torbits,psi
      if(tlines .ge. 14000.) then
          close(unit=8)
          close(unit=9)
          close(unit=10)
          open(unit=8,file='pitch',status='new')
          open(unit=9,file='roll',status='new')
          open(unit=10,file='yaw',status='new')
          tlines=0.
      end if
c
200   continue
c
      stop
      end
c

      subroutine haming(nxt)
c
```

```
c     haming is an ordinary differential equations integrator
c     it is a fourth order predictor-corrector algorithm
c     which means that it carries along the last four
c     values of the state vector, and extrapolates these
c     values to obtain the next value (the prediction part)
c     and then corrects the extrapolated value to find a
c     new value for the state vector.
c
c     the value nxt in the call specifies which of the 4 values
c     of the state vector is the "next" one.
c     nxt is updated by haming automatically, and is zero on
c     the first call
c
c     the user supplies an external routine rhs(nxt) which
c     evaluates the equations of motion
c
      common /ham/ x,y(7,4),f(7,4),errest(7),n,h,i01,i02,i03,m,ll,
     +             w,e,sma,u,n4
      double precision x,y,f,errest,h,hh,xo,tol,i01,i02,i03,m,ll,
     +                 w,e,sma,u,n4
c
c     all of the good stuff is in this common block.
c     x is the independent variable ( time )
c     y(7,4) is the state vector- 4 copies of it, with nxt
c                 pointing at the next one
c     f(7,4) are the equations of motion, again four copies
c                 a call to rhs(nxt) updates an entry in f
c     errest is an estimate of the truncation error - normally not
c                 used
c     n is the number of equations being integrated
c     h is the time step
c
      tol = 1.0d-08
c     switch on starting algorithm or normal propagation
      if(nxt) 190,10,200
c
c     this is hamings starting algorithm....a predictor - corrector
c     needs 4 values of the state vector, and you only have one- the
c     initial conditions.
c     haming uses a Picard iteration (slow and painfull) to get the
c     other three.
c     if it fails, nxt will still be zero upon exit, otherwise
c     nxt will be 1, and you are all set to go
c
10    xo = x
      hh = h/2.0d+00
      call rhs(1)
      do 40 l = 2,4
      x = x + hh
      do 20 i = 1,n
20    y(i,l) = y(i,l-1) + hh*f(i,l-1)
      call rhs(l)
```

```
      x = x + hh
      do 30 i = 1,n
30    y(i,1) = y(i,1-1) + h*f(i,1)
40    call rhs(1)
      jsw = -10
50    isw = 1
      do 120 i = 1,n
      hh = y(i,1) + h*( 9.0d+00*f(i,1) + 19.0d+00*f(i,2)
     1     - 5.0d+00*f(i,3) + f(i,4) ) / 24.0d+00
      if( dabs( hh - y(i,2)) .lt. tol ) go to 70
      isw = 0
70    y(i,2) = hh
      hh = y(i,1) + h*( f(i,1) + 4.0d+00*f(i,2) + f(i,3))/3.0d+00
      if( dabs( hh-y(i,3)) .lt. tol ) go to 90
      isw = 0
90    y(i,3) = hh
      hh = y(i,1) + h*( 3.0d+00*f(i,1) + 9.0d+00*f(i,2)
     1     + 9.0d+00*f(i,3)
     1     + 3.0d+00*f(i,4) ) / 8.0d+00
      if( dabs(hh-y(i,4)) .lt. tol ) go to 110
      isw = 0
110   y(i,4) = hh
120   continue
      x = xo
      do 130 l = 2,4
      x = x + h
130   call rhs(l)
      if(isw) 140,140,150
140   jsw = jsw + 1
      if(jsw) 50,280,280
150   x = xo
      isw = 1
      jsw = 1
      do 160 i = 1,n
160   errest(i) = 0.0
      nxt = 1
      go to 280
190   jsw = 2
      nxt = iabs(nxt)
c
c     this is hamings normal propagation loop -
c
200   x = x + h
      npl = mod(nxt,4) + 1
      go to (210,230),isw
c     permute the index nxt modulo 4
210   go to (270,270,270,220),nxt
220   isw = 2
230   nm2 = mod(npl,4) + 1
      nml = mod(nm2,4) + 1
      npo = mod(nml,4) + 1
c
```

```
c     this is the predictor part
c
      do 240 i = 1,n
      f(i,nm2) = y(i,npl) + 4.0d+00*h*( 2.0d+00*f(i,npo) - f(i,nm1)
     1     + 2.0d+00*f(i,nm2) ) / 3.0d+00
240   y(i,npl) = f(i,nm2) - 0.925619835d+00 * errest(i)
c
c     now the corrector - fix up the extrapolated state
c     based on the better value of the equations of motion
c
      call rhs(npl)
      do 250 i = 1,n
      y(i,npl) = ( 9.0d+00*y(i,npo) - y(i,nm2)
     1     + 3.0d+00*h*( f(i,npl)
     1     + 2.0d+00*f(i,npo) - f(i,nm1) ) ) / 8.0d+00
      errest(i) = f(i,nm2) - y(i,npl)
250   y(i,npl) = y(i,npl) + 0.0743801653d+00 * errest(i)
      go to (260,270),jsw
260   call rhs(npl)
270   nxt = npl
280   return
      end

      subroutine rhs(nxt)
c
c     rhs is the right - hand - side subroutine, customized
c     to the particular set of odes being integrated
c
      common /ham/ t,x(7,4),f(7,4),errest(7),n,h,i01,i02,i03,m,l1,
     +             w,e,sma,u,n4
      double precision t,x,f,errest,h,i01,i02,i03,m,l1,w,e,sma,u,
     +                 n4,z,a,r1,r,n1,n2,n3,i1,i2,i3,b
      dimension z(7),r(3),a(3,3)
c
c  variable description
c
c  calculate current values of inertia
      i1 = i01
      i2 = i02 + m*((.5*l1*sin(w*t))**2)
      i3 = i03 + m*((.5*l1*sin(w*t))**2)
c
c  convert variable names
      z(1) = x(1,nxt)
      z(2) = x(2,nxt)
      z(3) = x(3,nxt)
      z(4) = x(4,nxt)
      z(5) = x(5,nxt)
      z(6) = x(6,nxt)
      z(7) = x(7,nxt)
c
c  calculate direction cosine matrix
      a(1,1) = z(1)**2 - z(2)**2 - z(3)**2 + z(4)**2
```

```
      a(1,2) = 2*(z(1)*z(2) + z(3)*z(4))
      a(1,3) = 2*(z(1)*z(3) - z(2)*z(4))
      a(2,1) = 2*(z(1)*z(2) - z(3)*z(4))
      a(2,2) = -z(1)**2 + z(2)**2 - z(3)**2 + z(4)**2
      a(2,3) = 2*(z(2)*z(3) + z(1)*z(4))
      a(3,1) = 2*(z(1)*z(3) + z(2)*z(4))
      a(3,2) = 2*(z(2)*z(3) - z(1)*z(4))
      a(3,3) = -z(1)**2 - z(2)**2 + z(3)**2 + z(4)**2
c
c  compute r1 (length of orbit)
      r1 = sma*(1 - e*cos(n4*t))
c
c  calculate radius vector components
      r(1) = a(1,1)*r1
      r(2) = a(2,1)*r1
      r(3) = a(3,1)*r1
c
c  calculate gravity gradient torque n
      b = (3*u)/(r1**5)
      n1 = b*(i3-i2)*r(2)*r(3)
      n2 = b*(i1-i3)*r(1)*r(3)
      n3 = b*(i2-i1)*r(1)*r(2)
c
c  write equations of motion
c
      f(1,nxt) = 0.5*(x(2,nxt)*(x(7,nxt)-a(3,3)*n4)-x(3,nxt)*
     +    (x(6,nxt)-a(2,3)*n4)+x(4,nxt)*(x(5,nxt)-a(1,3)*n4))
c
      f(2,nxt) = 0.5*(-x(1,nxt)*(x(7,nxt)-a(3,3)*n4)+x(3,nxt)*
     +    (x(5,nxt)-a(1,3)*n4)+x(4,nxt)*(x(6,nxt)-a(2,3)*n4))
c
      f(3,nxt) = 0.5*(x(1,nxt)*(x(6,nxt)-a(2,3)*n4)-x(2,nxt)*
     +    (x(5,nxt)-a(1,3)*n4)+x(4,nxt)*(x(7,nxt)-a(3,3)*n4))
c
      f(4,nxt) = 0.5*(-x(1,nxt)*(x(5,nxt)-a(1,3)*n4)-x(2,nxt)*
     +    (x(6,nxt)-a(2,3)*n4)-x(3,nxt)*(x(7,nxt)-a(3,3)*n4))
c
      f(5,nxt) = (n1+(i2-i3)*x(6,nxt)*x(7,nxt))/i1
c
      f(6,nxt) = (n2+(i3-i1)*x(7,nxt)*x(5,nxt)-(0.5*w*m*l1**2*
     +          sin(w*t)*cos(w*t))*x(6,nxt))/i2
c
      f(7,nxt) = (n3+(i1-i2)*x(5,nxt)*x(6,nxt)-(0.5*w*m*l1**2*
     +          sin(w*t)*cos(w*t))*x(7,nxt))/i3
c
      return
      end
```

Bibliography

Breakwell, J.V. and Ralph Pringle, Jr. "Nonlinear Resonance Affecting Gravity Gradient Stability," International Astronautical Congress, Athens Greece: 305-325 (September 1965)

Chan, John D. An Analysis of Space Station Motion Subject to the Parametric Excitation of Periodic Elevator Motion, M.S. Thesis AFIT/GA/AA/86-D-2. School of Engineering, Air Force Institute of Technology (AU), Wright-Patterson AFB OH, December 1986 (AD-A179-235).

Chubb, W.B., et al. "Flight Performance of Skylab Attitude and Pointing Control System," J Spacecraft, 12, 220-227, 1975.

Debra, Daniel B. and R.H. Delp. "Rigid Body Attitude Stability and Natural Frequencies in a Circular Orbit," Journal of the Astronautical Sciences, 8: 14-17 (Spring 1961)

Hayashi, Chihiro. Nonlinear Oscillations in Physical Systems. New York: McGraw-Hill Book Company, 1964

Hughes, P.C. Spacecraft Attitude Dynamics. New York: John Wiley and Sons, Inc., 1986.

Kaplan, Marshall H. Modern Spacecraft Dynamics & Control. New York: John Wiley & Sons, 1976.

Meirovitch, Leonard. Methods of Analytical Dynamics. New York: McGraw-Hill Book Company, 1970.

Nayfeh, A.H. and D.T. Mook. Nonlinear Oscillations. New York: John Wiley & Sons, 1979.

Thomson, W.T. and Y.C. Fung. "Instability of Spinning Space Stations Due to Crew Motion," AIAA Journal, 3, 1082-1087, 1965.

Wertz, J.R. Spacecraft Attitude Determination and Control. Boston: D. Reidel Publishing Co., 1985.

Vita

Captain Thomas E. Williams [redacted] in 1980 and attended Embry-Riddle Aeronautical University, from which he received the degree of Bachelor of Science in Aeronautical Enginnering in April 1984. Upon graduation, he received a commission in the USAF through the ROTC program. He went on active duty in May 1984 and served as a stability and control engineer at the Aeronautical Systems Division, Wright-Patterson AFB, OH, until entering the School of Engineering, Air Force Institute of Technology, in June 1987.

[redacted]

REPORT DOCUMENTATION PAGE

Form Approved
OMB No. 0704-0188

1a. REPORT SECURITY CLASSIFICATION UNCLASSIFIED	1b. RESTRICTIVE MARKINGS
2a. SECURITY CLASSIFICATION AUTHORITY	3. DISTRIBUTION/AVAILABILITY OF REPORT Approved for public release; distribution unlimited
2b. DECLASSIFICATION/DOWNGRADING SCHEDULE	
4. PERFORMING ORGANIZATION REPORT NUMBER(S) AFIT/GSO/AA/88D-2	5. MONITORING ORGANIZATION REPORT NUMBER(S)
6a. NAME OF PERFORMING ORGANIZATION School of Engineering 6b. OFFICE SYMBOL (If applicable) AFIT/ENY	7a. NAME OF MONITORING ORGANIZATION
6c. ADDRESS (City, State, and ZIP Code) AIR FORCE INSTITUTE OF TECHNOLOGY WRIGHT-PATTERSON AFB, OHIO 45433	7b. ADDRESS (City, State, and ZIP Code)
8a. NAME OF FUNDING/SPONSORING ORGANIZATION 8b. OFFICE SYMBOL (If applicable)	9. PROCUREMENT INSTRUMENT IDENTIFICATION NUMBER
8c. ADDRESS (City, State, and ZIP Code)	10. SOURCE OF FUNDING NUMBERS PROGRAM ELEMENT NO. / PROJECT NO. / TASK NO / WORK UNIT ACCESSION NO.

11. TITLE (Include Security Classification)
AN ANALYSIS OF THE ATTITUDE STABILITY OF A SPACE STATION SUBJECT TO PARAMETRIC EXCITATION OF PERIODIC MASS MOTION

12. PERSONAL AUTHOR(S)
THOMAS E. WILLIAMS, CAPT, USAF

13a. TYPE OF REPORT	13b. TIME COVERED	14. DATE OF REPORT (Year, Month, Day)	15. PAGE COUNT
M.S. THESIS	FROM _____ TO _____	1988 DECEMBER	102

16. SUPPLEMENTARY NOTATION

17. COSATI CODES			18. SUBJECT TERMS (Continue on reverse if necessary and identify by block number)
FIELD	GROUP	SUB-GROUP	
22	01		ASTRONAUTICS, SATELLITE ATTITUDE SPACE STATIONS
22	05		

19. ABSTRACT (Continue on reverse if necessary and identify by block number)

THESIS ADVISOR: Curtis H. Spenny
Assistant Professor of Aerospace and Systems Engineering

ABSTRACT ON BACK

12 Jan 1989

20. DISTRIBUTION/AVAILABILITY OF ABSTRACT ☒ UNCLASSIFIED/UNLIMITED ☐ SAME AS RPT. ☐ DTIC USERS	21. ABSTRACT SECURITY CLASSIFICATION UNCLASSIFIED
22a. NAME OF RESPONSIBLE INDIVIDUAL Curtis H. Spenny, Assistant Professor	22b. TELEPHONE (Include Area Code) 513-255-3517 22c. OFFICE SYMBOL AFIT/ENY

DD Form 1473, JUN 86 *Previous editions are obsolete.*

The future space station will contain a mechanism that transports mass across large distances of its surface. Accordingly, this study will derive the equations of attitude motion for a gravity-gradient stabilized space station whose moments of inertia are varying with time. The equations are linearized, after which Hill's Equation is used to determine pitch stability, while the Method of Multiple Scales is used to determine the roll/yaw stability of the system. Results show that for certain frequencies of mass motion, attitude motion can grow unboundedly with time. Consequently, the shape of the classical Lagrange stability region is altered.